

Department of Precision and Microsystems Engineering

Vibration Isolation

On the determination of direct disturbance forces

D.B.C. Lakerveld

Report no : MSD 2013.020
Coach : dr. ir. R.A.J. van Ostayen
Coach Mapper : dr. ir. R.M.L. Ellenbroek
Professor : prof. ir. R.H. Munnig Schmidt
Specialisation : Mechatronic System Design
Type of report : Master thesis

Vibration Isolation

On the determination of direct disturbance forces

Author: D.B.C. Lakerveld
Date: July 2, 2013
Report No: MSD 2013.020
Type of report: Master Thesis
Student No: 1318039
Institute: Delft University of Technology
Faculty of Mechanical Engineering
Department of Precision and Microsystems Engineering

Board of Examiners:

Prof. Ir. R.H. Munnig Schmidt	Precision and Microsystems Eng., 3Me, TU Delft
Dr. Ir. R.A.J. van Ostayen	Precision and Microsystems Eng., 3Me, TU Delft
Dr. Ir. R.M.L. Ellenbroek	Mapper Lithography B.V., Delft
Dr. Ir. M. Langelaar	Precision and Microsystems Eng., 3Me, TU Delft

Preface

This thesis focuses on the properties, characterization and performance of vibration isolation systems. Specifically, the thesis treats the experimental measurement of flow-induced forces.

This master thesis is the final hurdle in achieving the grade of Master of Science in Mechanical Engineering with a specialisation in Precision and Microsystems Engineering at the Delft University of Technology, faculty 3mE. The project is performed in collaboration with the company Mapper Lithography, Delft, The Netherlands.

Management summary

In the electron-beam lithography tool produced at Mapper lithography, a wafer placed on a positioning stage is aligned with the electron optics. The electron optics are isolated from floor vibrations and direct disturbance forces by the use of a passive vibration isolation system. The main challenge of this thesis is to reduce the error in alignment between the electron optics and the wafer to 1 nm $3\text{-}\sigma$ RMS. To meet the challenge, the passive vibration isolation system is characterized by use of a dynamic error budgeting model. The uncharacterised direct disturbance forces acting on the system are identified as the performance limiting factor. The magnitude and spectral distribution of these forces are investigated by use of a test setup. The results show that the forces are much larger than currently accounted for. Based on the results recommendations are done to meet the challenge. The main challenge can only be met if a solution is found for suppressing or eliminating the direct disturbance forces caused by the water cooling system.

Acknowledgements

Finally! My thesis is finished!

Of course I would like to thank several people for their invaluable contribution. First of all I would like to thank my supervisor at Mapper, Rogier Ellenbroek, for his advice and guidance. I owe him many thanks for the good reviews of my work and showing me the importance of keeping a wide scope. Furthermore I would like to thank my supervisor from the TU Delft, Ron van Ostayen, for his feedback during our regular updates and his great patience in completion of this project. Special thanks to Jan van Eijk for his participation in one of these regular updates. This meeting marked a positive shift in the execution of the project. Also thanks to the great members of the Mapper CON department for providing a pleasant work environment.

And of course I really want to thank my parents, brother and sister for all their love and support they have given me during my years of education and especially during finishing this thesis. I could not have done it without you.

Success is not final...Failure is not fatal...It's the courage to continue that counts
WINSTON CHURCHILL

And now abide Faith, Hope, Love, these three; but the greatest of these is Love.
1 CORINTHIANS 13:13 , NEW KING JAMES BIBLE

Contents

1	Introduction	1
1.1	Context	1
1.2	E-beam Lithography; The Mapper machine	2
1.3	Vibration Isolation	4
1.4	Challenge definition	5
1.5	Outline of thesis	6
2	Vibration isolation	7
2.1	Introduction	7
2.2	Vibration isolation; theory and practice	8
2.2.1	A basic model	8
2.2.2	Application of vibration isolation	10
2.2.3	Floor vibrations	11
2.3	The Mapper machine	12
3	Dynamic error budgeting	15
3.1	Introduction	15
3.2	Theoretical background	17
3.3	System modelling	19
3.3.1	Disturbance sources	20
3.3.2	Vibration isolation system	21
3.3.3	Positioning stage	23
3.3.4	Resulting spectra	23
3.4	Parameter variations	25
3.5	Conclusions	27
4	Determining Direct Disturbance Forces	29
4.1	Introduction	29
4.2	Direct disturbance forces in the Mapper machine	29
4.3	Determining the DDF by the cooling system	30
4.3.1	The experimental stand	30
4.3.2	The investigated components	32
4.4	Resulting direct disturbance forces	33

4.4.1	Measurement scenarios	33
4.4.2	Measurement results	34
4.4.3	Discussion of the measurement results	40
4.5	Conclusion	41
5	Discussion	43
5.1	Introduction	43
5.2	Evaluation of the realized research goals	43
5.2.1	Vibration isolation	43
5.2.2	Dynamic error budgeting	44
5.2.3	Determining direct disturbance forces	45
5.3	Conclusions	46
6	Conclusions	47
6.1	Introduction	47
6.2	Conclusions	47
6.3	Recommendations	49
6.3.1	Continuation	49
6.3.2	Design recommendations	50
A	Vibration isolation system review	53
A.1	Introduction	53
A.2	Passive vibration isolation systems	53
A.2.1	Vertical isolators	53
A.2.2	Horizontal isolators	55
A.2.3	Damping	57
A.3	Active vibration isolation systems	60
A.3.1	Sensors	60
A.3.2	Actuators	64
A.3.3	Isolation strategy and control	66
B	Dynamic error budgeting model	69
B.1	Introduction	69
B.2	Dynamic error budgeting Matlab model	69
B.3	Results changing parameters of model	73
B.3.1	Stiffness of vibration isolation system	75
B.3.2	Damping of the vibration isolation system	79
B.3.3	Weighth of the isolated mass	83
B.3.4	Cross-talk	86
B.3.5	Direct disturbance forces: magnitude and spectral distribution	88
B.3.6	Floor vibration spectrum; magnitude and spectral distribution	91
B.3.7	ShS bandwidth	93

C Vibronix datasheet	95
C.1 DEB model of Vibronix	97
Bibliography	106

Glossary

Abbreviation	Description
AA	Aperature Array
ASD	Amplitude Spectral Density
CAS	Cumulative Amplitude Spectrum
CPS	Cumulative Power Spectrum
CPU	Central Processing Unit i.e. processor
CRT	Cathode Ray Tube
DDF	Direct Disturbance Force
DEB	Dynamic Error Budgeting
DOF	Degrees of Freedom
EO	Electron Optics
IC	Integrated Circuit
MOF	Metro-Optics Frame
PID	Proportional-Integral-Derivative
PSD	Power Spectral Density
RMS	Root Means Square
ROM	Rough Order of Magnitude
ShS	Short Stroke Stage
TV	Television
VC	Vibration Criteria
VIM	Vibration Isolation Module

Variable	Description	Units
a	Acceleration	[m/s ²]
ASD	Amplitude Spectral Density	[SI/√Hz]
c	Damping coefficient	[Ns/m]
C_x	Cumulative Power Spectrum	[SI ²]
$C(s)$	Compliance	[SI/N]
CAS	Cumulative Amplitude Spectrum	[SI]
CAS_{Floor}	Resulting CAS by floor vibrations	[m]
CAS_{Floor}	Resulting CAS by DDF	[m]
CPS_{Floor}	Resulting CPS by floor vibrations	[m ²]
CPS_{Floor}	Resulting CPS by DDF	[m ²]
ζ	Damping ratio	[-]
x_f	Displacement of Floor	[m]
x_{MOF}	Displacement of MOF	[m]
x_w	Displacement of Wafer	[m]
F_d	Direct Disturbance Force	[N]
e	Error	[m]
F	Force	[N]
g	Gravity constant (9.81)	[m/s ²]
m	Mass	[kg]
f_0	Natural frequency	[Hz]
ω_n	Natural frequency	[rad/s]
PSD_{DDF}	Force PSD of DEB model	[N ² /Hz]
PSD_F	Force PSD of DEB model test setup	[N ² /Hz]
PSD_F	PSD of DEB model test setup	[(m/s ²) ² /Hz]
S_x	Power Spectral Density	[SI ² /Hz]
H	Transfer function	[-]
$T(s)$	Transmissibility	[-]
$T_{DDF}(s)$	DDF Transfer function	[m ² /N ²]
T_{Fl}	Floor displacement transfer function	[-]
E_x	Signal Energy	[SI ²]
μ_x	Signal Mean	[SI]
\bar{x}^2	Signal Power	[SI ²]
σ_x^2	Signal Variance	[SI]
k	Stiffness	[N/m]

*"I think there is a world market for
maybe five computers"*

THOMAS WATSON
Chairman of IBM, 1943

Chapter 1

Introduction

1.1 Context

Laptops, notebooks, ultrabooks, tablets, desktop computers and smartphones. All kinds of appliances of which we can hardly remember to ever have lived without them. These examples of digital technology are common goods in modern day information society, being increasingly integrated in the personal life of citizens worldwide. The wide availability of computational power and storage capacity has boosted progress in science and industry and has resulted in systems of unprecedented size like the internet with currently 2,4 billion users worldwide [1] or social media like Facebook with 1 billion active members [2].

Surprisingly, this digital revolution was sparked by the invention of one of its smallest components; *the transistor*. The replacement of vacuum tubes by solid-state transistors in computer designs and the invention of the *integrated circuit* (IC), an electronic circuit created on a small plate of semiconductor material, mark the beginning of wide-spread use of the computer and its capabilities.

The transistor is the fundamental building block of the *central processing unit* (CPU) i.e. processor which is the core of every computer. The CPU performs all the basic arithmetical, logical and input/output operations for the computer to process information. The CPU is a single silicon chip which contains billions of transistors. The transistors 'process' binary information (1 and 0) by arrangement of multiple transistors in logic gates via Boolean logic.

The rapidity of development of the computer is well-illustrated by *Moore's Law*. This 'law', stated in 1965 by Gordon E. Moore, describes the trend that the number of transistors on an integrated circuit doubles approximately every two years. Together with the improvement of the transistors themselves, the trend predicts a doubling of CPU performance over each period [5, 6]. Moore's Law has been accurate for over 50 years, see figure 1.1a, and is therefore used as a roadmap for decisions, planning and future

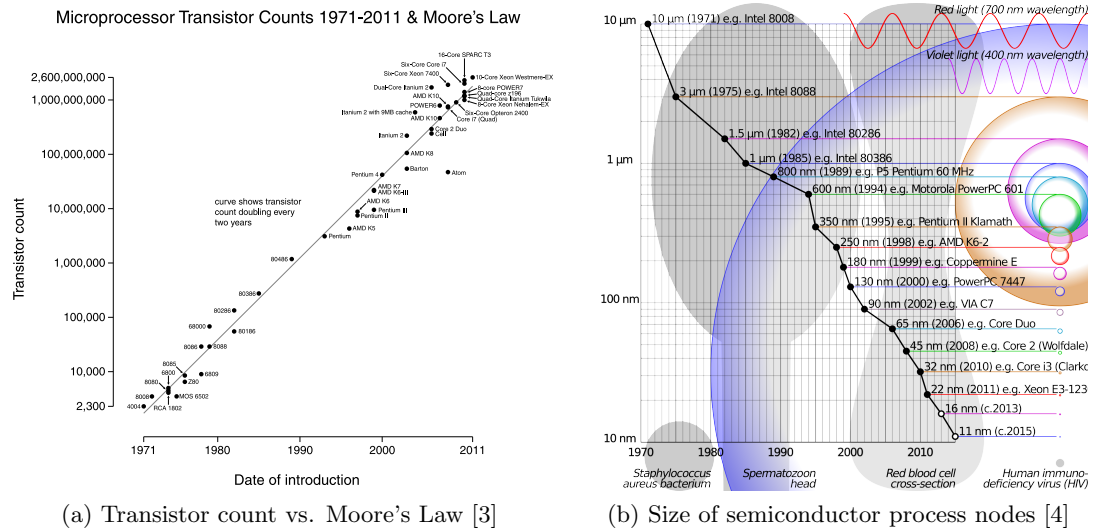


Figure 1.1: The law of Moore is sustained by decreasing the size of the transistors. The smaller features can only be produced by the use of ever better Lithography tools.

developments in the semiconductor industry [7].

In order to 'obey the law' ever smaller transistors have to be produced, see figure 1.1b. The feature size of current state-of-the-art commercial processor is 22 nm, which is about 4500 times smaller than the width of an average human hair. The small structures of integrated circuits such as transistors are produced by the use of *Lithography tools*. Lithography tools write the 2D-patterns of an electric circuit on a silicon wafer by selective exposure of a resist layer. The material at the exposed areas is removed by chemical etching and this process is repeated several times. The resulting exposed silicon wafer contains a complex semi-3D electric circuit specific for the desired functionality of the produced ICs [8]. The miniaturization of transistors is realized by the development of ever better Lithography tools capable of accurately producing the smaller features.

In conventional lithography tools light passing through an optical mask is used to expose the wafer in a way similar to the working principles of a slide-projector. With the increasingly smaller features of IC's, the use of light to create the features brings in more and more complexities and disadvantages. For the next step in the fabrication of semiconductor devices therefore also other methods of lithography are considered. One of those alternatives is the use of Electron Beam Lithography (or E-Beam Lithography).

1.2 E-beam Lithography; The Mapper machine

Instead of using light, E-Beam Lithography makes use of beams of electrons to expose the resist layer. This results in a very different production process which can be best compared to the working principles of a CRT TV. Instead of creating the desired pattern

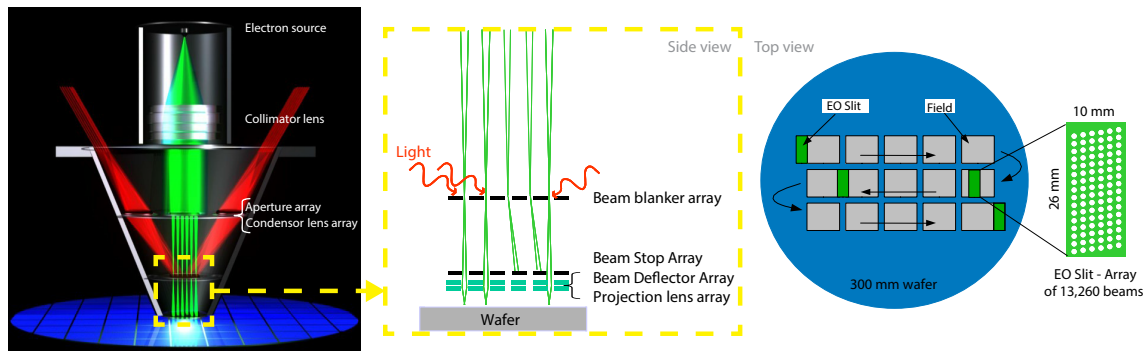


Figure 1.2: The working principle of the Mapper e-beam lithography tool. Left an overview of the electron optics (EO) is shown. In the middle a close-up of the beam switching process is displayed. At the right, the process for exposure of a full wafer is shown. Adapted from [10].

passively by blocking light with a mask, the pattern is created actively by steering the electron beam and selectively exposing the wafer 'pixel by pixel'.

The main advantage of e-beam lithography is that the wavelength of electrons is much smaller than that of light. This makes that far smaller features can be produced and overcomes traditional problems like the diffraction limit of light. Furthermore e-beam lithography excludes the use of a mask. This brings in a large cost-reduction especially for small series of IC's and makes the production process more flexible. Other advantages are the low costs and required space per machine. For production of large series of IC's the used surface per machine in an important factor due to the high cost of cleanroom space. The small size of the machines is beneficial for the ratio of exposed wafers per square meter of cleanroom space. The low costs per machine make that also smaller companies and institutions will be able to afford a machine capable of producing small series of high-end IC's.

The limitation holding back this method of lithography is the low throughput. A full wafer exposure takes far more time compared to conventional photolithography. This disadvantage is to be overcome by writing with many parallel beams simultaneously called massively-parallel e-beam writing. One of the developers of such a commercially competitive e-beam lithography tools is the Dutch company Mapper Lithography B.V. [9].

The working principle of the Mapper e-beam lithography tool is shown in figure 1.2. An electron beam originating from the electron source is collimated and cut into 13.260 separate bundles. Every independent bundle can be steered by optically-switched electrostatic lenses when passing through the beam blanker array. The bundles then pass the beam stop array which is a simple array of holes which are aligned with the electrostatic lenses. By steering a bundle away from its corresponding hole, the bundle is blocked and the wafer remains unexposed at the 'pixel'. Any design can be produced by sending a simple bitmap of the 2D-pattern to the beam blanker array by use of an optical circuit. The passing bundles are deflected and focused by the beam deflector array and the projection lens array, writing a $2\mu\text{m}$ line on the wafer. The 13.260 bundles

thereby expose an area of 26x26 mm. In order to fully expose a circular 300 mm wafer, the wafer is moved relative to the electron beam by use of a high-precision stage [10].

1.3 Vibration Isolation

With the decreasing size of the features, so decreases the room for errors. In order to attain a correct stitching between the tiled exposed fields and a correct overlay between different layers, the correct alignment between the electron beams and the wafer becomes very important. The total overlay error allowed is 7 nm 3- σ RMS. As contribution to this combined sum, the horizontal alignment in the Mapper machine allows a misalignment of only 1.8 nm 3- σ RMS. In order to achieve this high positional accuracy, the system must be isolated from the disturbances acting upon it.

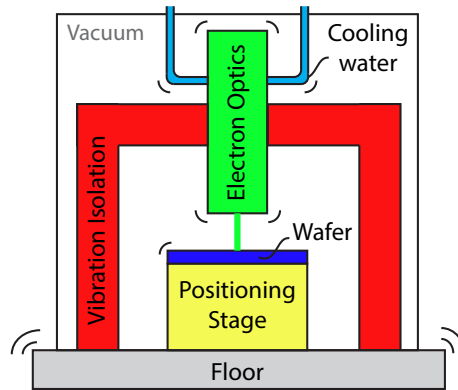


Figure 1.3: Vibration isolation is used to isolate a payload, the electron optics, from direct disturbances and floor vibrations. When using only passive components a fundamental trade-off between ground-disturbance and direct-disturbance rejection exist.

An important disturbance acting on the system is the vibration of the floor upon which the machine is mounted. The electron optics are isolated from this disturbance source by the use of a *Vibration Isolation System*. The vibration isolation system uses a low stiffness mounting to connect the payload to the ground. This results in a good ground-disturbance rejection of the system. The low stiffness mounting however makes the system sensitive for disturbances acting directly on the payload and so results in a poor direct-disturbance rejection of the system. Next to the floor vibrations, disturbances acting directly on the payload are present in the Mapper machine. These forces arise from the use of a water cooling system used to cool the electron optics.

When using only passive components, this results in a fundamental trade-off between the ground-disturbance rejection and the direct-disturbance rejection of the vibration isolation system. The configuration of the design has to be balanced such that the combined misalignment by both the floor vibrations and the direct disturbances remains below the

allowed error budget. As contribution to the allowed horizontal misalignment of 1.8 nm 3- σ RMS, the error currently allowed by the floor vibrations and direct disturbances is 1.39 nm 3- σ RMS.

1.4 Challenge definition

The use of a passive vibration isolation system and the presence of both floor vibrations and direct disturbance forces makes an interesting design challenge. This sets the following challenge to be discussed in this thesis:

Reduce the error in alignment between the electron optics and the wafer caused by the disturbances acting on the vibration isolation system to 1 nm 3- σ RMS.

The following research goals are derived from this challenge:

- Determine the design properties of vibration isolation systems. Investigate the current state-of-the-art of vibration isolation systems as discussed in literature and compare the design of the Mapper vibration isolation system.
- Determine the influence of the design properties on the performance of the Mapper vibration isolation system. Create a model to predict the change in performance of the system when the parameters of the system are adjusted.
- Characterize the performance limiting factors. Make a detailed analysis of the properties of the limiting factor.
- Discuss the results and determine solutions in order to improve the performance of the vibration isolation system. Discuss the representativeness of the research for the performance of the system realized in practice.

The research is performed in the following phases;

First the available literature on vibration isolation system is studied. Next the performance and different parameters of the Mapper system are investigated by the use of dynamic error budgeting. Based on the results from the system modelling, the direct disturbance forces caused by the cooling system are characterized by use of an experimental stand. Next, the obtained overview is discussed to determine if and how the set challenge is to be met. This results in a set of recommendations and conclusions based on the performed research.

1.5 Outline of thesis

The thesis focuses on vibration isolation with an emphasis on the determination of forces caused by flow of water through components mounted on an isolated load.

The research goals are treated by the chapters consecutively. In Chapter 2 the properties of vibration isolation systems are discussed. The properties and limitations of different vibration isolation systems and its components are discussed. Furthermore, the vibration isolation system used by Mapper is described. An overview of the different components and strategies is given in Appendix A. The performance of the system is analysed in Chapter 3 by use of a dynamic error budgeting model. First, a summary of the theory of dynamic error budgeting is provided. The properties of the created model are described and the results are discussed. By changing the model parameters the performance limiting parameters are determined. Based on the results of the dynamic error budgeting study, an indication of the forces caused by the use of the water cooling system is obtained in Chapter 4. The experimental stand used to acquire the indication is described and the results of several components are discussed. Chapter 5 discusses the obtained results and evaluates the used tools and methods. The final conclusions to the main challenge of the thesis are given in Chapter 6. Recommendations are done regarding the continuation of the research and possible design changes.

Chapter 2

Vibration isolation

In this chapter, first the theory and practice of vibration isolation systems is discussed. The basic design parameters of passive and active vibration isolation systems are discussed. The theory is illustrated by a basic model of a vibration isolation system. Furthermore the basic design of the vibration isolation system used in the Mapper machine is described.

2.1 Introduction

The performance of many high precision systems directly depends on how well disturbances from the environment can be diminished. The theory and practice of attenuation of floor vibrations and direct disturbances by use of vibration isolation system is therefore extensively discussed in literature.

The vibration isolation systems discussed in literature primarily focus on the suppression of floor vibrations. Many research effort is put in creating 'silent' mounts or platforms on which different systems can be mounted such as AIMS [11, 12] or the Hummingbird platform [13]. Very sophisticated system designs are used in the large-scale laser interferometer systems used to detect cosmic gravitational waves. These make use of cascaded vibration isolation systems since extremely low levels of vibrations need to be attained in order to detect these waves [14]. Different systems configurations are used in the renown facilities as AIGO [15], GEO 600 [16], LIGO [17] and VIRGO [18].

The working principle of these high-performance vibration isolation systems is often based on the basic behaviour of spring-mass-damper systems and in practices relies on the use of basic mechanical components such as pendulums, springs and dampers. By use of active components limitations of the passive components can be compromised.

To gain insight in the functioning of the Mapper system, first an overview of the properties of vibration isolation systems is obtained.

2.2 Vibration isolation; theory and practice

In this section the basic properties of vibration isolation systems are discussed. An overview is given of the application of and used components in passive and active vibration isolation systems. The theory is illustrated by a basic model of a vibration isolation system.

2.2.1 A basic model

A basic passive vibration isolation system can be modelled as shown in figure 2.1.

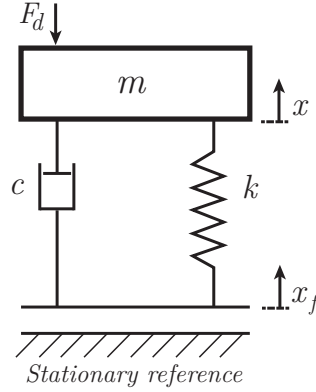


Figure 2.1: A basic passive vibration isolation system consisting of a spring k , damper c and mass m . The disturbances acting on the system are the floor vibrations x_f and the direct disturbance forces F_d .

The equation of motion of this basic model is given by:

$$m\ddot{x} + c(\dot{x} - \dot{x}_f) + k(x - x_f) = F_d \quad (2.1)$$

by transformation to the Laplace domain the equation can be rewritten to:

$$(ms^2 + cs + k)x = (cs + k)x_f + F_d \quad (2.2)$$

By definition of the natural frequency of the system $\omega_n = \sqrt{k/m}$ and the damping ratio $\zeta = c/2\sqrt{km} = c/2m\omega_n$ the motion of the payload can be defined as:

$$x = \frac{2\zeta\omega_n s + \omega_n^2}{s^2 + 2\zeta\omega_n s + \omega_n^2} x_f + \frac{1}{m(s^2 + 2\zeta\omega_n s + \omega_n^2)} F_d \quad (2.3)$$

The velocity and acceleration of the payload and the floor can be easily determined by multiplying these displacements x and x_f in equation 2.3 with s and s^2 respectively. Two important properties of the model can be derived from the equation;

$$\text{Transmissibility } T(s) \quad \frac{x}{x_f} = \frac{2\zeta\omega_n s + \omega_n^2}{s^2 + 2\zeta\omega_n s + \omega_n^2} \quad (2.4)$$

$$\text{Compliancy } C(s) \quad \frac{x}{F_d} = \frac{1}{m(s^2 + 2\zeta\omega_n s + \omega_n^2)} \quad (2.5)$$

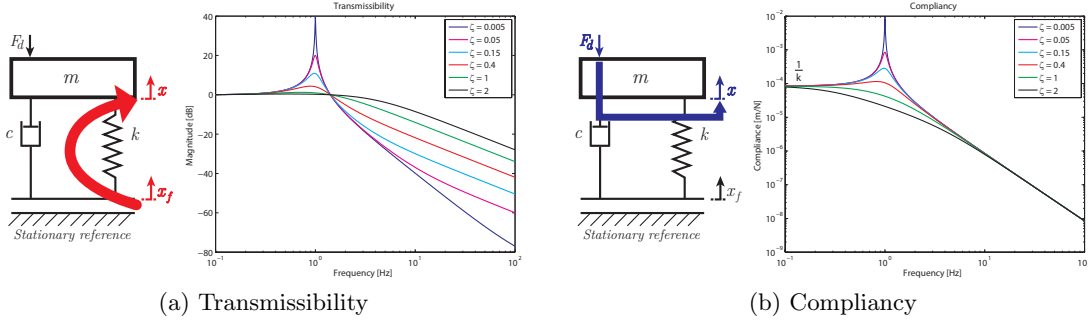


Figure 2.2: The transmissibility indicates the transfer of floor vibrations while the compliancy indicates the transfer of direct disturbance forces to the motion of the payload. The transfer functions under different levels of damping are shown.

The transmissibility, equation 2.4, describes the transmission of floor movement to movement of the isolated mass, while the compliancy, equation 2.5, describes the transmission of forces acting directly on the isolated mass to movement of the isolated mass. These properties determine the resulting performance of the vibration isolation system, as shown in figure 2.2.

As can be noted from the transmissibility in figure 2.2a, the system isolates the payload from floor vibrations at frequencies above $\omega > \sqrt{2}\omega_n$. Around ω_n the floor vibrations are amplified while at frequencies $\omega \ll \omega_n$ the floor vibrations are transferred one-on-one. By decreasing the natural frequency ω_n the transmissibility is improved. Damping reduces the magnitude around ω_n but limits the $1/f^2$ decrease in magnitude for frequencies $\omega \gg \omega_n$ where the system behaviour is determined by the rigid-body motion of the payload (*roll-off*).

The compliancy differs from the transmissibility. Disturbances at low frequencies are also suppressed since the compliancy at $\omega \ll \omega_n$ is determined by $1/k$. Furthermore the damping reduces the magnitude around ω_n without limiting the roll-off after ω_n . For displacements, the compliancy can be improved without compromising the transmissibility by proportionally increasing both stiffness k as mass m while maintaining a constant ζ . This results in maintaining an equal ω_n with equal damping resulting in a equal transmissibility. The compliancy is however improved since its starting magnitude is determined by $1/k$. By increasing the stiffness, the overall magnitude of the compliancy decreases resulting in a better direct disturbance rejection.

The compliancy and transmissibility are however connected resulting in a fundamental trade-off between the two. The fundamental trade-off can be noted by examination of the acceleration of the payload;

$$\ddot{x} = \frac{2\zeta\omega_n s + \omega_n^2}{s^2 + 2\zeta\omega_n s + \omega_n^2} \ddot{x}_f + \frac{s^2}{m(s^2 + 2\zeta\omega_n s + \omega_n^2)} F_d \quad (2.6)$$

From this equation, the dimensionless compliancy function, referred to as the sensitivity

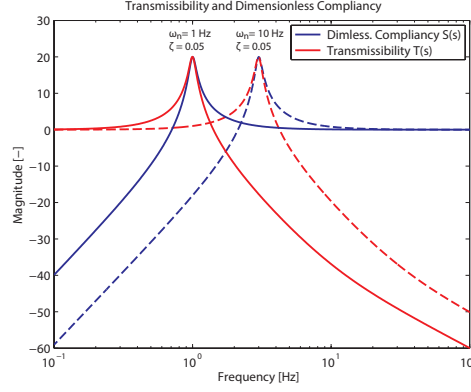


Figure 2.3: The relation between the compliancy and transmissibility for acceleration of the payload shows that a fundamental trade-off exist between suppressing both disturbance sources.

function, is obtained by:

$$S(s) = m \frac{\ddot{x}}{F_d} = \frac{s^2}{s^2 + 2\zeta\omega_n s + \omega_n^2} \quad (2.7)$$

One can note that the transmissibility function now exactly forms the complementary sensitivity function:

$$T(s) = \frac{\ddot{x}}{\ddot{x}_f} = \frac{2\zeta\omega_n s + \omega_n^2}{s^2 + 2\zeta\omega_n s + \omega_n^2} \quad (2.8)$$

where

$$S(s) + T(s) = 1 \quad (2.9)$$

The relation as displayed in figure 2.3 shows that, for accelerations, direct disturbances and floor vibrations cannot be rejected at the same frequency. This fundamental trade-off has been noted by Subrahmanyam and Trumper [19]. The trade-off holds for both passive vibration isolation systems as well as active system using only displacement or velocity feedback relative to the ground.

2.2.2 Application of vibration isolation

While the actual realization can be simple, the design of vibration isolation systems covers many aspects. The goal of a vibration isolation system is to isolate the motion of a payload from its environment. The three most common functional requirements for vibration isolation systems are:

- Floor vibration isolation
Isolate the motion of the payload from ground motion. Attenuate the absolute payload motion due to ground motion or attenuate the force transmitted to the ground by payload motion. The performance is often expressed by the transmissibility of the system.

- Direct disturbance rejection
Isolate the motion of the payload from forces acting directly on the payload. The forces acting on the payload are indicated as *Direct Disturbance Forces* (DDF). The performance is often expressed by the compliancy of the system.
- Position alignment
Isolate the payload from ground motion and DDF in order to maintain the relative position of the payload to some reference. The performance is often expressed by the resulting error in the alignment between the payload and the reference.

In order to meet the functional requirement the vibration isolation system acts on different parameters, as also illustrated by figure 2.1. The basic parameters on which the vibration isolation system acts are;

- Relative motion between the isolated payload and the ground and/or intermediate platforms; relative position and velocity.
- Motion of the isolated payload; absolute position, velocity or acceleration
- Base motion; absolute acceleration

The vibration isolation systems make use of different components to act on the parameters. Based on the used components the vibration isolation systems can be divided in two different categories; passive and active vibration isolation. An overview of the relevant parameters and components used in the design of vibration isolation systems is given in Appendix A.

2.2.3 Floor vibrations

The vibration of the floor is one of the main disturbance sources acting on the vibration isolation system determining its resulting performance. In order to correctly evaluate and compare the performance of a vibration isolation system, a proper shared standard for the existing floor vibrations is required.

The accepted standard are the Bolt, Beranek and Newman Inc. (BBN) Vibration Criteria originally proposed by Gordon in 1991 [20] and reviewed in 1999 [21] and 2005 [22], better known as the *VC criteria*. Before the introduction of this standard, different companies used their own different standards making it difficult to correctly compare the performance of a different systems. The VC criteria are given by one-third octave band (terts band) spectra with a specified by a RMS velocity input per given tert band and are also shown in figure 3.3a. Originally the bands span the range of 4-100 Hz, but currently VC-C and the criteria below start from 1 Hz due to the increased use of pneumatic springs. Below 1 Hz the New High Noise Model (NHNM) from the Albuquerque Seismological Lab [23] can be used but this is not common for typical industrial applications.

Next to the VC-criteria, still different models exist (e.g. NIST) and the use of the VC-criteria is often considered an upper limit for the actual vibration level present. If a

correct prediction of the system performance is to be made it is best to perform longterm (24 hours) on-site measurements in order to characterize the floor vibrations present at a designated site, as also proposed by several authors [24,25]. More background on floor dynamics is given by Boogaard [26].

Due to the focus on suppressing floor vibrations, the actual effectiveness of vibration isolation systems found in literature can sometimes be misleading when only the transmissibility is shown without showing the resulting acceleration level at the isolated load. Often very low natural frequencies are used to achieve a low transmissibility, making the passive system sensitive for DDF such as acoustic noise increasing the acceleration level of the load.

2.3 The Mapper machine

As described in chapter 1 the use of a vibration isolation system is essential for realization of the high positional accuracy required for the next generation of lithography tools. As stated, the e-beam lithography tool developed at Mapper Lithography also makes use of a vibration isolation system to isolate the used electron optics. The vibration isolation used in the Mapper tool is illustrated by figure 2.4. The isolation system exist out of two sections;

The first section consist of a passive vibration isolation system, spring k and damper c , supporting the electron optics in the Metro-Optics Frame (*MOF*). The passive vibration isolation system, having low natural frequencies in all 6 DOF, provides a good attenuation of floor vibrations x_f but makes the system more sensitive for the direct disturbance forces F_d acting directly on the MOF. This is expressed by a low transmissibility and a high compliancy.

The second section of the system consists of a positioning stage which aligns the wafer with the electron optics. The positioning stage consist of a long-stroke and short-stroke stage. The longstroke stage performs the coarse positioning (*Stepping, Scanning*) while the short-stroke stage performs the fine positioning. The short-stroke stage consists of a gravity compensator k_{grav} in parallel with zero-stiffness actuators F and carries the wafer on mass m . The positioning stage makes use of an optical measurement system determining the relative position, δx , between the electron optics and the wafer. It is assumed that no floor vibrations pass through the positioning stage. Other disturbance sources (e.g. from electronics) acting on the positioning stage are neglected.

The functional requirement of the vibration isolation system is to isolate the MOF from its environment such that a correct alignment between the wafer and electron optics can be maintained by the stage. The performance of the system is determined by the resulting error e . The error e is the resulting misalignment between the position of the MOF, x_{MOF} , and the position of the wafer, x_w . Since this error results directly on the wafer it plays an important role in the performance of the Mapper machine as a whole.

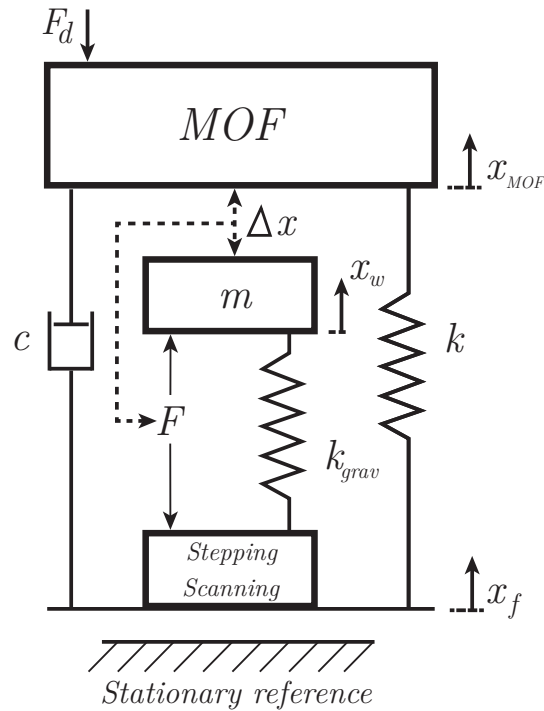


Figure 2.4: Lay-out of the vibration isolation system used in the Mapper e-beam lithography tool

In comparison with the basic model of a vibration isolation model, the behaviour of the Mapper vibration isolation system differs in two important ways. First of all is the isolated payload, the MOF, used as a reference for the positioning stage. The stage can correctly follow the position of MOF at low frequencies, below its bandwidth, but cannot follow around and above the stage bandwidth. This decreases the importance of suppressing low frequency vibrations of the MOF but increases the importance of vibrations of the MOF around the stage bandwidth.

Second important difference is the existence of direct disturbance forces acting upon the MOF. Although the system is operating in vacuum direct disturbance forces act on the MOF due to the use of a cooling system. The presence of the DDF makes that the fundamental trade-off for passive isolation systems, between transmissibility and compliancy becomes relevant. Lowering the eigenfrequency will decrease the effect of low frequent floor vibration but increases the effect of the direct disturbance forces. These factors cause that in order to obtain a lower error in the alignment, simply lowering the natural frequencies of the used passive vibration isolation system is not sufficient. The effect of the different parameters of the vibration isolation system on the resulting performance is discussed in the next chapter.

"If you want to find the secrets of the universe, think in terms of energy, frequency and vibration"

NIKOLA TESLA

Chapter 3

Dynamic error budgeting

In this chapter, first the theoretical background of dynamic error budgeting is discussed. Next the simulation model of the Mapper vibration isolation system is described. This is followed by a study on parameter changes in this model. The chapter ends with conclusions from the dynamic error budgeting study on the Mapper vibration isolation system.

3.1 Introduction

According to *Moore's law*, suppliers of Lithography tools for the semi-conductor industry need to improve the performance of their systems in a predicted time span. Lithography tools have to ever become more productive and above all; more accurate. This increasing demand on the performance inherently increases the complexity and costs of these high precision mechatronic systems. The development of these systems is highly knowledge-extensive, time consuming and very expensive. Systems are developed modularly and consist of multiple subsystems. This tendency stresses the importance of the design of these systems, demanding that the systems must be first-time-right. The final build system must satisfy all the specifications at once since no significant changes can be made in the post-design phase. It is therefore important that a designer can predict the system performance a-priori, enabling him to asses and improve the final system performance before being materialized.

The performance of a high precision mechatronic system is often defined by the error e , which results under influence of disturbances d attenuated by the sub-systems under control by controller C . During the design, methods are used to focus on this error e as the performance indicator of the mechatronic system. A common method is the use of *error budgeting*. In this method every disturbance source is attributed a budget to which it may contribute to a specified final resulting error. The propagation of a disturbance to the output is often determined by rules of thumb which are based on harmonic simulations.

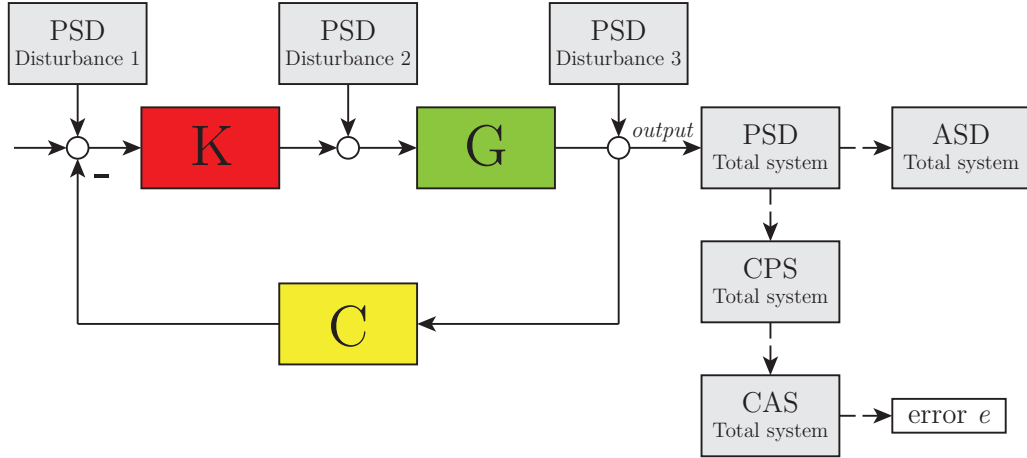


Figure 3.1: In dynamic error budgeting, every stochastic disturbance source is represented by its power spectral density and propagates to the output of the system being filtered by the squared frequency dependent models of the system components. The resulting power spectral is the weighted sum of the separate contributions of the disturbance sources and is used to determine the performance of the system. For precision system this performance is often expressed by the resulting error e

However, since almost all the disturbances in mechatronic systems are of stochastic nature, modelled by their *Power Spectral Density* (PSD), these rules of thumb do not apply. According to the theory of *Spectral Analysis*, the propagation of stochastic disturbances can however be modelled by the use of frequency dependent models. This resulted in the theory of frequency dependent error budgeting, also known as *Dynamic Error Budgeting* (DEB).

In this method, the PSD resulting at the output is the weighted sum of PSDs resulting from each respective disturbance source after being filtered by the squared transfer function from source to output. By use of spectral analysis, the PSDs can be analysed and reworked into a *Amplitude Spectral Density* (ASD), *Cumulative Power Spectrum* (CPS) and a *Cumulative Amplitude Spectrum* (CAS) stating the resulting error e by the stochastic disturbances.

This design approach is clearly described in the works of Monkhurst [27, 28] and Jabben [24]. For the application of this design approach, a short summary of the theory extensively described in by Monkhurst and Jabben is provided in the following section.

3.2 Theoretical background

In order to apply dynamic error budgeting to a system model the following assumptions are made on the system and the disturbances:

- The system is assumed to be linear, time invariant.
- The disturbances are stationary
- The disturbances are uncorrelated
- Since the disturbances are modelled by their PSDs only ergodic stochastic disturbances are allowed.
- Not all the disturbances have a normal distribution. It is assumed that, by use of the *Central Limit Theorem*, the output will approach a normal distribution for an increasing number of disturbances.

A stationary stochastic signal $x(t)$ can be described by its mean, power and variance:

$$\text{Mean} \quad \mu_x = \lim_{T \rightarrow \infty} \frac{1}{2T} \int_{-T}^T x(t) dt \quad (3.1)$$

$$\text{Power} \quad \bar{x}^2 = \lim_{T \rightarrow \infty} \frac{1}{2T} \int_{-T}^T x(t)^2 dt \quad (3.2)$$

$$\text{Variance} \quad \sigma_x^2 = \bar{x}^2 - \mu_x^2 \quad (3.3)$$

Here the power (3.2) is expressed by the mathematical definition of signal power [SI²] rather than physical power [J/s].

For the determination of the PSD the time domain properties must be translated to the frequency domain. By use of *Parseval's Theorem* the time domain energy can be related to the frequency domain energy. The energy of finite duration non-periodic signals is described by:

$$\text{Energy} \quad E_s = \int_{-\infty}^{\infty} x(t)^2 dt \quad (3.4)$$

Parseval's Theorem than states relates the time domain energy to the frequency energy by stating that:

$$\text{Energy} \quad E_s = \int_{-\infty}^{\infty} x(t)^2 dt = \int_{-\infty}^{\infty} |X(f)|^2 df \quad (3.5)$$

where $X(f)$ is the Fourier transform of time signal $x(t)$:

$$X(f) = \int_{-\infty}^{\infty} x(t) e^{-2\pi jft} dt \quad (3.6)$$

The PSD describes the power distribution over frequency of a the time signal $x(t)$ with units $[\text{SI}^2/\text{Hz}]$. The area below the PSD denotes the power or, when having a zero mean, the variance. By Parsevals theorem also the signal power in the time domain can be related to the frequency domain by:

$$\text{Power} \quad \bar{x}^2 = \lim_{T \rightarrow \infty} \frac{1}{2T} \int_{-T}^T x(t)^2 dt = \lim_{T \rightarrow \infty} \frac{1}{2T} \int_{-\infty}^{\infty} |X_T(f)|^2 df = \int_{-\infty}^{\infty} \lim_{T \rightarrow \infty} \frac{|X_T(f)|^2}{2T} df \quad (3.7)$$

where $X_T(f)$ is the Fourier transform of $x(t)$ on the interval $-T \leq t \leq T$. The resulting term in the integral is referred to as the two-sided PSD $S_x(f)$ as it describes the signal power over frequency. In practice the one-sided PSD is used which is only defined on positive frequency axis but still contains all the signal power. The one-sided PSD is therefore simply defined as double the two-sided PSD while having half the frequency range.

$$S_{x\text{-one-sided}}(f) = \lim_{T \rightarrow \infty} \frac{|X_T(f)|^2}{T} \quad 0 \leq f \leq \infty \quad (3.8)$$

In this report $S_x(f)$ always refers to a one-sided PSD.

The propagation of a signal $d(t)$ to the output is determined by multiplying its PSD S_d with the squared magnitude of the corresponding frequency dependent transfer function $H(j2\pi f)$.

$$S_x(f) = |H(j2\pi f)|^2 S_d(f) \quad (3.9)$$

The resulting PSD of the output is simply the linear sum of each of these resulting PSDs of the input signals.

By using zero-mean signals, the variance μ_x^2 equals the power \bar{x}^2 of the signal. Since a PSD describes the power over frequency, the integral over frequency states the power, and thus the variance, of the output signal.

$$\bar{x}^2 = \int_0^{\infty} S_x(f) df \quad (3.10)$$

$$\sigma_x^2 = \bar{x}^2 \quad (3.11)$$

For the correct analysis of the performance of the system, the PSD can be moulded into more descriptive functions. An important function is the *Cumulative Power Spectrum* (CPS), which clearly shows how much power is added at which frequency.

$$C_x(f_o) = \int_0^{f_o} S_x(f) df \quad (3.12)$$

The performance can most effectively be improved by reducing the largest power inputs distinguished in the CPS. It is therefore the main tool for analysis to improve system

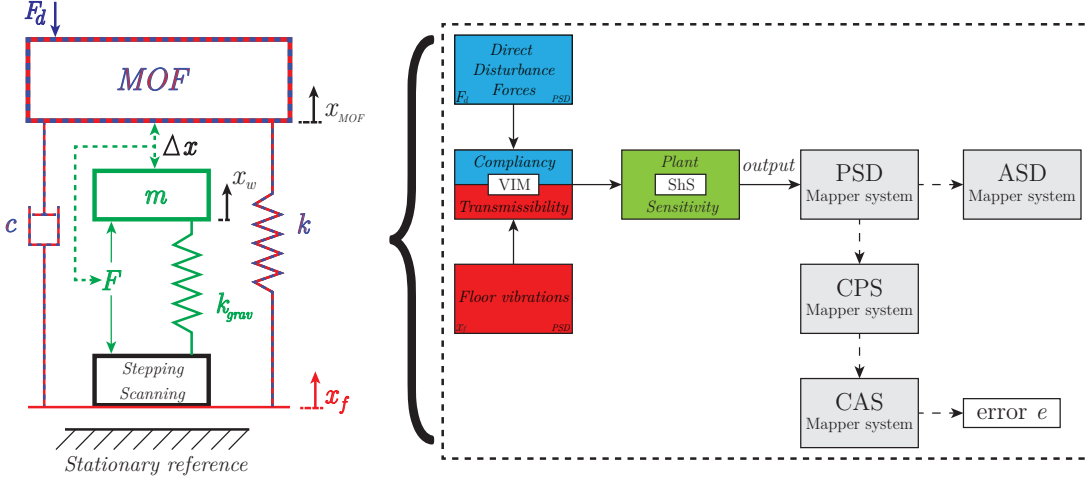


Figure 3.2: The dynamic error budgeting model of the Mapper system consist of two disturbance sources, direct disturbance forces F_d and floor vibrations x_f , which are 'filtered' by the squared model of the vibration isolation system (VIM) and the positioning stage (ShS) over frequency.

performance by dynamic error budgeting.

Other useful spectral functions are the square-root versions of the PSD and the CPS, the *Amplitude Spectral Density* (ASD) and *Cumulative Amplitude Spectrum* (CAS).

$$ASD = \sqrt{|S_x(f)|} \quad (3.13)$$

$$CAS = \sqrt{|C_x(f)|} \quad (3.14)$$

The CAS [SI], at its final value, equals the standard deviation σ_x of the signal. While the CPS is best used for showing at which frequency most of the power, and thus of the resulting error is added, the CAS is most useful in comparing the performance with the specifications since most specifications are set in terms of σ -values. The ASD [SI/ \sqrt{Hz}] is often used by suppliers to indicate the noise performance of electrical components e.g. sensors.

In this report a signal-norm of $3\text{-}\sigma$ RMS is used to determine the performance of the system. For a stochastic variable with a normal distribution, this norm indicates that 99,7% of the realized values are within the bounds of the $3\text{-}\sigma$ value.

3.3 System modelling

The theory of dynamic error budgeting is used to model the performance of the high precision mechatronic system being produced at Mapper Lithography. The most important parts of the created model are shown in Appendix B. The modelled system consists of a passive vibration isolation system of which the isolated mass is used as reference for a positioning stage. The positioning stage aligns the position of the stage with the

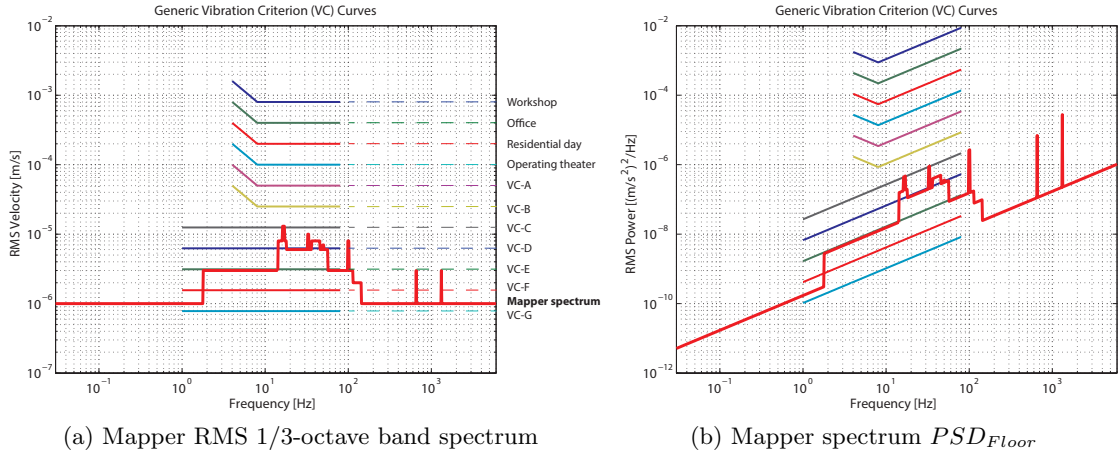


Figure 3.3: The Mapper spectrum spans a much larger frequency range than the VC-criteria and has additional input at known equipment frequencies. In the 1-100 Hz range, the spectrum is similar to a mixed VC-D / VC-E spectrum with peaks up to a VC-C level.

isolated mass. The final resulting error e in the alignment between the isolated mass and the positioning stage indicates the performance of the system. The DEB system model, as shown in figure 3.2, consists of two disturbance sources and two plant models. The disturbance sources are the displacements of the floor and the forces acting directly on the isolated load. Both disturbance sources act upon the vibration isolation system. The two plants represent the model of the vibration isolation system and the positioning stage over frequency. The system performance is analysed in one DOF with a contribution by cross-talk from three other directions.

In this section the disturbance sources and the frequency dependent models of the system are described.

3.3.1 Disturbance sources

The direct disturbance forces and the floor vibrations are both given in RMS values measured in 1/3-octave band spectra. These spectra are converted to PSDs in order to be used in the DEB model. Next the origin of both these spectra is discussed.

Floor vibrations

As discussed in section 2.2.3 floor vibrations are often specified by the categories stated in the VC-criteria. These criteria often lead to an overestimation of the situation in practice [25]. Therefore Mapper makes use of a custom floor spectrum (Mapper floor spectrum) which is based on floor measurements performed at various operating locations of early Mapper prototype machines. This spectrum spans a larger frequency range than regular VC-criteria and additional input is added at known frequencies coming from equipment mounted close-by or inside the machine. The Mapper floor spectrum

is shown in figure 3.3a and spans a range from 0.03 up to 6000 Hz. Due to the large range, this adds up to an input of about 83 mm/s^2 RMS, while a VC-D spectrum adds up to only $6,5 \text{ mm/s}^2$ RMS. For the determination of the resulting error, the Mapper spectrum PSD is integrated to a displacement spectrum, indicated as PSD_{Floor} . The input of the displacement PSD of the Mapper spectrum is $11 \mu\text{m}$ RMS while a VC-D has a displacement input of $2 \mu\text{m}$ RMS.

Direct disturbance forces

Since the isolated load is placed in a vacuum no acoustic disturbances act on the system. Furthermore, during operation, no components mounted on the isolated load are moving. The force disturbance sources are therefore limited to the cooling system and the cabling connected to the isolated load. It is chosen to neglect the latter, which leaves the cooling system as the main contributor to direct disturbance forces (DDF) acting on the isolated load.

In contrast to the floor vibrations, direct disturbance forces acting on vibration isolation systems are far less well-documented. Where floor vibrations are omni-present and easy characterizable, direct disturbance forces are often strongly dependent on the environment and geometry of a system and are often difficult to determine. This also holds for forces caused by the use of a cooling system, which are strongly dependent on flow, pressure and geometry of the system. Up to date, no sources have been found providing a categorization for occurring force levels experienced by use of tubing or known cooling components.

Due to the uncertainty of the forces caused by the cooling system it is decided to first determine which level of direct disturbance forces is allowed in order for the system to be within specification. The budget left after filtering the floor vibrations by its corresponding transfer function may be attributed by the direct disturbance forces. By knowing the available resulting error budget and the intermediate transfer function a budget for the applied direct disturbance forces can be determined. First an arbitrary force distribution is used in order to determine a resulting error which is within the budget, which is also shown in 3.6a. The PSD of the force distribution is indicated as PSD_{DDF} .

3.3.2 Vibration isolation system

The vibration isolation system is described by the equations of the transmissibility $T(s)$ and the compliancy $C(s)$ respectively. Theoretically these properties are defined by the basic equations 2.4 and 2.5, which result infinite attenuation at infinite frequency. In practise however the attenuation at increasing frequency is limited, for instance by internal dynamics of the components of the system. To account for this behaviour, a pair of high frequency zero is added to the basic equations resulting in the limited

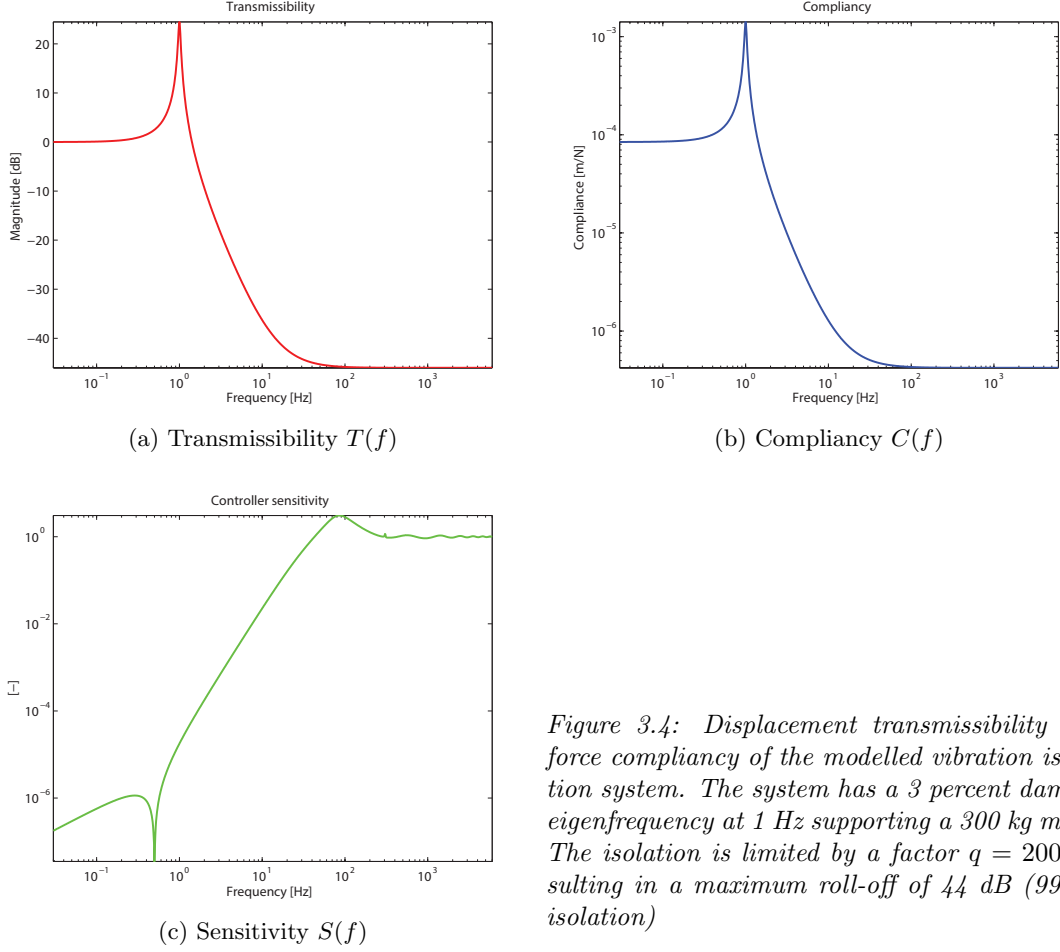


Figure 3.4: Displacement transmissibility and force compliancy of the modelled vibration isolation system. The system has a 3 percent damped eigenfrequency at 1 Hz supporting a 300 kg mass. The isolation is limited by a factor $q = 200$ resulting in a maximum roll-off of 44 dB (99,5% isolation)

transmissibility $T(s)$ (3.15) and the limited compliancy $C(s)$ (3.16) respectively:

$$T(s) = \frac{s^2 + (2q\zeta\omega_n + \frac{\omega_n}{2\zeta})s + q\omega_n^2}{q(s^2 + 2\zeta\omega_n s + \omega_n)} \quad (3.15)$$

$$C(s) = \frac{s^2 + 2\omega_n\sqrt{q}s + q\omega_n}{mq\omega_n^2(s^2 + 2\zeta\omega_n s + \omega_n^2)} \quad (3.16)$$

where $\omega_n = 2\pi f_0 = 2\pi(1.0)$ is the natural frequency in $[rad/s]$, $\zeta = 0.3[-]$ the damping ratio and $m = 300[kg]$ the weight of the isolated load. In practice, the isolation at increasing frequency after the passing the eigenfrequency is limited. The high frequency dynamics present in the system limit the attenuation and can even cause an increase of the transfer functions. This effect is accounted for by adding a high frequency zero in the transfer functions, limiting the high frequency isolation to a maximum factor q . With the given properties, this maximum isolation level is reached around 90 Hz. The transmissibility T and compliancy C of the system are shown in figure 3.4a and 3.4b.

3.3.3 Positioning stage

The ability of the positioning stage to reject disturbances is represented by the resulting sensitivity function of this feedback controlled system. This important transfer function, which is in the *Gang of Four* [8], is defined as:

$$S(s) = \frac{1}{1 + G(s)C(s)} \quad (3.17)$$

where G is the plant model under feedback control by controller C . The sensitivity function indicates how output disturbances influence the output of the total system. If $|S(s)| < 1$ the disturbances are attenuated while if $|S(s)| > 1$ the disturbances are amplified.

The positioning stage, as described in section 2.3, is modelled by an actuated load of 22 kilogram on a 0,5 Hz suspension, under control by a 75 Hz bandwidth controller having an output delay of 9,26 milliseconds. The resulting sensitivity function of this system is shown in figure 3.4c. As can be noted, the positioning system has a good disturbance rejection at low frequencies but amplifies disturbances around the bandwidth of the controller.

3.3.4 Resulting spectra

By multiplying the squared transmissibility and compliancy with the squared sensitivity function, the transfer function of the total system results, as shown in figure 3.5:

$$T_{Fl}(s) = T(s)^2 S(s)^2 \quad (3.18)$$

$$T_{DDF}(s) = C(s)^2 S(s)^2 \quad (3.19)$$

The transfer functions of the combined system give an important insight in the system behaviour. The addition of the positioning stage to the classical vibration isolation system has a profound effect on the disturbance rejection of the total system. While the classical vibration isolation problem has little disturbance rejection at low frequencies, improving after its natural frequency, this combined system has very high disturbance rejection at low frequencies which decreases when nearing the positioning stage bandwidth. This shows that the system is most sensitive to disturbances in the frequency range around the positioning stage bandwidth, so between 20-100 Hz.

When multiplying the disturbance sources with the corresponding transfer functions, the resulting error e in alignment between the isolated mass and the positioning stage can be determined. The resulting 1- σ spectra are defined by:

$$CPS_{Floor}(f) = \int_0^{f_o} T_{Fl}(f) PSD_{Floor}(f) df \quad (3.20)$$

$$CAS_{Floor}(f) = \sqrt{|CPS_{Floor}(f)|} \quad (3.21)$$

$$CPS_{DDF}(s) = \int_0^{f_o} T_{DDF}(f) PSD_{DDF}(f) df \quad (3.22)$$

$$CAS_{DDF}(f) = \sqrt{|CPS_{DDF}(f)|} \quad (3.23)$$

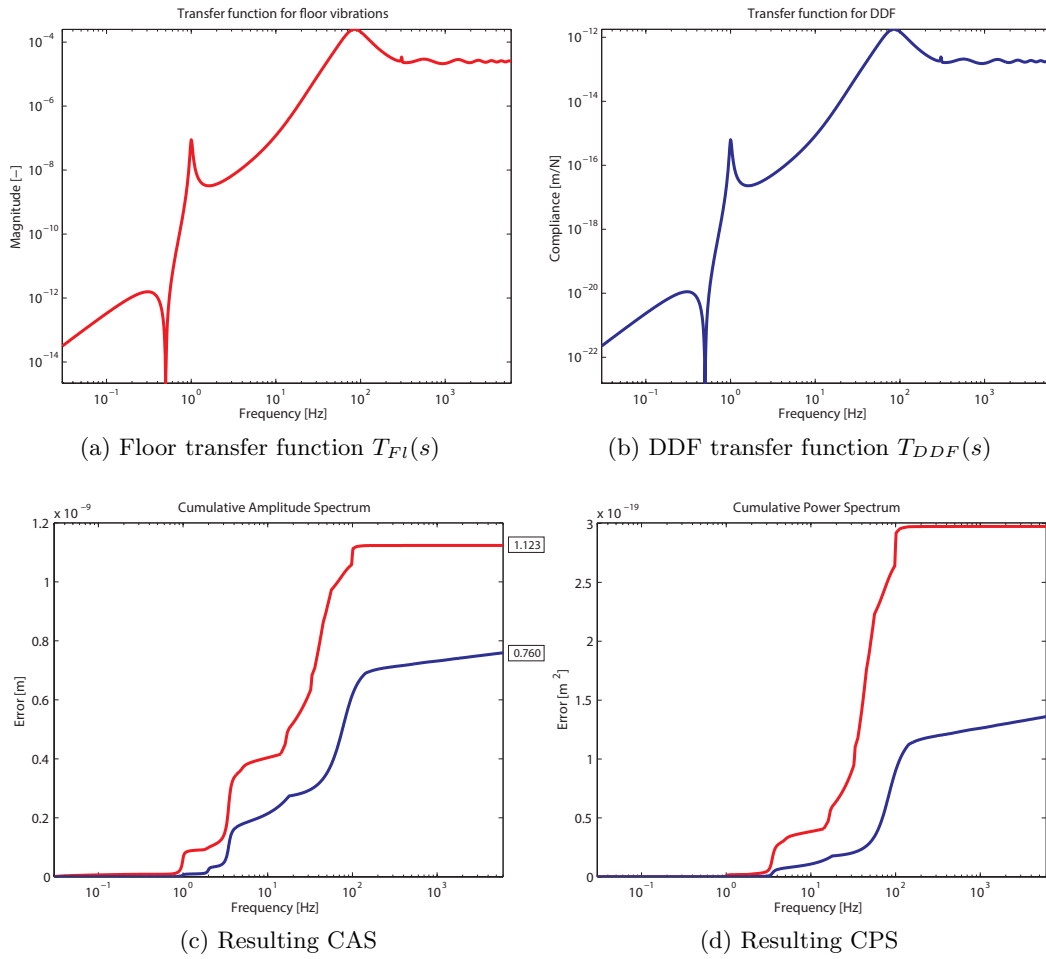


Figure 3.5: When ‘filtering’ the disturbance spectra with the corresponding transfer functions T_{Fl} and T_{DDF} , the CAS and CPS can be obtained. The CAS shows the resulting 3-sigma error e by the disturbances. The CPS shows that most of this resulting error is added in the 20-100 Hz range. When comparing the CAS and CPS, the low frequency additions are visually enlarged in the CAS.

The available error 3- σ budget for the floor vibrations and the direct disturbance forces is 1.39 nm. In the model, the resulting error by the floor vibrations is 1.123 nm error while the resulting error by direct disturbance forces is 0.760 nm. This adds up to a resulting error of 1.356 nm.

The resulting error spectra show the build up of the error over frequency. When analysing the CAS (figure 3.5c) it seems like a large contribution to the resulting error is done at low frequency. The CPS, figure 3.5d, however shows a build up in which the contributions at higher frequencies, around the bandwidth of the controller, are much more

prominent. Since the largest power contributions make for the largest contribution to the resulting error, the CPS best shows the proportion of error build-up at different frequencies. It is so the preferred tool for correctly analysing the system performance [8]. For this analysis it is best to use a linear scale y-scale to correctly show the proportions.

3.4 Parameter variations

In order to determine the robustness of the system model, the effect of the parameters of the system model is studied. By variation of the different inputs and system properties, it is determined how sensitive the modelled system is for variation of its parameters. The goal is to determine which and how parameters should be tuned in order to improve the performance of the system. The results of this study are discussed in Appendix B.3. In this section the most important conclusion of this study are discussed.

The existence of the DDF in the model cause that a correct balance in the fundamental trade-off between transmissibility and compliancy becomes important. The traditional solution of decreasing the natural frequency of the passive vibration isolation system in order to improve its overall disturbance rejection is not applicable. However, since the attenuation of the compliancy function before the natural frequency is determined by $1/k$, a higher stiffness improves the DDF rejection behaviour. The DDF rejection can therefore be improved without compromising the floor vibration rejection by proportionally increasing the weight and stiffness of the system, resulting in an equal natural frequency of the system. This has no influence on the floor vibration rejection because the eigenfrequency is not changed but improves the DDF rejection by the increase of the stiffness. It however stresses the demands on (mounting) stiffnesses in order to control the occurrence of internal dynamics due to the increased weight.

As also shown in figure 3.5a and 3.5b, the high frequency disturbance rejection is determined by the sensitivity function of the positioning stage and the maximum suppression level q used in the vibration isolation system model. The use of factor q is justified in order to create a more realistic system behaviour but its exact level has significant effect on the resulting performance. E.g. if the maximum suppression level is increased from 46 dB ($q = 200$) to 50 dB ($q = 316$) the performance increases by 26%. It is therefore important to have a correct indication for the applied q which should be validated by reality. It also shows that the high frequency behaviour of the vibration isolation system is important in the effectiveness of the system. It urges the importance of achieving a high roll-off after passing the natural frequency and having a large spectral spacing between the natural frequency and the spurious modes. Achieving a high maximum suppression level and taking good care of the internal dynamics are just as important as creating a low natural frequency.

Observing the results of changing the applied direct disturbance force brings us to the most important conclusion. As discussed, first the available budget for the DDF is

determined by the budget left after the determination of the error by floor vibrations. This due to the large uncertainty on the occurring forces. Any DDF spectrum is allowed as long as, after being filtered by the transfer function T_{DDF} , the total resulting error is still within budget. In this perspective transfer function T_{DDF} can be viewed as a 'weighting' function to determine the resulting error by any given input spectrum. Due to the complexity and dependency on the geometry, only basic *rough order of magnitude* (ROM) calculations have been performed in order to approximate the DDF input spectrum. One of the ROM calculations [29], which is a dimensional analysis of a straight piece of tube representative for one of the components of the cooling system, was used as input to the model. While having equivalent magnitude to the set requirement, the difference in spectral distribution causes that the resulting error is far above budget. The variation showed that even small differences in the force amplitudes or spectral distribution have a large effect on the resulting error. Moreover, the ROM calculations indicate that most of the forces are acting in the sensitive range of the system, the 20-100 Hz band.

The goal of the DEB model is to determine the influence of the different parameters on the resulting performance. The large effect on the performance by the DDF shows that in order to make a correct statement about the performance of the system, a representative approximation of the acting DDF must be determined.

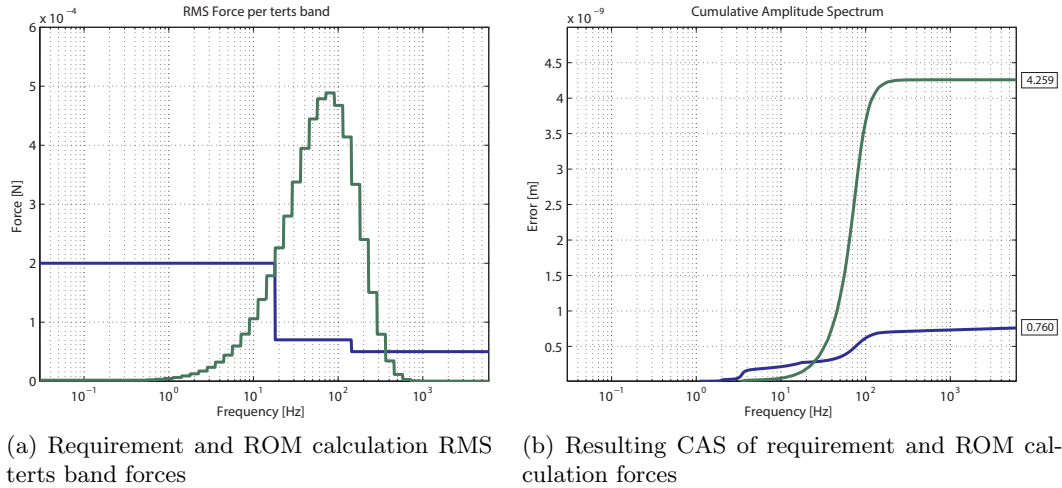


Figure 3.6: The calculated ROM forces (green) from [29] result in a much higher 3- σ error as allowed by the budget. An arbitrary in-spec force distribution is shown in blue. The variation of the force amplitude and spectral distribution showed that the resulting performance is highly dependent on the applied DDF spectrum. In order for the DEB model to be functional a correct approximation of the DDF spectrum is critical.

3.5 Conclusions

Dynamic error budgeting is a very useful tool for the performance analysis of the Mapper system. The DEB model shows that, by addition of the positioning stage, the resulting transfer functions for the disturbances are very different than those of the classical passive vibration isolation system. The Mapper system shows to be most sensitive for floor and DDF disturbances in 20-100 Hz range. The disturbance rejection in this range is determined by the bandwidth of the positioning stage and the maximum attained roll-off.

The variation of the different parameters most clearly indicates that the performance of the system is very dependent on the applied direct disturbance forces spectrum. The available budget for the DDF is very small and requires that the DDF remain very small, especially in the sensitive range of the system. Early rough order of magnitude calculations however indicate that the forces might very well be higher and moreover dominantly act in the 20-100 Hz range. Applying the calculated ROM spectra result in large out-of-spec error levels. The uncertainty on the DDF therefore compromises the representativeness of the resulting performance from the system model in comparison with the system performance to be expected in reality.

Based on the result from the DEB model of the system and the resulting error by variation of the parameters, it is concluded that it is most important to first create an understanding and proper indication of the resulting direct disturbance forces by use of the cooling system in the 20-100 Hz range. The acquisition of an indicative spectrum for the DDF in this range is discussed in chapter 4.

"Water is the driving force of all nature"

LEONARDO DA VINCI

Chapter 4

Determining Direct Disturbance Forces

In this chapter, first a description is given of the cooling system used in the Mapper machine. Next the experimental stand used to determine the cooling forces is described. This is followed by the results from measurements performed on the experimental stand to determine the acting forces. Furthermore, the measured force spectra are used as an input for the created dynamic error budgeting model.

4.1 Introduction

The dynamic error budgeting has shown that in order to make a representative indication of the performance of the Mapper system, a correct characterization of the direct disturbance forces acting on the isolated load of the machine must come available. The main contribution to the DDF comes from the use of a water cooling system to control the temperature of several subsystems mounted on the isolated load. Each of the subsystems requires a specified flow at a given pressure in order to maintain a correct temperature. The study of forces caused by the use of water flow to cool components is not common. Due to its dependency on many factors such as flow, pressure and geometry it is difficult to attain a correct numerical approximation of the acting forces. An approximation of the forces is therefore obtained by use of an experimental stand which is used to measure the forces caused by water flow through different components. The results from this experimental stand can be used as an input to the dynamic error budgeting model in order to determine the stage position error by the measured forces.

4.2 Direct disturbance forces in the Mapper machine

The Mapper closed-circuit cooling system consist of a pressure regulated pump providing flow for cooling of five different subsystems. Each subsystem is given an error budget of 0.35 nm, resulting in a total DDF error budget of 0.783 nm. All the components are

offered a specified (turbulent) flow at a constant pressure. The flow is provided to the components by flexible, vacuum-proof tubing constructed such that a minimal amount of stiffness is added parallel to the vibration isolation system.

4.3 Determining the DDF by the cooling system

In this section first an introduction on the used experimental stand is given and its performance is discussed. Next the components to be characterized by the setup are described. An overview of the properties of the test setup is given in Appendix C.

4.3.1 The experimental stand

Concept. An experimental stand is created to characterize forces caused by flow of water through a mounted geometry. The basic idea of the test setup, called *Vibronix*, is to mount a component provided with water cooling on a very compliant suspension and measure its resulting accelerations. By knowing the mass participating in the acceleration, the forces can be related to the measured accelerations via $F = ma$.

The compliant suspension is created by a two-stage passive vibration isolation system. First the component is mounted on a plate (isolated load) which is suspended from lightweight flexible pendulums (stage 1). The pendulums hang in a closed frame which is mounted on a heavy granite table. This heavy granite table is mounted on low stiffness air mounts which are connected to the floor (stage 2). This concept and the realized test setup are shown in figure 4.1.

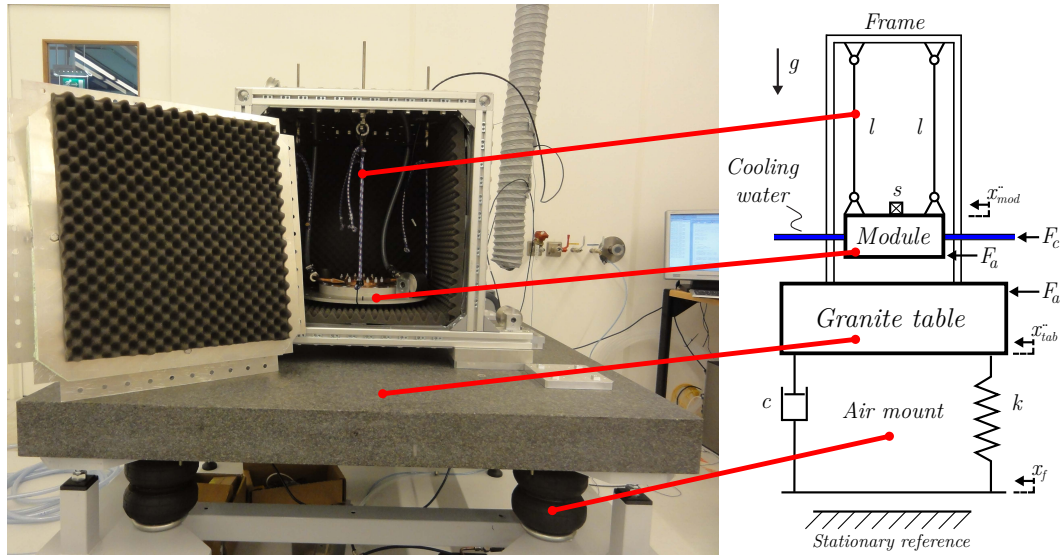


Figure 4.1: The realized and concept version of the experimental stand used to determine forces resulting from water flowing through the mounted component in the setup. The test setup is able to measure accelerations of $3 * 10^{-7}(m/s^2)/\sqrt{Hz}$ in the 20-100 Hz frequency range.

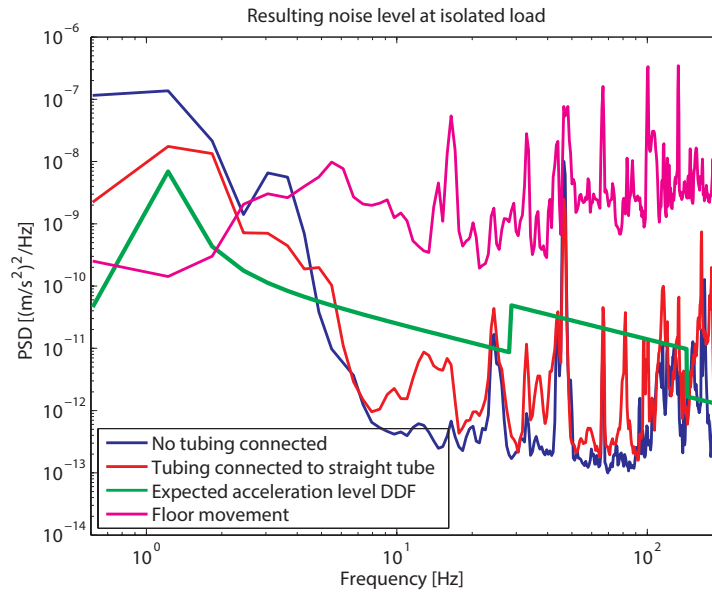


Figure 4.2: The resulting PSD at the isolated load. The blue line indicates the performance when no component is mounted on the isolated load. The red line indicates the performance when the straight tube is mounted and connected by tubing. The green line indicates the expected PSD of DDF allowed to stay within the error budget. The magenta line shows the floor vibration level. The measurements are performed in horizontal direction with the box frame closed.

Modelling. The viability of the concept is determined by the use of a dynamic error budgeting model, as described in section C.1. The setup is modelled as a three-body spring-mass-damper. The disturbances acting on this system are floor vibrations and the expected DDF caused by water flow through a component. As discussed in chapter 3, the largest direct disturbance forces are expected at higher frequencies. Therefore an arbitrary DDF spectrum $PSD_F[N^2/Hz]$ is specified which complies to the DDF error budget having the largest forces in the 30-140 Hz range. The parameters of the model are set by maximizing the expected accelerations of the isolated load by the DDF in respect to the interfering floor disturbances. Furthermore, the resulting acceleration level is compared with the noise properties of several acceleration sensors and noise by analog-to-digital conversion in order to determine the signal-to-noise ratio when measuring the accelerations in practice. The properties of the setup components such as the sensor, DAQ card, weight of the isolated load and stiffness and damping of the suspension.

Construction. Next to the floor vibrations, acoustic disturbances acting directly on the isolated load and internal dynamics can interfere with the results. In order to avoid acoustic disturbance of the isolated load, the isolated load hangs in a tightly sealed closed box frame. The double walled side plates of the frame consist of a sandwich of PUR foam, aluminum plate and extrusion profile. The PUR foam provides damping of the acoustic disturbances and damps any unaccounted structural resonances. Additionally,

Component	Weight [gr.]
Real AA	7439
Dummy AA	6466
Rectangular component	6100
Straight tube	4722
Tubing connected	4397
No component	4296

Table 4.1: Weight of the isolated load with indicated component mounted

acoustic egg-crate foam is added to the inside of the frame. In the mechanical design of the test setup special care has been taken that no internal dynamics show up below 200 Hz. The structural dynamics are evaluated by the use of finite element analysis.

To measure the accelerations of the isolated load, use has been made of an Endevco[®] model 86 piezoelectric accelerometer. This sensor is selected due to the claimed very low noise properties, having the best available noise properties in a measurement range from 1 to 100 Hz. Furthermore, this sensor was already available at Mapper Lithography. The model 86 has a voltage sensitivity of 10 V/g and a residual spectral noise of about $1 \cdot 10^{-7} (m/s^2)/\sqrt{Hz}$ at 10 Hz and $4 \cdot 10^{-8} (m/s^2)/\sqrt{Hz}$ at 100 Hz [30]. The sensor has its first eigenfrequency at 215 Hz which limits the accurate measurement range to about 100 Hz. The sensor signal is measured and logged by use of a National Instruments 4472 series, NI PCI-4472B data acquisition card [31].

Performance. The performance of the setup is shown in figure 4.2. The setup shows a minimum noise level of about $1 \cdot 10^{-13} (m/s^2)^2/Hz$ at 70 Hz. It is suspected that the minimum is set by the noise properties of the used Endevco[®] sensors being less good than specified. The PSD of the floor accelerations, figure 4.2, has some clear peaks at distinct frequencies which also show in the movement of the isolated load. A strong noise peak shows around 50 Hz. In figure 4.2, the resulting PSD at the isolated load due to the expected DDF spectrum PSD_F is shown in green. Except for some narrow peaks at distinct frequencies, the setup performance is situated well below this level. This shows that the setup is able to measure forces in the frequency range from 20 to 100 Hz which are smaller than required by the force error budget. It indicates that the setup is applicable for the intended measurements.

4.3.2 The investigated components

The components tested in the setup are shown in figure C.2 in Appendix C. The experimental stand is focused around the characterization of one of the main components of one of the cooled subsystems, the *Aperture Array* (AA). In the Mapper machine, the AA requires the largest flow of cooling water. In order to maintain a correct temperature, the AA requires a flow of 13,6 L/min at a pressure of 3 bars. The design of the cooling

circuit inside the AA incorporates a diverging tube connector, 10 separate 1 mm tubes followed by a merging tube connector. Both tube connectors are followed by 90 degree bends. The AA can be connected to the providing circuit by the use of Swagelok[®] connectors.

In order to obtain a good indication of the results the behaviour of three other components is also investigated. The results of these components are used for comparison and indicate how changes in the tested component influence the resulting force spectrum. By mounting (almost) no geometry between the connecting tubes, the minimal noise level by the flow can be determined being a reference for mounting any other geometry in between. Since the forces are related to the accelerations via $F = ma$ the weight of the components is an important factor in the interpretation of the results. The weight of the isolated load of the setup with the respective components mounted is shown in table 4.1.

4.4 Resulting direct disturbance forces

This section discusses the scenarios used to characterize the described components. Next the measurement results of the different components in the different scenarios are shown.

4.4.1 Measurement scenarios

The components are tested in two different scenarios.

In the first scenario the components are tested under different flow levels. The rectangular component, dummy AA, straight tube and real AA, figure C.2, are investigated by this scenario. The flow to the setup is provided by a pump which is similar to the one used to supply the Mapper machine. The closed-circuit pump is connected to the inlet and outlet of the setup by use of 2×15 meters of flexible tubing.

In the second scenario the setup is tested under a single flow level while using the actual pump used to supply the Mapper machine. The pump supplied a flow of 6.4 L/min with a pressure of 3.98 bar at the output of the pump. The straight tube and real AA are investigated in this scenario. Furthermore the flexible tubing was connected to the isolated plate without mounting a component in between, figure C.2. The pump is connected to the inlet and outlet of the setup by use of 2×40 meters of flexible tubing. For practical reasons only a limited amount of tests could be performed in this scenario.

In both scenarios a pump is used to supply the flow to the setup. It is decided to use a pump to create similar flow conditions at the inlet of the setup as expected in the Mapper machine. Since the goal is to obtain an indication of the occurring DDF as to be expected in the Mapper machine, the use of a representative pump is more similar to the actual situation. It is expected to give a better indication of the DDF occurring in the Mapper machine.

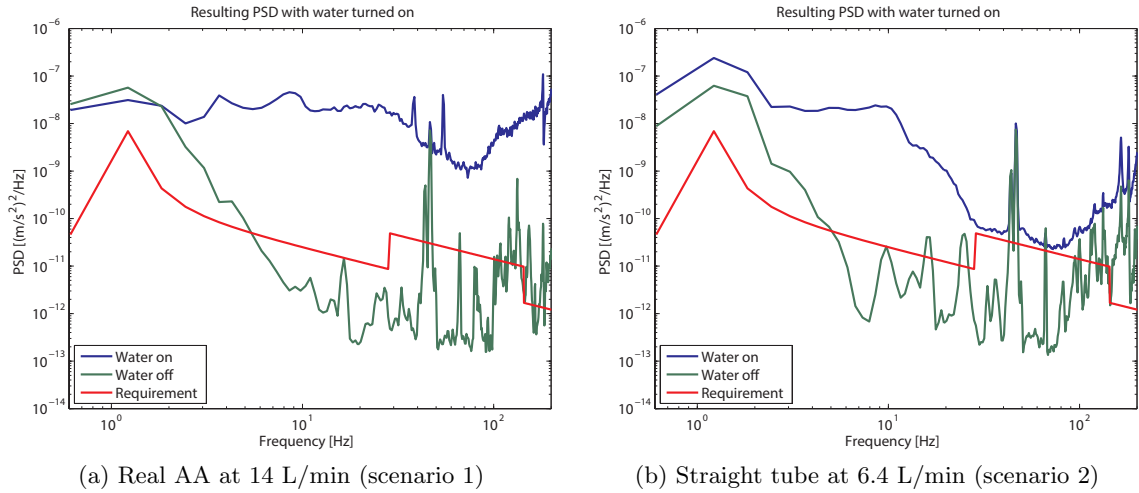


Figure 4.3: Example of resulting PSDs over the 0.6-200 Hz range when offering a specified flow to the mounted component

4.4.2 Measurement results

The results of scenario 1 and 2 are shown in figure 4.4 to 4.7. The results of the scenarios are shown in two types of plots; a PSD with units $[N^2/Hz]$ (force PSD) and a CAS $[m]$.

Force PSD. The force PSDs are created by multiplying the accelerations in the 20-100 Hz range with the weight of the isolated load as indicated in table 4.1. The bottom green line always shows the PSD at the isolated load before the pump was switched on, being the noise floor for the set of measurements. The sharp-edged requirement line shows the expected force PSD PSD_F which complies to the entire(!) error budget by DDF of the Mapper machine. The legend to these plots is given in their corresponding CAS. All shown measurement results are performed in the horizontal direction. Each line is an average of at least 10 repeated measurements.

CAS. The CAS shows the resulting error when the acquired force PSDs are used as input to the DEB model as described in chapter 3. The measured force PSDs are effectively 'weighted' by the transfer function T_{DDF} from equation 3.19. This results the expected error if the measured forces would be acting in the Mapper machine. The entire error budget for DDF in the Mapper machine is set to 0.783 nm. The arbitrary force spectrum adds in 0.32 nm of error in the 20-100 Hz range. As stated, all errors are given in $3\text{-}\sigma$ values.

An indication of the change in the PSD when supplying a flow is shown in figure 4.3. Both subfigures show a significant increase of the PSD when a flow is provided to the tested component. Again the sharp-edged red line shows the expected PSD resulting from PSD_F which complies to the entire error budget by DDF of the Mapper machine. The figure shows that, with the water turned on, the lower bound of the effective measurement range is set by the effect of resonances of the compliant components while the upper bound is set by the first eigenfrequency of the sensor causing an increase of the sensor transfer function from about 100 Hz. As discussed the effective measurement range is therefore limited from 20-100 Hz. Further results are therefore only plotted over this frequency range.

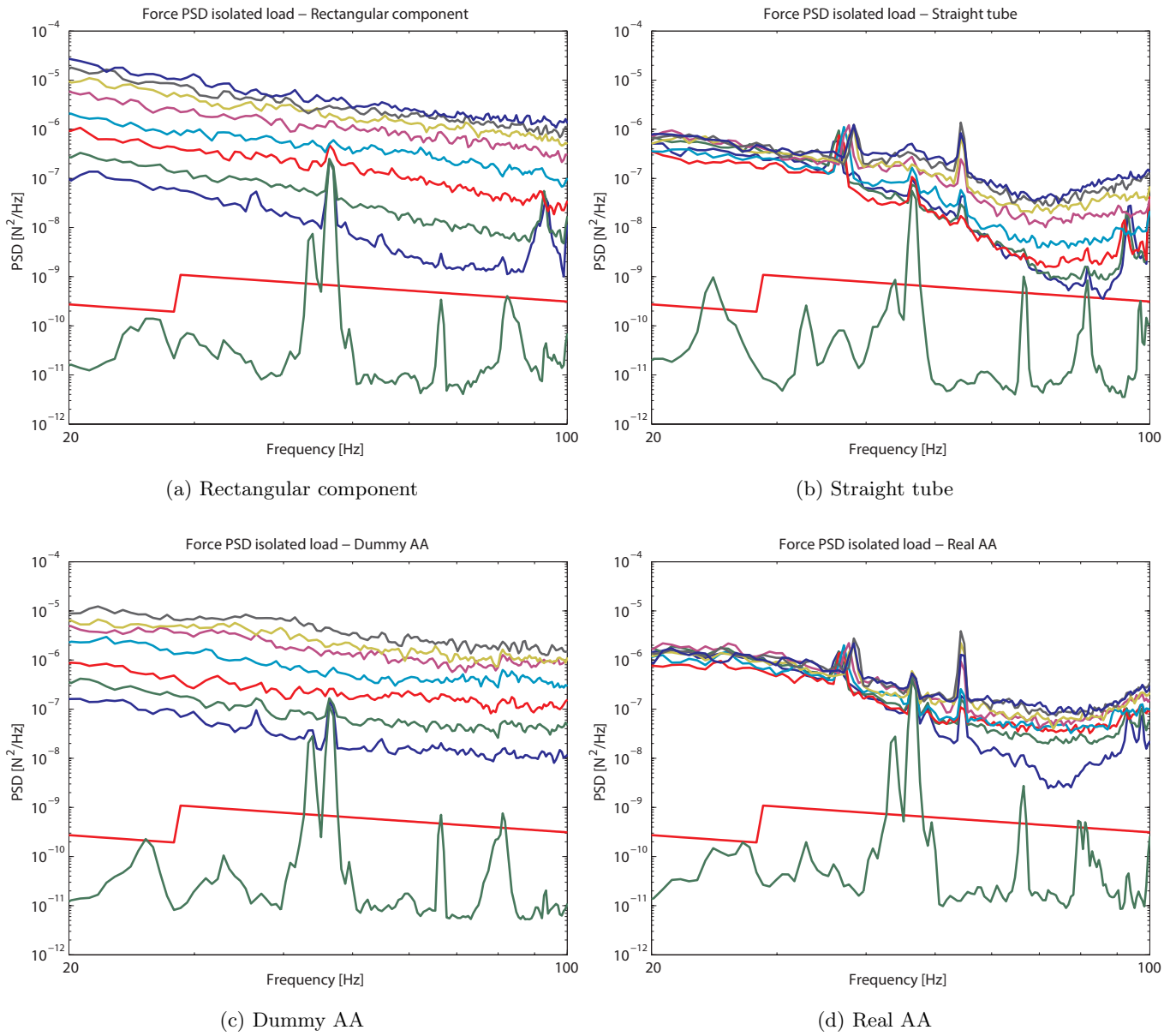


Figure 4.4: Results of scenario 1 - variation of the flow. Force PSD's in the 20-100 Hz range. The legend to the lines is given in the corresponding results in figure 4.5.

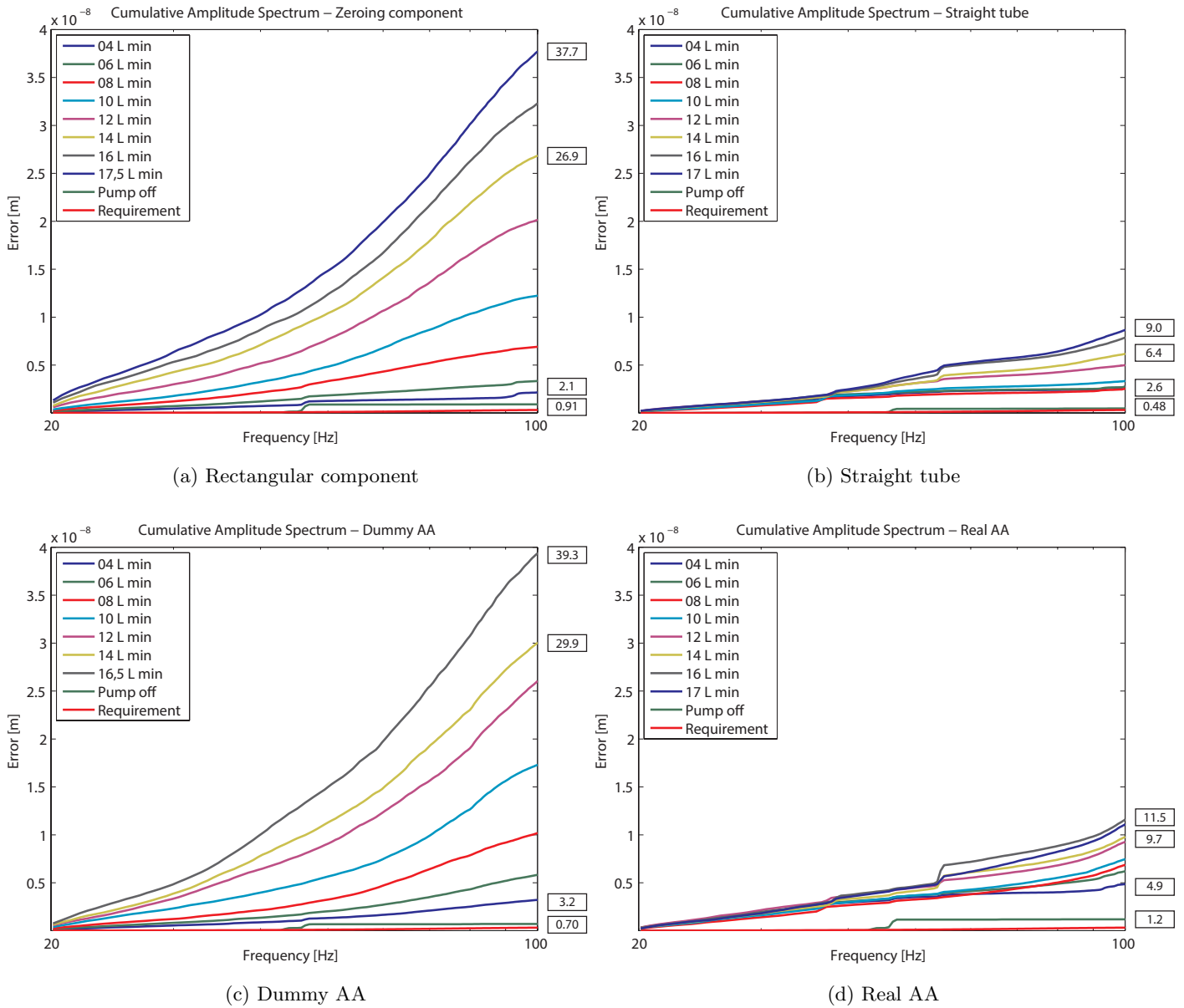
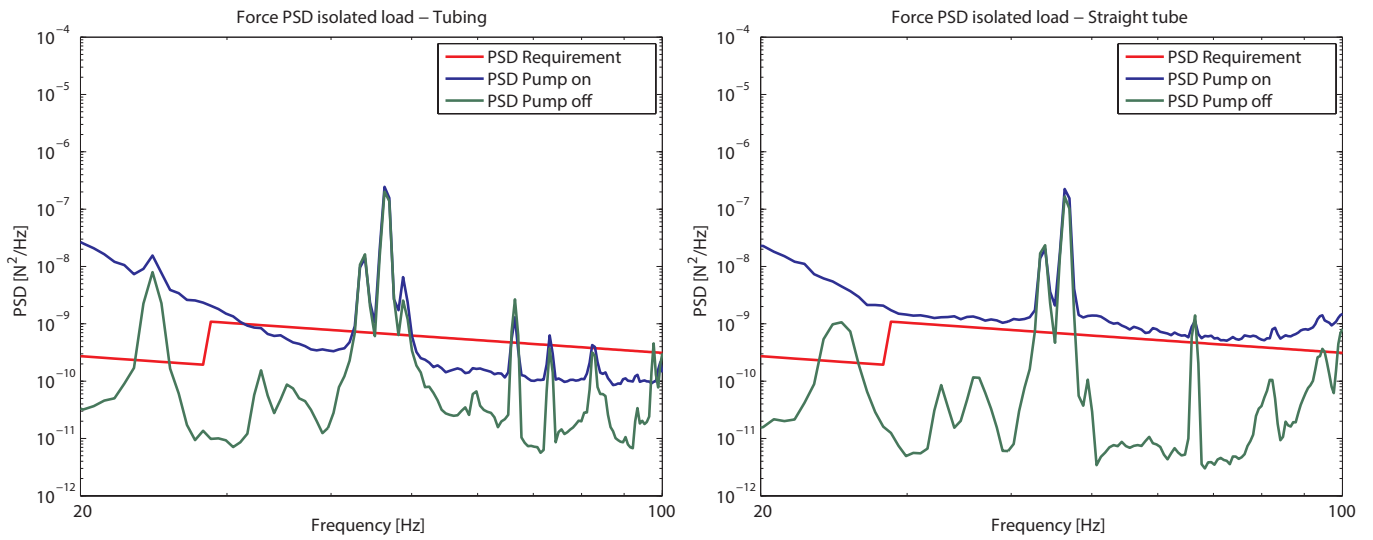
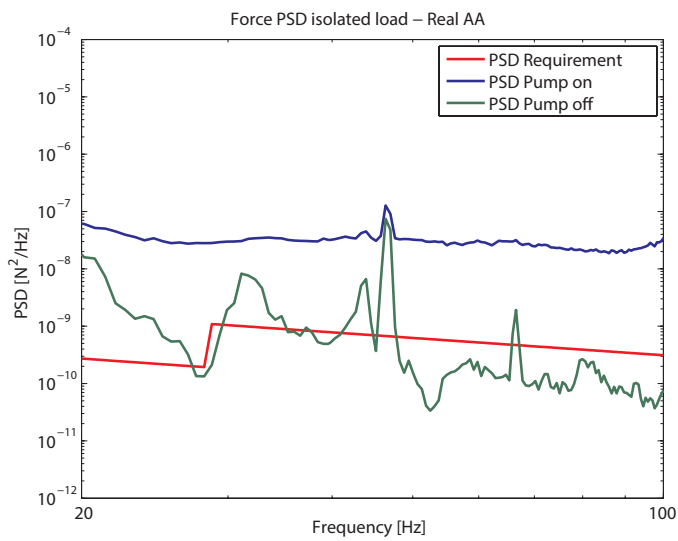


Figure 4.5: Results of scenario 1 - variation of the flow. Weighted PSD's in the 20-100 Hz range. Resulting error by the measured PSD's weighted by T_{DDF} . The indicated errors [nm] are, from bottom to top, the results when inputting the PSD from; pump off, 04 L/min (minimum flow), 14 L/min and the maximum attained flow level. The error by the in-spec forces in the error band is 0.32 nm while the budget for the entire machine is 0.783 nm.



(a) Tubing connected to plate

(b) Straight tube



(c) Real AA

Figure 4.6: Results of scenario 2 - Constant flow. Force PSD's in the 20-100 Hz range.

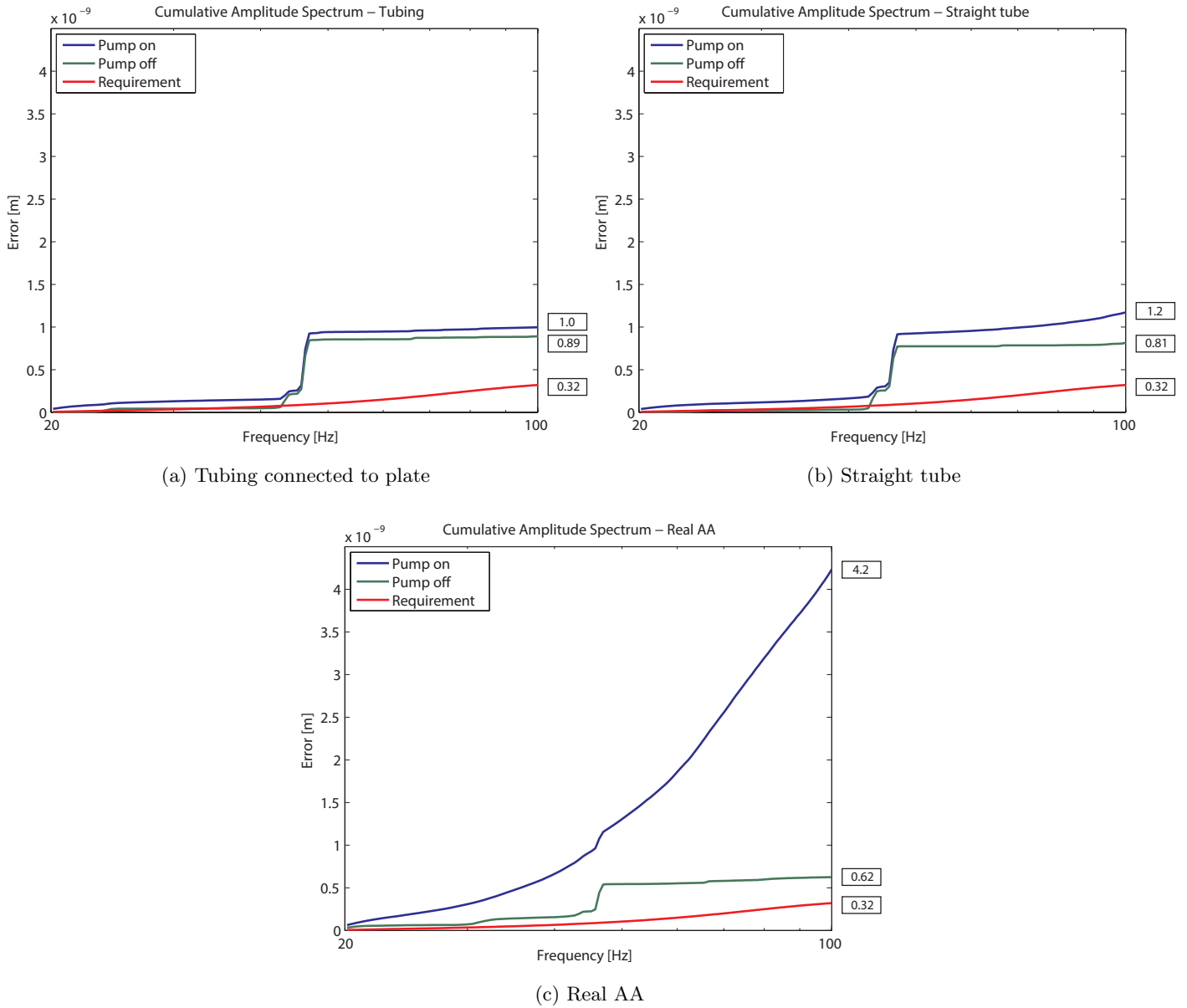


Figure 4.7: Results of scenario 2 - Constant flow. Weighted PSD's in the 20-100 Hz range. Resulting error by the measured PSD's weighted by T_{DDF} . The error by the in-spec forces in the error band is 0.32 nm while the budget for the entire machine is 0.783 nm.

4.4.3 Discussion of the measurement results

Overall. All results show forces which are larger than allowed by the available error budget. In both scenarios, offering a minimal flow or mounting a component with minimal geometry results in forces and errors which are still larger than the budget. It is important to note that the budget for all the DDF acting in the Mapper machine is 0.783 nm while the large resulting errors only come from single components.

When comparing scenario 1 and 2, it can be noted that the differences in the flow conditions (used pump and length of input tubing) also influence the resulting forces. The response in scenario 2, when using the real pump and very long entrance tubing, overall result in smaller forces especially in the range below 60 Hz. Disturbances caused by the pump are damped out by the increased length of the tubing while the entrance pressure at the component is reduced. It can be concluded that, next to the geometry of the tested component, the resulting forces are determined by the conditions under which the flow is provided.

The distinct contribution in the PSDs between 40 and 50 Hz causes that the measurements with the pump turned off (bottom green line) often result in an error larger than the stated budget. When the distinct contribution is filtered from the pump off measurement, the resulting error commonly stays well below the error budget.

Scenario 1. The results of scenario 1 are shown in figure 4.4 and 4.5. To compare the results, the rectangular component acts as a reference for the dummy AA while the straight tube acts as a reference for the real AA. When looking at these plots it can be seen that figure 4.4a and 4.4c look much different from figure 4.4b and 4.4d. Both the rectangular component as well as the dummy AA have a response which clearly varies under the amount of flow but is rather level and gradual. It is suspected that the response is dominated by the t-shaped connectors incorporated in the design. It is known that these often result high levels of vibrations due to the abrupt change of the flow direction. The straight tube and more specifically the real AA have a far more constant response which varies little under flow especially below 35 Hz. Also some clear resonance peaks show up especially around 55 Hz which can not be directly related to mechanical or floor vibrations. What also stands out is that both the dummy AA as well as the real AA seem to have a larger force input at higher frequency in respect to the references. This is suspected to be caused by the smaller features in the components which results in high frequency vibrations.

The influence of the higher input at higher frequencies becomes more evident when the measured force PSDs are weighted with the DDF transfer function T_{DDF} . As discussed this transfer function has a higher amplitude at higher frequencies. Therefore, although the plots of the references seem quite similar, the high frequency vibrations cause a larger error with the dummy AA and real AA.

Scenario 2. All the forces measured in scenario 2 are smaller than the forces measured in scenario 1. The effect of using a different pump and using 40 meters of flexible tubing before entering the setup have a beneficial effect on the resulting force level. Due to the accurate control on the output pressure of the pump and the long length of flexible tubing, the contribution by the pump in scenario 2 is considered to be minimal. The forces measured with the tubing connected to the isolated load, figure 4.6a, the PSD even approaches the PSD with the pump turned off. When subtracting the resulting errors in this situation, the resulting error of $\sqrt{1.0^2 - 0.89^2} = 0.46nm$ is however still above the set budget. Mounting the straight tube result a force PSD with a similar spectral distribution to mounting the tubing but scales the magnitude with a factor 10. In respect to scenario 1 no distinct resonance peaks show up. The real AA resulted in a very constant force response over the specified measurement range. The absence of clear resonance peaks also makes that the flow-induced forces seems to have an input similar to that of white noise. Unfortunately, the floor vibrations are higher during this measurement due to constructional activities nearby the building were the measurements are performed. The spectral distribution and magnitude of the resulting PSD when testing the real AA is significantly different from that of testing the tubing or straight tube. The difference is most probably caused by the difference in geometry of the mounted component. Since the conditions on the flow are constant, this is an indication that the appearance of higher forces is related to the change in the tested geometry. Also in this scenario, the resulting error by the measured forces is higher than allowed by the budget.

4.5 Conclusion

A test setup is created which is able to determine accelerations with a minimum of $3 * 10^{-7}(m/s^2)/\sqrt{Hz}$ in the frequency band of 20-100 Hz. This setup is used to determine occurring accelerations when offering a flow to a component mounted. Several components are tested in two different scenarios in which the set flow, used pump and tubing length before entering and exiting the setup are different. The measured accelerations are related to forces by $F = ma$ which gives a PSD of the forces in the frequency band. This force PSD is weighted by the transfer function for DDF which resulted from the DEB model of chapter 3, stating the resulting error when the measured force would be acting on the Mapper machine. The results show that the geometry of the mounted component does influence the resulting level of forces. In both scenarios, the resulting errors by the determined force PSDs exceed the DDF error budget set for the entire Mapper machine.

"The fewer the facts, the stronger the opinion"

ARNOLD H. GLASGOW

Chapter 5

Discussion

5.1 Introduction

In this chapter the contents and results of the previous chapters are evaluated. The relation of the different results to the goal of the thesis is discussed. The results are related to the research goals derived from the main challenge of the thesis. The validity and accurateness of the different models and methods is evaluated to determine the representativeness of the research for the performance of the system realized in practice.

5.2 Evaluation of the realized research goals

In Chapter 1 the main challenge of the thesis is defined and four research goals are defined. Each of the previous chapters has addressed one of the research goals. The following section discusses how each of the goals has been answered and evaluates the obtained result.

5.2.1 Vibration isolation

Determine the design properties of vibration isolation systems. Investigate the current state-of-the-art of vibration isolation systems as discussed in literature and compare the design of the Mapper vibration isolation system.

In Chapter 2 and Appendix A the design properties of vibration isolation systems is discussed. Vibration isolation systems are divided into two categories; active and passive isolation systems. Passive systems make use of horizontal and vertical isolators combined with a damping mechanism to attenuate the natural frequency. Active systems use actuators and sensors placed in a specific configuration and using a selected control strategy to overcome the limitations of the used passive components. Passive systems commonly make use of pendulums and air springs while active system commonly make use of geophones and Lorentz actuators.

The Mapper vibration isolation consists out of two sections; a passive vibration isolation isolating the electron optics and a positioning stage which aligns a wafer with the isolated electron optics. The addition of the positioning stage aligning to the isolated load is an important difference in respect to system designs discussed in literature. By expressing the performance of the system by the resulting error in alignment between the isolated load and the stage instead of the resulting motion of the isolated load, very different spectral transfer functions for the disturbance sources result. This changes the importance of the different design parameters. The evaluated literature contains no examples of isolation loads being used as a reference for a second system and the disturbance transfer function is only expressed by the resulting transmissibility. Also the presence of both floor vibrations and direct disturbance forces is an important difference; almost all systems discussed in literature are focussed on the suppression of floor vibrations.

The requirement on the suppression of floor vibrations makes that a suspension with a low natural frequency is required in horizontal direction. The addition of active components to improve the suppression of low frequency floor vibration is considered unnecessary due to the addition of the positioning stage. It would add additional complexity and costs and take more space while the low frequency vibrations of the MOF are well suppressed by the positioning stage. Due to the different natural frequencies for horizontal and vertical isolation, the system in practice is sensitive for parasitic stiffness and crosstalk. This increases the importance of minimizing crosstalk.

5.2.2 Dynamic error budgeting

Determine the influence of the design properties on the performance of the Mapper vibration isolation system. Create a model to predict the performance of the system when changing the parameters of the system.

In Chapter 3 a dynamic error budgeting model is created to analyse the properties of the Mapper vibration isolation system. This model is created to investigate the performance and influence of the different parameters of the Mapper vibration isolation system. The disturbances are modelled by representative power spectral densities. The system parameters vary the transfer functions which attenuate the disturbances. The resulting power spectral density are analysed by transformation to cumulative amplitude and cumulative power spectra.

The investigation of the influence of the different parameters indicated that the performance of the system is strongly dependent on the acting direct disturbance forces. According to the model, only minimal direct disturbance forces are allowed while rough estimations show that much larger forces are to be expected. Therefore the uncertainty on the direct disturbance forces can be considered the limiting factor for characterizing and further improving the system performance. In order to improve the system performance the direct disturbance forces are to be characterized.

Several remarks can be made regarding the used methods and the results of the dynamic error budgeting.

First of all it is questionable if the model is still representative for considering results in (sub-)nanometre range. In order to obtain an alignment error of 1 nanometre in practice every parameter has to be tuned correctly and every disturbance has to be accounted for. The dynamic error budgeting model consists of idealized estimations of the real system behaviour which have a limited accuracy. To ensure the representativeness of the model, every parameter of the model should be therefore always be augmented with solid experimental data either from test setups or the realized system. This way the discrepancy between the modelled and actual forces caused by water flow could have been identified earlier. For mechatronic systems, reality is always less ideal than the idealized model.

The research from the start is mostly focused on vibration isolation systems. The variation of the parameters of the model is therefore mainly focused on investigating the effect of changing the parameters of the vibration isolation system rather than those of positioning stage. By treating the parameters of the positioning stage during the study as a given has left its influence on the performance of the system underexposed. However, the variation and possible optimization of the theoretic model of the system could have been a full study at its own. The determination of the direct disturbance forces was however considered a more valuable and useful contribution to determining and improving the Mapper system performance. In practice the resulting sensitivity of the controller is dependent on having correct controller settings. Any improvement of the controller which results in an improvement of the performance is beneficial so good care should be taken with realizing the stage controller.

With modelling, as always, it should be remembered that 'in theory, practice and theory are the same, but in practice they are not' (Einstein).

5.2.3 Determining direct disturbance forces

Characterize the performance limiting factors. Make a detailed analysis of the properties of the limiting factor.

In Chapter 4 the direct disturbance forces which were identified as the performance limiting factor have been characterized. The main source of direct disturbance forces is the use of water cooling system used to cool components mounted on the isolated load. The direct disturbance forces caused by the flow of water through a component are characterized by the use of an experimental test setup. The test setup is first focused on characterizing the forces caused by the Aperture Array. Three other components are also tested in order to compare the different results. The components are tested in two different scenarios. The scenarios differed in the used length of entrance tubing, pump and set flow. The results showed that the results are influenced by the provided flow and the geometry of the component under investigation. In both scenarios the resulting

forces are significantly higher than the specified requirement.

Due to its experimental nature, the study on the direct disturbance forces holds its limitations. Remarks can be made on several parts of this study. First of all, the experimental setup does only measure in a single degree of freedom. Therefore the measured forces are only an approximation of the total forces caused by the water flow. An extension of the setup to measuring in 6 DOF is however currently not possible due to the limited volume inside the closed frame and the limited space on the plate on which the components are mounted. This size limitation also limits which components can be tested. Another issue concerns the connection of the component to the tubing. To prevent the tubing to interfere with pendulums or the sides of the closed frame, the routing of the tubing differs per component, changing the directional stiffness of the setup. Furthermore the vibration or whip of the tubing also contributes to the resulting vibrations. Although this influence is only limited, as determined by mounting the 'straight tube' component, it would be better to have an equal connection of the tubing to the component mounted in the setup. Challenge for this connector would be to provide a flow while preventing transmission of external non-flow related disturbances to the isolated load and also preventing transmission of forces by vibration of the connecting tubing itself.

Overall the characterization of the flow-induced forces by the use of a test setup needs a more structured approach. A more structured approach is necessary to identify the influence of the three main factors determining the resulting forces; the used pump, the flow conditions (e.g. flow and pressure) and the geometry of the component. Although some of these factors are connected, such as pressure drop over a certain geometry, a more separated approach can result in better understanding of what causes the largest contribution to the forces. For example flow could be provided by use of a pressure vessel instead of a pump to cut out the contribution of the pump to the current results. The approach used in the current study however is sufficient to obtain a first indication of the forces in acting in the real system which uses a similar pump, tubing and components. The study provided the information necessary at this moment which could be performed in the time available.

5.3 Conclusions

It can be concluded that each part of the research has tried to address a subgoal derived from the main challenge. Each part of the research left room for different improvements. Based on this discussion of the result, conclusions and recommendations are given in the following chapter.

*"The whole is more than the sum of
the parts"*

ARISTOTLE
Metaphysica

Chapter 6

Conclusions

This chapter provides the conclusions and recommendations based on the performed research. The main challenge set at the start of the research is evaluated. Recommendations are given for the possible continuation of the research and the design of the Mapper system.

6.1 Introduction

The definition of the main challenge marked the start of this report. The main challenge is defined as:

Reduce the error in alignment between the electron optics and the wafer caused by the disturbances acting on the vibration isolation system to 1 nm 3- σ RMS.

Based on the derived research goals, the work performed sought to answer and contribute to this challenge. The evaluation of the work resulted in a set of conclusions and recommendations which are discussed next.

6.2 Conclusions

The main challenge is separated into four different research goals. From the first research goal an overview of vibration isolation systems resulted. The study on vibration isolation systems provides a solid overview into their relevant properties and parameters. It provides an important framework for identifying the problem of achieving the challenge by analysis of vibration isolation systems discussed in literature. This information showed to be essential for correct assessment of the further results during the study.

The second research goals resulted in an analysis of the Mapper system by use of a dynamic error budgeting model. Dynamic error budgeting has shown to be a very effective tool to identify the influence of different parameters on the performance of the

mechatronic system. The study on the influence of the different parameters helped to identify the parameters to further characterize and improve in order to meet the set challenge.

The analysis showed that in order to be able to correctly improve the Mapper system a better indication of the acting direct disturbance forces is to be acquired. Without a correct approximation of the acting force disturbances no realistic prediction of the system performance can be obtained. The acting disturbances determine the necessary attenuation of the system and thereby sets the requirement for the different parameters. The determination of the direct disturbance forces therefore answers to the third research goal. The largest forces acting on the vibration isolation system arise from the use of a water cooling system. A test setup, called Vibronix, is created to measure forces caused by the water cooling of components. The setup measures the accelerations resulting from supplying a flow to a component which is mounted on an isolated load. By assumption of a fully decoupled mass undergoing rigid body motion, the forces are determined by $F = ma$ over a limited frequency band. By using the resulting forces as input to the dynamic error budgeting model the effect on the performance, error e , of the system is determined.

After verification of its performance, the setup is first used to characterize the forces caused by the Aperature Array, the largest consumer of cooling water. Also three other components are characterized to compare the results for different geometries. The components are tested in two different scenarios. The results show a relation between the geometry of the component and the resulting forces. Most importantly the results show forces much higher than stated by the current requirement resulting in an error e much larger than budgeted for. The experimental research with the test setup is not conclusive in covering all the aspects related to the influence of using water cooled components on an isolated load. The obtained results however provide a first indication of the direct disturbance forces to be expected and offer a first reliable indication of the influence of the actual forces on the performance of the Mapper system.

The fourth research goal is fulfilled with the discussion the research answering the research goals and the recommendations for meeting the challenge. The discussion of the results showed that each method and tool used during the research has its own limitations and room for improvement. Main remarks are the underexposed influence of the stage controller in the dynamic error budgeting model and desire of a more structured approach to determining the individual contributions to the flow-induced forces. This reflection is important to determine where the current deficiencies are and how the research can be improved.

The research provides the following conclusions to the main challenge;

- Dynamic error budgeting is an essential tool for assessing the performance of a mechatronic system.

- The limiting factor for predicting and improving the system performance are the unknown direct disturbance forces.
- The results from the Vibronix setup show that the forces to be expected are significantly larger than the available budget.
- The main challenge can only be met if a solution is found for suppressing or eliminating the flow-induced forces.

6.3 Recommendations

With the conclusion of the main challenge and the respective research goals, recommendations can be done for possible solutions and further research. The recommendations are divided in two sections; continuation of the research and design recommendations.

6.3.1 Continuation

Any continuation of the research should first center around the further characterization of the flow-induced forces. A well structured research plan should be formulated to create a good step-by-step understanding of the flow-induced forces. It is advised to separately investigate the contribution of; the pump, the flow conditions at input of the component and the geometry of the component. The influence of the pump can be excluded from the measurements by letting the flow be provided by the use of a water tower or pressurized water tank. Due to the relatively high pressure required, the use of a pressurized water tank is advised. The influence of geometry can be characterized by starting with a basic component and incrementally make small adjustments to its geometry. It should be tried to backup and verify the results from these measurement by simple numerical calculations.

However, since literature provides only little information on determining forces caused by water flow through an arbitrary geometry, the research is primarily to be founded upon experimental measurements by use of a test setup. Vibronix currently limits the size of the components to be characterized and measures only in 1 DOF. An upgrade or redesign of Vibronix is therefore advised preferably incorporating 6 DOF measurement and making it suitable for characterization of all separate water cooled components of the Mapper system.

A goal for the continued research should be to devise a design rule by which an estimation of the resulting forces can be made for supplying a specified flow to a specified geometry. This would provide designers a tool to assess the flow-induced forces during the design phase of a component, enabling him to compare and minimize the resulting forces for different design concepts. This tackles the problem, as it should, during the design instead of only measuring the force resulting from a component after it has been realized. Furthermore, it is recommended to determine the effect of the flow-induced forces on the actual Mapper system when completed. This in order to verify the results from this

study and to determine if the system meets the desired performance and requirements when having the cooling system switched on.

6.3.2 Design recommendations

Also recommendations can be done for improvement of the current and future design of the Mapper system. The Mapper system is divided in two sections for which different recommendations can be done.

Only little attention has been spent on possible improvement of the positioning stage performance. It is therefore recommended that further research is performed on the possibilities of improving the stage performance. The feasibility and performance gain by adding additional control functions should be investigated.

Due to the magnitude of the measured direct disturbance forces, in the future it might be necessary to redesign the vibration isolation system. Although this currently is for later concern, the future design should be better capable of suppressing direct disturbance forces. The use of a passive vibration isolation system is advised. The compliancy to accelerations of a passive system can be improved without compromising the transmissibility by proportionally increasing the mass of the isolated load and the suspension stiffness. For a redesign it is advised to use the provided literature survey as a guideline to creating design concepts.

Based on the Vibronix measurements, the following simple design rules can already be formulated to minimize flow-induced forces from a cooled component:

- Prevent abrupt changes in the tubing diameter
- Prevent the use of abrupt turns (eg. 90 degree turns) in components
- Minimize the required amount of flow

The results have also shown the importance of verifying if a concept or design complies to its requirements. Before the execution of this study, the use of water cooling had already been decided upon and all of the necessary designs and components were in advanced design state with final designs being materialized. During the design the set requirement on the allowed interface forces for meeting the stated error budget was however neglected. None of the realized designs were checked on meeting the imposed interface requirement. This resulted that the effect of the actual occurring flow-induced forces has long been overlooked. If a requirement or budget is stated but no verification is performed to check if a design meets the set requirement, stating the requirement is pointless. It should always be verified if a design meets its requirements. The verification should be performed in the concept phase of the design rather than with a finished product to prevent production of products unfit for use. Although this approach will take more time during the design, it will prove to be more cost-effective and time-effective overall.

Appendix A

Vibration isolation system review

A.1 Introduction

In this appendix an overview is provided of the relevant parameters and components used in the design of vibration isolation systems. The overview is based on an extensive literature survey into vibration isolation systems. Several overviews of the properties of vibration isolation systems exist but are lengthy. The goal of this study is to give a compact but complete overview of this field. Therefore comprehensive algebraic analysis of the components or further details are often left out but can always be found in the related citations. Very complete and often used references are the works of Zuo [32], Ibrahim [33] and Winterflood [14] on passive isolators, van Eijk [25] on active systems and van der Poel [34] on active hard-mount systems.

This study divides vibration isolation systems in two categories; passive and active systems. For passive systems we discuss horizontal isolators, vertical isolators and damping. For the active systems we discuss sensors, actuators and the isolation strategy and control. The focus for the sensors is on geophones and accelerometers while the focus for actuators is on electromagnetic and piezoelectric actuators.

A.2 Passive vibration isolation systems

Passive systems solemnly make use of passive components like springs and dampers. Both spring and damper act on relative motion between the payload and the ground. The system design is subdivided in vertical and horizontal isolators. Vertical isolators must support the weight of the payload against gravitational force and so generally store large amounts of energy. Horizontal isolators overall store much less energy but often need careful alignment.

A.2.1 Vertical isolators

To obtain a low natural frequency to the vibration isolation system a low stiffness suspension is necessary. Since the spring must support the payload's mass, the use of a

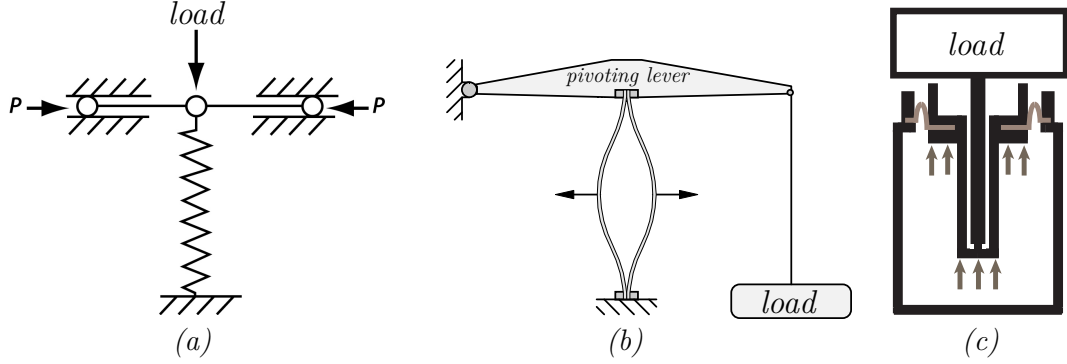


Figure A.1: Three different types of vertical isolators; a non-linear stiffness mechanism (a) from [35, 36], a constrained Euler column (b) from [14] and a Gimbal pneumatic isolator (c) from [12, 37]

conventional linear spring results in large static sag. The static sag of a linear spring is defined by $\Delta_g = g/(4 * \pi^2 f_n^2)$ so in order to obtain a natural frequency of 1 Hz a static sag of 0,248m results. This is not acceptable for most applications. Therefore other means are used to obtain a low natural frequency of the system. The most common means to attain a very low natural frequency (<2 Hz) in vertical isolators are the use of pneumatic springs, post-buckled beams or by employing non-linear stiffness mechanisms. For higher natural frequencies conventional metal or rubber springs often suffice.

Non-linear stiffness mechanisms are often obtained by employing elements with negative stiffness. Positive stiffness occurs when the deformation of the spring is in the same direction as the applied force, corresponding to a restoring force that returns the spring to its neutral position. For negative stiffness this directional relationship between force and displacement of a spring is reversed. Instead of opposing the deformation, a negative spring assists the imposed deformation. Since the deformation is assisted, energy is added to the system. This is possible by preload of the element or by using an energy supply. Furthermore, a system with only negative stiffness is in unstable equilibrium since any disturbance is assisted in moving away from the equilibrium. The negative stiffness is therefore compensated by positive springs in order to attain a net zero stiffness around the working point of the vibration isolation system. Non-linear stiffness mechanisms for vibration isolation using negative stiffness have been reported by Platus [35, 36] and Carella [38]. Platus is also the founder of Minus K which offers commercial vibration isolators using a negative stiffness mechanism [39].

Another application of a non-linear mechanism for vertical vibration isolation is the use of post-buckled beams, also referred to as Euler columns. By making use of beam in the post-buckled situation a very low stiffness results. The energy stored in a linear spring is defined by $E_{pot} = \frac{1}{2} kx^2$. In the pre-buckling situation the stiffness is very high and the deflection is very small. E_{pot} scales with x^2 so very little energy is stored. By

defining the working range of the isolator on the onset of buckling hardly any static energy of supporting the payload is stored in the spring element. This makes that only dynamic energy is stored in the element during operation. Since the displacement of the payload and ground is generally very small only little energy has to be stored which makes that only little spring material is needed. When defining a maximum deflection of 0,5 mm in a 1 Hz system, the Euler column would only need 1/250 of the weight of a linear equivalent. When assuming that the internal modes scale roughly proportional with the square root of the mass, the internal modes would be $\sqrt{250} \approx 16$ times higher and the effect of the modes reduced with 1/250 mass ratio. By analysis it can be found that the natural frequency of a system using a post-buckled spring only depends on the weight of the spring; $\omega_n = \sqrt{\frac{g}{2l}}$. An Euler column can thus attain the same natural frequency as an equivalent pendulum system ($\omega_n = \sqrt{\frac{g}{l}}$) in half the length. The Euler columns is extensively studied in the works by Winterflood [14].

Non-linear stiffness mechanisms can obtain sub-hertz natural frequencies with only little static sag. The mechanisms often introduce additional hysteretic damping. Hysteretic damping is preferred over viscous damping since the $1/f^2$ roll-off above the natural frequency is maintained. Non-linear stiffness mechanisms however offer a limited position adjustment and require regular tuning. A very good overview of the many types of non-linear stiffness mechanisms for both vertical as horizontal isolators is given by Ibrahim [33].

Pneumatic springs have a wide-spread use in vibration isolation systems. A pneumatic spring consist of a pressure vessel and piston or diaphragm and uses the entrapped air as a resilient element. Its stiffness is generally given as:

$$k_{air} = \frac{\gamma p A^2}{V} \quad (\text{A.1})$$

where A is the effective area of the diaphragm, p and V are the pressure and volume in working condition and γ is the specific heat ratio. At low frequencies (<3 Hz) the compression is adiabatic and γ approaches 1.4 while at high frequencies the compression is isothermal and γ approaches 1.0. Pneumatic springs are commonly used in the design of both conventional as well as high end optical tables [40, 41].

A.2.2 Horizontal isolators

Low frequency horizontal isolation by mechanical means is dominated by the use of pendulums. The simplicity of this suspension technique makes its use very attractive since by just suspending a payload by a string already a very low natural frequency can be obtained. The natural frequency of a simple pendulum system is only dependent on the pendulum length l since:

$$f_n = \frac{1}{2\pi} \sqrt{\frac{g}{l}} \quad (\text{A.2})$$

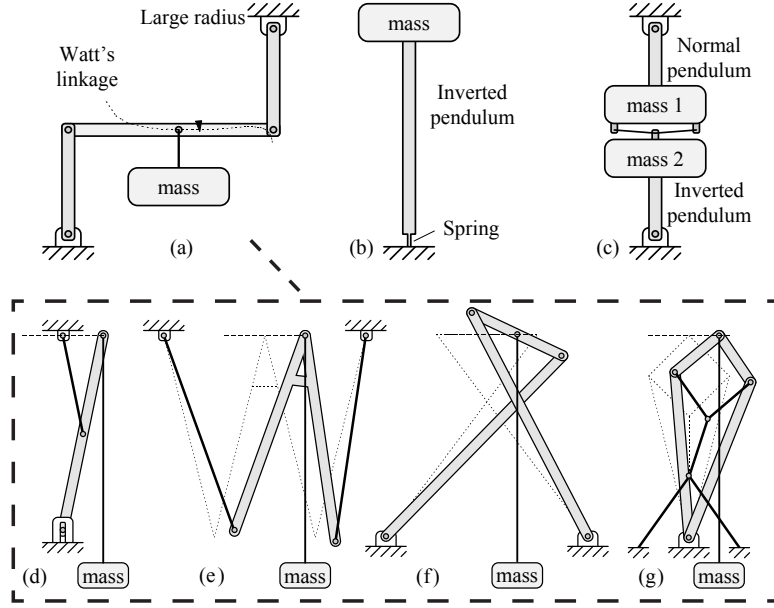


Figure A.2: Three categories of pendulum systems; (a) geometrical, (b) counter sprung and (c) counter weighted. Different geometrical configurations are the; (d) Scott-Russel linkage, (e) Roberts linkage, (f) Chebyshev linkage and (g) Peaucellier Cell linkage. From [14]

Another basic example of the use of pendulums is its inverted version, the inverted pendulum. Effectively the inverted pendulums is employs the gravitational force as a negative spring while compensating this stiffness with the positive stiffness of the pendulums hinge. The natural frequency of an inverted pendulum therefore does depend on the mass of the payload m :

$$f_n = \frac{1}{2\pi} \sqrt{\frac{k}{m} - \frac{g}{l}} \quad (\text{A.3})$$

Different advanced pendulum structures have been used in several gravitational wave detectors [15–18]. The used horizontal isolators consist of a pre-isolator, which mainly distinguishes itself by its size and mass, in combination with a cascaded system of pendulums. These advanced pendulum systems can be divided in three categories; geometrical types, counter sprung pendulums or counter weighted pendulums. See figure A.2.

Geometrical types make use of a construction with a specific geometry (a linkage) in order to make the payload suspension point to move in a flat horizontal plane. They aim to keep the stored energy as low as possible by preventing vertical displacements. Examples are the Scott-Russel linkage, Roberts linkage, Chebyshev linkage and the Peaucellier Cell linkage [14].

The counter sprung pendulum systems make use of a spring to counteract the negative stiffness of the gravitational force acting on a hinge point. The effective realizations of a counter sprung pendulum system is the inverted pendulum. Counter sprung pendulum

systems are often used as pre-isolators [15, 42].

Counter weighted systems use a pendulum suspended mass to counter-act the gravitational force acting on an inverted pendulum. No implementations of this type of system has been reported in literature. More details on the construction and performance of these types of systems can be found in the works of Ibrahim [33] and Winterflood [14].

An important parameter in the design of pendulum system which is often overlooked is the center of percussion effect. For every rigid body undergoing both a translation and rotation in a plane, a point may be found which is momentarily stationary with respect to the plane. A rigid body which is accelerated by a force which is not in line with its center of mass will undergo both rotational as well as translational acceleration. Similarly a point can be found which momentarily undergoes no acceleration. This point is called the *center of percussion*. The position of the center of percussion is inherent to the point where the force is applied, the force impulse point, opposite of the center of mass. This effect is important for the design of pendulum systems since high frequent floor vibrations behave similarly to a force impulse. The pendulum will thus rotate around the center of percussion linked to the force impulse point at the base of the pendulum. The center of percussion will only rotate by the floor 'force impulse' and if another structure is attached to this point by use of a pivot almost no motion will be transmitted. If the payload is not connected at the pendulum's center of percussion the dynamic effect will limit the roll-off of the systems transmissibility function, flattening the transmissibility function at high frequencies. In order make correct use of pendulums, a correct tuning of the design is thus essential. By algebraic analysis of the center percussion effect in inverted pendulum systems [43, 44], it shows that there are three options to make the percussion point of an inverted pendulum coincide with the suspension point of a payload:

- to have a massless pendulum; unfeasible but shows that a lightweight pendulum is beneficial
- suspend the payload at the level of the percussion point; makes the pendulum suspend stick through the payload
- provide a counterweight below the elastic joint to make the percussion point to coincide with the elastic joint connected to the payload. This option is most used in practice

Surprisingly little standard texts on the center of percussion effect exist but its importance for vibration isolation is well documented by Winterflood [14].

A.2.3 Damping

Damping is very important in decreasing the magnitude around the natural frequency as well as in determining the high frequency response of the vibration isolation system. In this section we will shortly discuss the different damping mechanisms used in isolation

systems. A more comprehensive overview of damping mechanisms for vibration isolation can be found in different sources [32, 45, 46].

Different methods of damping exist; viscous damping, eddy current damping, hysteretic damping, piezoelectric damping and tuned-mass dampers.

Viscous damping is damping based on relative velocity. Viscous damping can be obtained by viscous fluid dampers and eddy current dampers. Viscous fluid dampers are based on Newton's law of viscosity stating that the shearing stress in a viscous fluid is proportional to the rate of shear strain. Energy is dissipated by flow of the fluid. General configurations are piston or diaphragm driven dampers or squeeze film damping. Recent interest has been in the use of electro-rheological and magneto-rheological fluids in order to tune the damping properties [47, 48].

Since viscous damping is proportional to the relative velocity between the payload and its base, a trade-off in the transmissibility for damping around the natural frequency and the high frequency roll-off exist as shown by equation 2.3 and its effect shown by figure 2.2a. At increased levels of damping, the magnitude around the natural frequency decreases but the high frequency roll-off moves from a $1/f^2$ slope to a $1/f$ slope.

Eddy-current dampers are based on the principle that when a conductor moves in a magnetic field, eddy-currents will be induced which dissipate energy when flowing through the resistance of the conductor. The opposing electromagnetic force by the eddy currents is proportional to the velocity relative to the field thus viscous damping is attained. More information on the dynamic characteristics of eddy current dampers is given by Tonoli [49] and practical realizations are discussed by Sodano [50] and in section 3.2.2 of Zuo [32].

Hysteretic dampers make use of the phenomena of hysteresis when loading and unloading a material. When a material or element does not comply to Hooke's law perfectly, energy is dissipated due to the plasticity of the element. The energy dissipated in each load-cycle corresponds to the area of the hysteresis loop resulting in the load-displacement diagram of a material or element. Hysteresis can also be interpreted as the phase lag between the loading stress and the strain of the material. This states that the materials Young's modulus in the frequency domain is generally a complex number $E(1 + j\nu)$ where ν is the material loss factor. This redefines the equation of motion of the basic vibration isolation system, equation 2.2, in the frequency domain ($s = j\omega$) as;

$$-m\omega^2 x + (1 + j\nu)k(x - x_f) = F_d \quad (\text{A.4})$$

and the transmissibility is then stated by;

$$\frac{x}{x_f} = \frac{k(1 + j\nu)}{-m\omega^2 + k(1 + j\nu)} = \frac{\omega_n(1 + j\nu)}{-\omega^2 + \omega_n^2(1 + j\nu)} \quad (\text{A.5})$$

The resulting transmissibility shows that hysteretic damping attenuates the magnitude peak without compromising high-frequency suppression. The high frequency magnitude

only increases by $\sqrt{1+\nu^2}$. High damping is attained by selection of a material with a high loss factor ν . Viscoelastic materials, such as rubbers, have high loss factors and are most used for this type of damping. Hysteretic damping is therefore often referred to as viscoelastic damping. The disadvantage of the use of viscoelastic materials is that the dynamic elastic modulus and the loss factor depend on the frequency. At increasing frequency the elastic modulus increases and the loss factor decreases. This makes the damper act more as a spring, adding to the suspension stiffness thereby increasing the transmittance of high frequency floor vibrations. Viscoelastic dampers are commonly based on the design methods of free-layer and constrained-layer damping, of which the damping parameters can be determined by the formulas given in [32].

Piezoelectric materials produce a voltage under strain. By shunting the piezoelectric material with a resistor, this property can be used to dissipate mechanical energy by conversion to electrical energy. The damping capabilities differ for the loading direction longitudinal (3-3 mode) or perpendicular (3-1 mode) to the poling direction of the material. For the most commonly used PZT material, the highest damping ratios result for longitudinal loading. Piezoelectric damping is dependent on the deformation of the material and so has the same characteristics as hysteretic damping. The shunted piezoelectric material itself behaves like viscoelastic material, its elastic modulus and loss factor being similarly dependent on frequency. More details and formulas on passive piezoelectric damping are given by [32, 51].

Piezoelectric elements have also been used to create active structural damping. Active control of a piezoelectric stack integrated as a structural component of a construction can be used to dampen structural resonances. This was proven by the Smart Lens Support (SLS) and the Piezo Active Lens Mount (PALM) created in the Smart Disc project [52, 53]. This however comes at the cost of decrease of mounting stiffness thereby lowering the natural frequency of the structure.

Tuned-mass damping attenuates the motion of the payload by deliberate introduction of an internal frequency of the payload coinciding with the natural frequency of the suspension. The internal frequency arises from the resonance of the tuned-mass damper consisting of a absorber mass, spring and damper capable of damping single or multiple degrees of freedom. By addition of the tuned-mass damper the original single mode at ω_n is split into two separate highly damped modes. In the transfer function this results in two separate resonance peaks around ω_n . The resulting lower frequency peak corresponds to the absorber mass and payload moving in phase whereas the higher frequency peak corresponds to the absorber mass and payload moving in counter-phase. This damping mechanism is based on the absolute motion of the payload and has no effect on the high frequency transmission. Tuned-mass damping can be considered a passive realization of the skyhook damping as proposed by Karnopp [54] as discussed in section A.3.3. A very good introduction into tuned mass dampers and the construction of a MDOF tuned-mass damper is given chapter 4 of Zuo [32].

A.3 Active vibration isolation systems

Active systems make use of a combination of both passive and active system components. Next to the passive spring and dampers, these systems make use of sensors, actuators and controllers. The active components are added in order to compensate and overcome limitations of passive systems. Generally, the main focus is on improving low frequency performance and breaking the trade-off between transmissibility and compliancy. Active control is based on feedback of relative or absolute payload motion or feedforward of ground motion. The main limitation of active systems is the generation of noise adding to the payloads movement.

Next to difference in the components used, the performance is greatly determined by the used isolation strategy (i.e. configuration of the components). A good review of the different existing isolation strategies is given by Collette [55]. Most active systems make use of an inertial reference, determining the absolute motion of the payload, while being mounted on the ground [11, 12] or on the payload [13].

A.3.1 Sensors

Sensors are used to measure the parameters of the vibration isolation system as discussed in section 2.2.2. Since the motion of the payload is very small, the resulting sensor signal is generally very small. The sensor's noise-level is therefore the most important property since it sets the threshold for which level of motion can be correctly measured.

Two categories of sensors are used; absolute or relative motion sensors. Absolute motion sensors measure motion in respect to an internal reference, in order to determine the absolute motion of a single component. The resulting signal is only valid in the frequency range in which the internal reference is stationary. Relative motion sensors measure the motion between separate system components in order to determine their relative motion. Most active vibration isolation systems make use of absolute motion sensors in the form of accelerometers and geophones.

Absolute motion sensors - Inertial referencing

In order to measure absolute motion, many mechanical sensors make use of *inertial referencing*. The motion sensing is not really absolute but is measured in respect to an inertial reference; a reference mass which is placed at a very low stiffness suspension. The low stiffness suspension offers a low natural frequency (1 Hz) such that the reference mass rapidly decouples from the base motion of the sensor. This way the reference mass can be used as an absolute reference with zero displacement, velocity and acceleration above the natural frequency and the absolute motion of an object can be measured relative to the stationary reference mass. However the frequency range (or *bandwidth*) in which this statement is valid is limited.

The reference mass and the low stiffness suspension form a basic spring mass system which properties limit the sensor properties. The bandwidth in which absolute motion can be measured is limited by the natural frequency and the higher (second, third) eigenfrequencies, the so-called spurious modes of the spring mass system. The sensitivity of

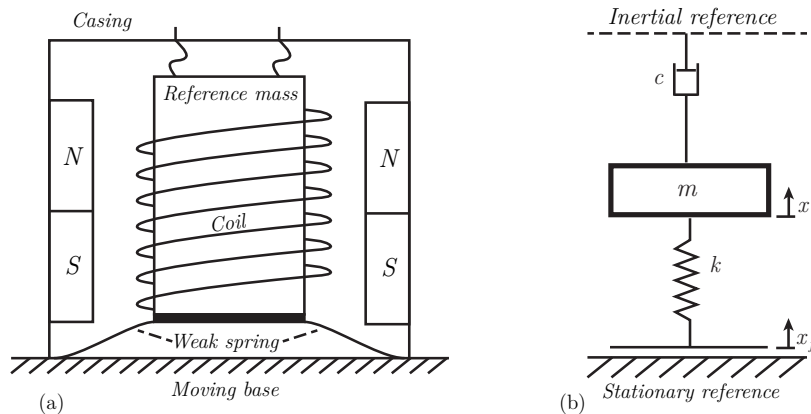


Figure A.3: A geophone (a) uses inertial referencing and is often used to obtain Skyhook damping (b) as proposed by Karnopp [54]

the sensor is directly linked to the motion of the reference mass.

Before the first eigenfrequency, the reference mass moves almost synchronous with the object to be measured and almost no relative motion can be detected. The sensor sensitivity is low and linearly increasing up to the eigenfrequency in the frequency domain. The low frequency performance of such a sensor can be improved by using stretching filters, increasing the measurement signal below the natural frequency. This is effective as long as the sensor offers a large enough signal-to-noise ratio. Low frequency noise is the limiting factor for sensors used for low-frequency active vibration isolation systems suppressing ground vibrations below 1 Hz.

Furthermore, for low-frequency measurements in horizontal direction, the tilt-to-horizontal coupling effect occurs. This effect states that motion by the change in gravitational force due to tilt around the perpendicular horizontal axis cannot be distinguished from horizontal motion. The tilt is thus misinterpreted for horizontal motion resulting in a incorrect actuation of the payload. At low frequencies, this effect becomes dominant over actual horizontal motion limiting the control performance below the natural frequency of the inertial reference [13].

The upper limit of the sensor bandwidth is set by the spurious modes of the reference mass on its suspension. The spurious modes induce motion of the reference mass in unwanted directions. This motion is detected by the sensor and causes instability of the controller. This generally limits the bandwidth to about a quarter of the second eigenfrequency of the reference mass. In practice it is extremely difficult to realize a second mode more than 100 times higher than the first mode. For example, with a natural frequency of 2 Hz the first spurious mode can be elevated to about 160-200 Hz, which limits the bandwidth to 40 Hz.

Geophones

Geophones measure the payloads absolute velocity. A geophone consists of a housing

containing a mass suspended on a weak spring. The mass constitutes of a magnet while the housing contains a coil, or vice versa. For frequencies larger than the ω_n of the internal suspension, the mass no longer follows the movement of the housing and remains stationary creating an *inertial reference*. The relative velocity between the stationary magnetic field and the coil moving with the housing causes a change of magnetic flux through the coil and thereby induces an EMF in the coil. The amplitude of the EMF is dependent on the relative velocity between coil and magnet. By increasing the flux rate of change the sensitivity of the sensor, given by the induced voltage per meter per second, is increased. A larger sensitivity results in a better signal-to-noise ratio. Geophones make use of relatively large inertial masses and are therefore relatively bulky. The main mechanical limitations of the geophone are stated in section A.3.1. A geophone directly measures the velocity needed for the damping so no extra noise is introduced by integration of low-frequency sensor noise opposed to using an accelerometer.

Geophones are most used in order to apply so-called sky-hook damping [54]. Damping is added proportional to the absolute velocity signal obtained in respect to the stationary 'sky', represented by the inertial reference in a geophone. Adding damping based on the velocity in relative to the stationary sky changes the equation of motion of the basic vibration isolation system, equation 2.1, into;

$$m\ddot{x} + c\dot{x} + k(x - x_f) = F_d \quad (\text{A.6})$$

and the transmissibility into;

$$\frac{x}{x_f} = \frac{\omega_n^2}{s^2 + 2\zeta\omega_n + \omega_n^2} \quad (\text{A.7})$$

The resulting transmissibility shows that by using damping based on absolute velocity attenuates the magnitude peak at ω_n without compromising the high-frequency suppression. The concept of sky-hook damping is often used in state-of-the-art active vibration system [25,56]. The main focus of these systems is on improving the suppression of floor vibrations for frequencies below 40 Hz.

Geophones are often used integrated in seismic measurement equipment. For industrial purposes geophones are available at main suppliers like Geospace [57] and Ion Geo [58]. Furthermore several companies have recently developed new innovative sensors:

Magnetic Innovations

For the use in a active vibration isolation systems, Dutch company Magnetic Innovations has developed a novel Geophone with excellent small signal behavior due to a very high sensitivity of 36.6 Vs/m. Magnetic Innovations claims to have broken the trade-off in obtaining a low natural frequency while maintaining high frequency spurious modes by using a magnetic spring giving the geophone a 1 Hz natural frequency and an effective bandwidth up to 40 Hz [59].

US Seismic Systems inc.

For the use in permanent oil field monitoring, the American company USSI has developed a fiber optic geophone claimed to have superior noise levels, 20x better than high performance magnet/coil geophones. By using a fiber bragg grating with time division multiplexing methodology, the system eliminates electronic sensor noise and electromagnetic cross-talk [60].

Accelerometers

Accelerometers determine the payloads absolute acceleration. They are often used in vibration isolation systems because of their large bandwidth and large amplitude range. The three main types are piezoelectric, capacitive and piezoresistive accelerometers.

Piezoelectric accelerometers

Piezoelectric accelerometers are the most common type of accelerometers. The sensors are based on the piezoelectric effect which states that a charge accumulates at the surface of the piezoelectric material when subjected to a mechanical stress. The accumulated charge is thus proportional to the applied force. By mounting a reference mass on stacks of piezoelectric element, the resulting charge is proportional to the acceleration of the mass via $F = ma$. By preloading the piezoelectric stacks both positive and negative accelerations can be measured. Different mechanical configurations are available based on different methods of loading the piezoelectric material (e.g shear, compression and bending) [8]. The sensor is operated in either voltage or charge mode. Charge mode accelerometers hold built-in conditioning electronics such as a charge amplifier to obtain a proper signal.

Capacitive accelerometers

A capacitive accelerometer works by fixing one electrode of a capacitor to a reference mass, which is suspended by flexure leaf springs or a membrane, and fixing the other electrode to the fixed world. The position of the reference mass in respect to the fixed world is a measure for the resulting acceleration. The relative position is measured by the change in capacitance of the capacitor. By using a Wheatstone bridge the change is modified into a signal proportional to the acceleration. Some sensors operate in closed-loop mode in which the reference mass is kept in position by supplying a control voltage proportional to the change in capacitance. Next to having a high sensitivity, the sensor can operate to 0 Hz frequency (DC acceleration). This makes them beneficial over piezoelectric sensors in active isolation systems since at low frequencies the system stability is not threatened due to the phase of the sensor signal. Modern capacitive accelerometers come in small packages since they are predominantly created by Micro Electro-Mechanical Systems (MEMS) technology. The often used comb-drive structure is produced easily by MEMS technology and can measure up to three orthogonal directions.

Piezoresistive accelerometers

Just as capacitive accelerometers, Piezoresistive Accelerometers are also mainly pro-

duced as a MEMS package. Piezoresistive, or strain gage, accelerometers are based on the effect that when a resistive material is stretched, becoming longer and thinner, its resistance increases. Typically, a reference mass is suspended by four separate beams equipped with strain gages. The acceleration of the mass causes the beam to deflect and so proportionally changing the resistance of the strain gages. By use of Wheatstone bridge this change can be related to the level of acceleration. By having a pair of strain gages per beam, accelerations in multiple directions can be measured. Piezoresistive sensors tend to have a larger frequency range than piezoelectric sensors, typically up to 2 kHz, but tend to have a lower sensitivity and require more electronics.

All these accelerometer types come with different properties for different applications. Many suppliers offer sensors specifically for vibration monitoring with their performance tailored to the application. Some main suppliers are; Endevco [61], Colibrys [62] and Bruel and Kjaer [63]. Relatively new are the so-called MEMS Geophones which are actually accelerometers designed to compete with the superior low frequency noise performance of magnet/coil geophones while still offering the advantages of MEMS accelerometers. Examples of recent innovations are:

Hewlett Packard (HP)

In connection to the CeNSE (Central Nervous System for the Earth) program [64], HP in cooperation with Shell are developing a novel MEMS seismic sensor [65] (a capacitive accelerometer) with a flat frequency response from DC up to 200 Hz with a claimed noise floor smaller than $10 \text{ ng}/\sqrt{\text{Hz}}$ which is a large improvement in respect to similar MEMS accelerometers. The sensor consists of a relatively large proof mass, to which one plate of a capacitor is attached while the other half is connected to the moving world. Unfortunately this sensor is not yet available for industrial use.

Sercel

The Sercel MEMS accelerometer was designed by CEA Leti and was industrialized by Tronics. According to Tronics [66], the sensor has a claimed noise floor of $10 \text{ ng}/\text{Hz}$ noise floor and a 0-800 Hz closed-loop bandwidth. The sensor is not separately available but is integrated into several of the Sercel [67] seismic products (DSU3 and DSU1).

A.3.2 Actuators

One of the most important properties of the actuators used in active isolation systems is their inherent stiffness. Since the actuators tend to act between the isolated mass and the fixed world, the actuator stiffness adds to the stiffness of the suspension. Actuators having zero stiffness are therefore preferred. Furthermore, the actuator is most effective when it is collocated with the sensors resulting in the most direct transfer function between the sensor signal and the actuator action.

The most common types of actuators used for vibration isolation are electromagnetic and piezoelectric actuators. The use of other types of actuators has also been reported such as conventional hydraulic and pneumatic actuators [68] or more exotic types such

as magnetorheological [69, 70], electrorheological [47, 48] or dielectric elastomer [71] actuators.

Electromagnetic actuators

Most active vibration isolation systems make use of electromagnetic actuators. The electromagnetic actuator is well suited for vibration isolation due to their advantageous stiffness properties. By construction, electromagnetic actuators have little mechanical stiffness between the fixed world and the actuated isolated mass so do not compromise the transmissibility of the isolation system.

Electromagnetic actuators generally come in two types; Voice coil, or Lorentz, actuators and reluctance actuators. A combination of both is called a hybrid actuator. Lorentz actuators are based on the effect that when a charged particle is moving through an electric and a magnetic field it experiences a force, the Lorentz force. By placing a wire which carries an electric current in a magnetic field it will experience the Lorentz force hence the functioning of the Lorentz actuator. The Lorentz force of the Lorentz actuator is linear dependent to the current and the magnetic field.

A reluctance actuator works by changing the reluctance of a magnetic circuit. A coil is used to create an electromagnet which pulls on a iron counterpart independently of the current direction through the coil. This pulling reluctance force is proportional to the current squared, resulting in non-linear control characteristics.

The most used type is the Lorentz actuator although the development of high performance reluctance actuators is gaining interest [72]. A disadvantage for the use of electromagnetic actuators is the existence of strong electric and magnetic fields which can affect the electron optics in e-beam lithography tools. Sufficient shielding is thus necessary. An example of the design of reluctance actuator and a 6 DOF Lorentz actuator is given by Nijssse [73]. Furthermore Mizuno has build a system using reluctance actuators and linearized zero-power control [74]. This system is focused on improving the compliancy of the vibration isolation system and uses only relative position sensors. A proper introduction on electromagnetic actuators and its properties is given in chapter 5 of the book of Munnig Schmidt [8].

Piezoelectric actuators

Another common actuator used in active configurations is the piezoelectric actuator. Just as piezoelectric sensors and shunted piezoelectric dampers, piezoelectric actuators make use of the piezoelectric effect. This effect is however used in the opposite way, by applying a voltage to the material a mechanical deformation is created. The actuators act in 3-3 or 3-1 mode. In 3-3 mode the strain is longitudinal to the poling direction. In 3-1 mode the strain is perpendicular to the poling direction. This deformation is however limited to about 0.1 percent of the actuators length. This limited stroke limits the a attenuation of low frequency vibrations having a large amplitude. By combination with a flexure the stroke can be increased. A disadvantage of piezoelectric actuators is the high level of hysteresis (up to 15%) and nonlinearity (up to 4%).

In contrast to electromagnetic actuators, piezoelectric actuators have a very high stiff-

ness. Where electromagnetic actuators can be used in parallel with a passive suspension, piezoelectric actuators are therefore used in series with passive suspensions. An example is using piezoelectric actuators to create an intermediate isolated platform on which another passive or active suspension can be mounted [37, 75, 76]. A comparison between an active system using a parallel Lorentz actuator or a piezoelectric actuator in series is given by Zuo [32, 56].

Piezoelectric actuators come in two types of material; lead zirconate titanate (PZT) and polyvinylidene fluoride (PVDF). PZT is a fragile ceramic. PZT actuators are most used and come as a piezoelectric stack or plate acting in 3-3 mode.

PVDF is a plastic polymer and is very flexible. PVDF actuators usually come as a piezoelectric film and operate in 3-1 mode. PVDF has a negative 3-3 mode piezoelectric coefficient meaning that it deforms (expand/compress) in the opposite direction as PZT when subjected to the same electric field. Much information on PVDF films is given in [77]. A well documented application is the creation of an active beam or plate by bonding a PVDF film or PZT plate to the structure creating a bending moment under an applied voltage [78, 79].

A.3.3 Isolation strategy and control

As in any mechatronic system, the resulting system performance is strongly determined by the effectiveness of the controller. Control strategies used for vibration isolation systems are classical feedback control, feedforward control, modal-space control, robust sliding control and adaptive control. Since the control method can be selected per system and due to the elaborateness and complexity of the control discipline, it is best to study the specific references and we will not elaborate on its details here. Details on several control strategies used for active vibration isolation are given by [32, 34, 80].

The goal of many active isolation system is to obtain 'skyhook' damping as described by Karnopp [54]. To break the trade-off between damping of the natural frequency and attenuation of high frequency vibrations with viscous dampers connected to a moving base, Karnopp proposed to connect the damper to a virtual inertial 'sky'. This way damping is applied proportional to the absolute velocity of the payload thus not compromising the high frequency attenuation. Since the inertial 'sky' does not physically exist, it is attempted to attain skyhook damping by control based on feedback of the velocity of the payload, as also shown in the discussion of the geophone.

Next to the selection of the correct components and having an effective control strategy, the performance of the active isolation system is determined by how the different components are configured in respect to each other. The system configuration determines if the system is able to distinguish both force and floor vibrations and determines which components are best to be used. Literature does not provide a comprehensive overview of the different possible configurations other than the overview given by Collette [55]. A configuration can be different per DOF and can be categorized by; single or multistage systems, relative or absolute motion measurement and using series or parallel actuators next to the passive suspension. An overview of possible single stage configurations is

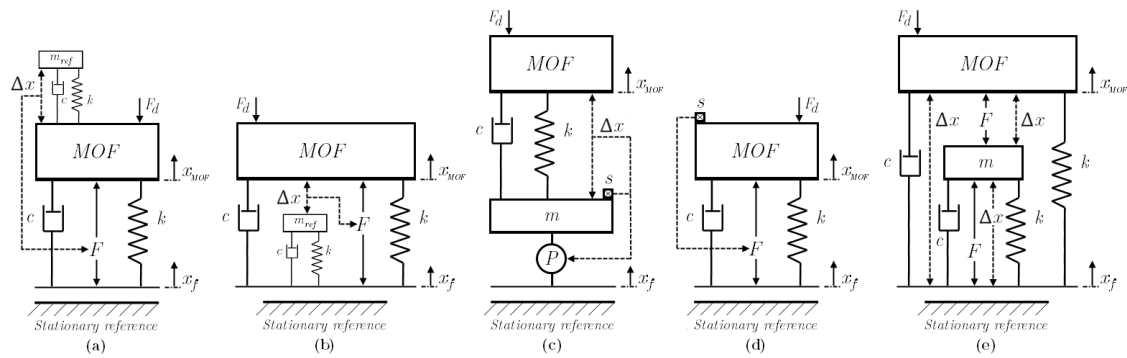


Figure A.4: Overview of the system configurations of different active vibration isolation systems. The isolated mass is indicated by MOF; (a) The Hummingbird platform [13] (b) The AIMS system [11, 12] (c) 'Hard mount' piezoelectric isolation system [37, 75, 76] (d) The MI-partners system [25] (e) The system by Mizuno [74]

given in figure A.5. The configuration can be selected per DOF. Series configurations make use of stiff actuators while parallel systems make use of non-stiff actuators. The most common active configuration is a single stage suspension with a parallel non-stiff actuator (e.g. Lorentz actuator) controlled by the signal from an collocated absolute motion sensor (e.g. geophone).

Figure A.4 shows the configuration of several systems described in literature. Configuration (a) and (b) both measure the position of the isolated mass in respect to an inertial reference and make use of an electromagnetic actuator parallel to a passive suspension. Configuration (b) is however also robust to direct disturbance forces, indicated by F_d . Configuration (c) uses a piezoelectric actuator in series with a passive suspension. Both relative and absolute motion sensor information, indicated by Δx and s , are used in the control of the actuator. Configuration (d) is similar to configuration (a) but uses a geophone to determine the velocity of the isolated mass. Configuration (e) uses only relative position sensors and reluctance actuators and aims to improve the compliancy of the passive suspension.

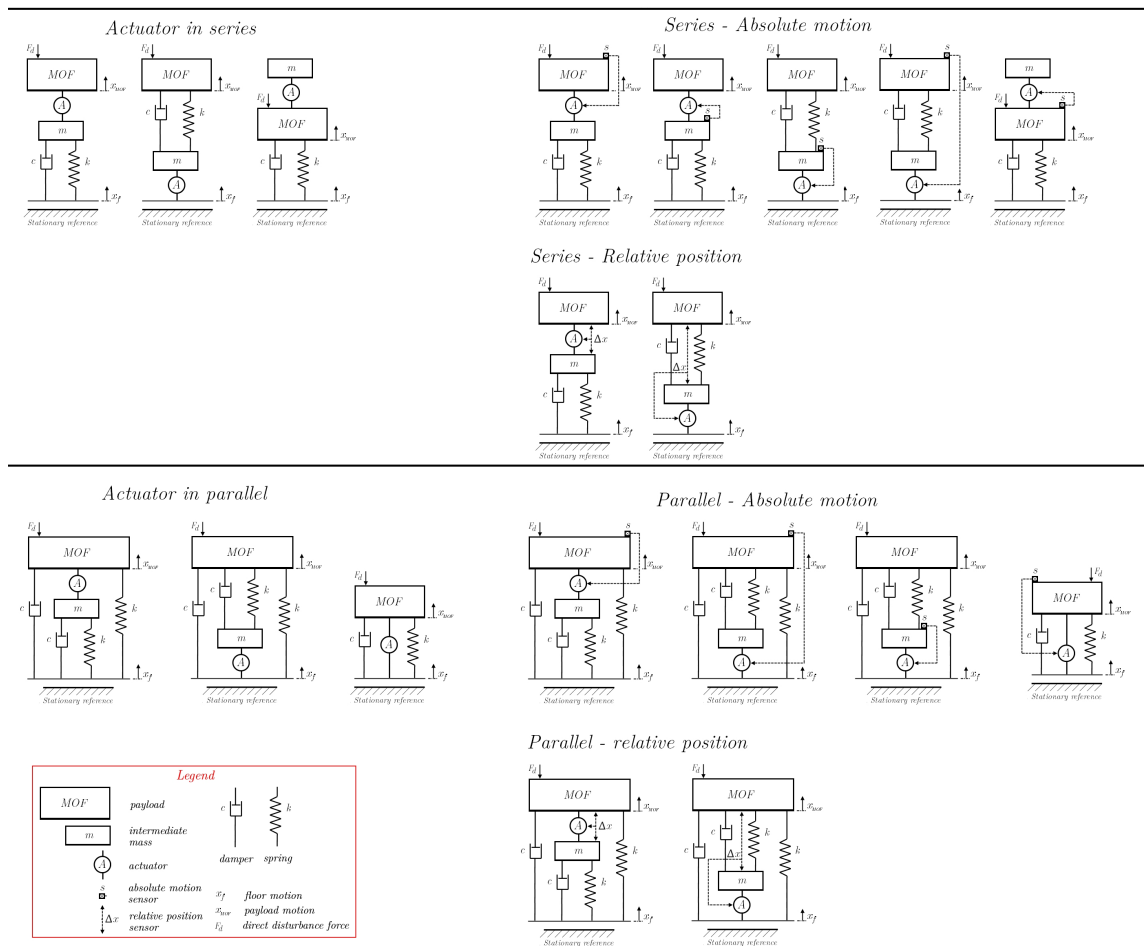


Figure A.5: Overview of single stage series and parallel configurations with the different sensor position for absolute and relative motion sensing.

Appendix B

Dynamic error budgeting model

B.1 Introduction

This appendix discusses the dynamic error budgeting model created in Matlab and the results when adjusting its parameters.

B.2 Dynamic error budgeting Matlab model

In this section, the main properties of the dynamic error budgeting model created in Matlab are highlighted. The code is self-explanatory by the comments given to the code. The following parameters of the model could be given as input:

```
1 %% Variables
2 m_MOF = -;           %[kg]           Weight of MOF
3 k_VIM = -;          %[N/m]           VIM Stiffness
4 zeta = -;           %[-]            Relative damping
5 BW = -;             %[Hz]           ShS bandwidth
6
7 k_VIM_Z = -;        %[N/m]           VIM Stiffness in Z
8 k_VIM_R = -;        %[N/m]           VIM Stiffness in Rx/Ry
9 k_VIM_Rz = -;       %[N/m]           VIM Stiffness in Rz
10
11 %% Rewriting parameters
12 wn = sqrt(k_VIM/m_MOF); %[rad/s]
13 wn_Hz = (1/(2*pi))*wn; %[Hz]
14 c_VIM = 2*sqrt(k_VIM*m_MOF)*zeta; %[N*s/m]   VIM Damping
15 Q_fac = 1/(2*zeta);   %[-]
16
17 % Cross-talk parameters
18 m_MOF_R = -;          %[kg*m^2] - Inertia of MOF in Rx/Ry
19 m_MOF_Rz = -;        %[kg*m^2] - Inertia of MOF in Rz
20
21 wn_Z = sqrt(k_VIM_Z/m_MOF); %[rad/s]   Cross-talk - natural
    frequency in Z
```

```

22 wn_R = sqrt(k_VIM_R/m_MOF_R);    %[rad/s]    Cross-talk - natural
    frequency in Rx/Ry
23 wn_Rz = sqrt(k_VIM_Rz/m_MOF_Rz); %[rad/s]    Natural frequency in Rz
24
25 zeta_Z = -;                      %[-] - relative damping in Z
26 zeta_R = -;                      %[-] - relative damping in Rx/Ry
27 zeta_Rz = -;                    %[-] - relative damping in Rx/Ry
28
29 Cross_Z = -;                    %[-] - Percentage of cross-talk from Z to X/Y
30 Cross_R = -;                    %[-] - Percentage of cross-talk from Rx/Ry to X/Y
31 Cross_Rz = -;                   %[-] - Percentage of cross-talk from Rz to X/Y
32
33 Floor_facZ = -;                 % Multiplication factor of floor spectrum PSD in Z
34 Floor_facR = -;                 % Multiplication factor of floor spectrum PSD in Rx/Ry
35 Floor_facRz = -;                % Multiplication factor of floor spectrum PSD in Rz
36
37 DDF_facZ = -;                   % Multiplication factor of direct disturbance force
    PSD in Z
38 DDF_facR = -;                   % Multiplication factor of direct disturbance force
    PSD in Rx/Ry
39 DDF_facRz = -;                  % Multiplication factor of direct disturbance force
    PSD in Rz
40
41 S_slit = -;                      % Beams at edge of the slit move with a certain arm -
    X/Y sensitive to Rz
42
43 Sup_max = -;                     % Maximum suppression factor in transmissibility and
    compliancy

```

The transmissibility and compliancy functions of the vibration isolation system are created by:

```

1 %% Transmissibility
2 Trans_tf = tf([1 2*Sup_max*zeta*wn+wn/(2*zeta) Sup_max*wn^2], Sup_max*[1
    2*zeta*wn wn^2]);
3 Trans_tf_points = freqresp(Trans_tf, Sampling_vector_w);    %
    determine sensitivity magnitude at frequency points of interest
4 Trans = squeeze(abs(Trans_tf_points));                      % create
    [1 length(Sampling_vector)] array out of freqresp response
5
6 %% Compliancy
7 Comp_tf = tf([1 2*wn*sqrt(Sup_max) Sup_max*wn^2], m_MOF*Sup_max*wn^2*[1
    2*zeta*wn wn^2]);
8 Comp_tf_points = freqresp(Comp_tf, Sampling_vector_w);    % determine
    sensitivity magnitude at frequency points of interest
9 Comp = squeeze(abs(Comp_tf_points));                        % create [1
    length(Sampling_vector)] array out of freqresp response

```

The sensitivity of the positioning stage is created by:

```

1 %% ShS controller sensitivity
2 % ShS properties
3 Md = -; % decoupling mass
4 Mm = -; % actuated mass
5 w0p = -; % resonance of compensated weak stiffness to
   fixed world
6 wlp = -; % first flexible resonance
7 k1 = (Md+Mm) * w0p^2; % weak stiffness to fixed world
8 k2 = Md * wlp^2; % stiffness of decoupling mass
9 b1 = -; % damping to the fixed world
10 b2 = -; % damping of the decoupling mass
11 Psro = tf([1 -2*0.1*2*pi*400 (2*pi*400)^2], (2*pi*400)^2);
12 % limitation of mass-line of the plant to include
   the effect of high frequency resonances (stop
   roll off), complex right half-plane zero pair
13
14 % Creating plant model
15 M = diag([Mm, Md]); % mass matrix
16 B = [b1+b2, -b2; -b2, b2]; % damping matrix
17 K = [k1+k2, -k2; -k2, k2]; % stiffness matrix
18
19 P = ss([zeros(2), eye(2); -M\K, -M\B], [zeros(2); inv(M)]*[1;0], [1 0 0
   0], 0) * Psro; % plant transfer function (1 DOF)
20
21 % Determining controller parameters
22 Wbw = 2*pi*BW; % rewrite BW from Hz to rad/s
23 Cp = 0.5*Wbw^2*(Md+Mm); % proportional gain per DOF (P-action)
24 Ci = 0.2*Cp*Wbw; % integrator gain per DOF (I-action)
25 Cd = 2/Wbw*Cp; % derivative gain per DOF (D-action)
26
27 C = tf([Cd Cp Ci], [1 0]) * tf((6*Wbw)^2, [1 2*0.7*6*Wbw (6*Wbw)^2]);
28 % 1 DOF controller transfer function - 6*Wbw is bandwidth of 2nd order
   roll-off filters
29 set(C, 'OutputDelay', 927e-6) % phase delay due to electronics
30
31 S_ss = inv(1+P*C); % sensitivity function of the controller

```

The resulting spectra (PSD, ASD, CPS and CAS) are created by:

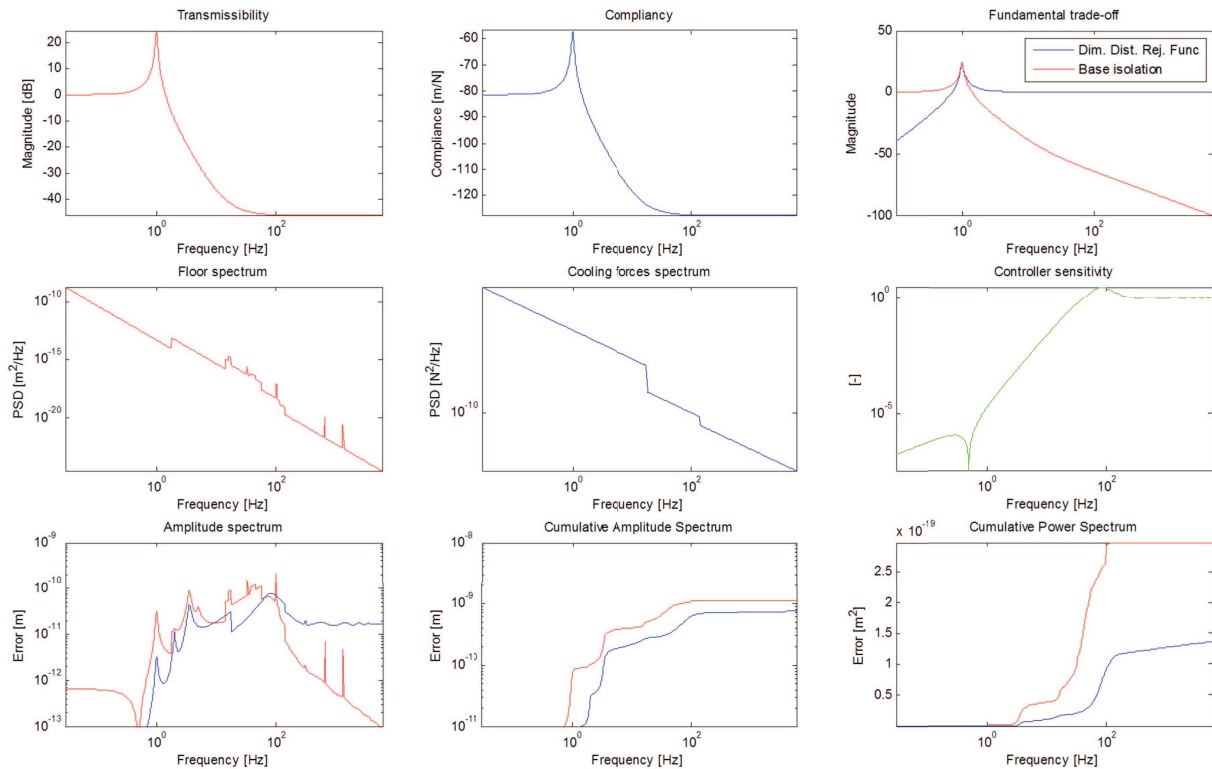
```

1 %% Dynamic error budgeting
2 % Creating different spectra with given input spectra
3
4 % Resulting PSD of floor vibrations after passing VIM
5 Cross_Talk_Floor =
    Floor_spec_Z.*Trans_ZToX.^2.*S.^2+Floor_spec_R.*Trans_RyToX.^2.*S.^2
    +Floor_spec_Rz.*Trans_RzToX.^2.*S.^2; % PSD of crosstalk contributions
6 Slit_Floor = (S_slit/2)^2*Floor_spec_Rz.*(Trans_RzToX/Cross_Rz).^2.*S.^2;
7 Floor_res_PSD = Floor_spec.*Trans.^2.*S.^2 + Cross_Talk_Floor +
    Slit_Floor; % [m^2/Hz] – Power Spectral Density function
8
9 % Resulting PSD of cooling vibrations after passing VIM
10 Cross_Talk_DDF = DDF_Z.*Comp_ZToX.^2.*S.^2+DDF_R.*Comp_RyToX.^2.*S.^2
    +DDF_Rz.*Comp_RzToX.^2.*S.^2; %PSD of crosstalk contributions
11 Slit_Force = (S_slit/2)^2*DDF_Rz.*(Comp_RzToX/Cross_Rz).^2.*S.^2;
12 Cooling_res_PSD = DDF.*Comp.^2.*S.^2 + Cross_Talk_DDF + Slit_Force;
    % [m^2/Hz] – Power Spectral Density function
13
14 % Frequency vector for integral calculation
15 dHz = diff(Sampling_vector); % determine frequency step
16
17 % Cumulative Power Spectrum
18 CPS_Floor = 3*sqrt(2*cumsum(Floor_res_PSD.*dHz).^2); % CPS =
    integral of PSD to frequency = equal to cumulative sum power from PSD
    times frequency band
19 CPS_Force = 3*sqrt(2*cumsum(Cooling_res_PSD.*dHz).^2); % – in 3
    sigma error including negative frequencies (the times 2)
20
21 % Amplitude Spectral Density
22 ASD_Floor = 3*sqrt(2*((Floor_res_PSD.^0.5).*dHz.^0.5).^2); % ASD =
    PSD^0.5 – in 3 sigma error including negative frequencies (the times
    2)
23 ASD_Force = 3*sqrt(2*((Cooling_res_PSD.^0.5).*dHz.^0.5).^2);
24
25 % Cumulative Amplitude Spectrum
26 CAS_Floor = 3*sqrt(2*(cumsum(Floor_res_PSD.*dHz).^0.5).^2); % CAS =
    CPS^0.5 – resulting amplitude error – in 3 sigma error including
    negative frequencies (the times 2)
27 CAS_Force = 3*sqrt(2*(cumsum(Cooling_res_PSD.*dHz).^0.5).^2);

```

B.3 Results changing parameters of model

The listed Matlab model produced the following result:



The VIM natural frequency is 1 Hz
 The VIM damping coefficient is 113.0973 Ns/m
 The VIM relative damping is 0.03
 The VIM Q factor is 16.6667

Resulting error by floor vibrations 1.1234 nm
 Resulting error by force disturbance 0.75958 nm
 The residual SUSA error is 1.1737 nm
 The residual MOF error is 1.3561 nm

Standard parameters of the model:

Parameter	Setting
Eigenfrequency VIM	1 Hz
Relative damping VIM	3%
Weight MOF	300 kg
Bandwidth ShS controller	75 Hz
<i>Crosstalk</i>	
Eigenfrequency VIM in Z	5 Hz
Eigenfrequency VIM in Rx/Ry	3.5 Hz
Eigenfrequency VIM in Rz	2 Hz
Relative damping in Z / Rx / Ry	0.06 (6%)
Relative damping in Rz	0.03 (3%)
Percentage of crosstalk Z and Rz	2 %
Percentage of crosstalk Rx/Ry	16%
Multiplication of floor spectrum in Z	1 x
Multiplication of floor spectrum in Rx/Ry/Rz	0.5 x
Multiplication of force spectrum in Z / Rz	10 x
Multiplication of force spectrum in Rx/Ry	2 x
Floor / Force / Sensitivity spectra	Mapper spectra
Frequency range	0 . . 6 kHz
Logarithmic sampling points	1000

These values are referred to as the standard parameters.

The results with these standard parameters can be compared with the error budgets:

Disturbance source	Budget	Result
Total budget (MOF budget)	1.39 nm	1.3561 nm
Floor	1.148 nm	1.1234 nm
Direct disturbance forces	0.783 nm	0.7596 nm
per cooled component	0.35 nm	0.3397 nm
SUSA budget	1.2 nm	1.1737 nm

The residual SUSA error is used for comparison with the budget given to SUSA. The SUSA budget contains the total floor vibration budget plus the budget of one cooled component. This budget is used at Mapper to check the performance of the SUSA subsystem.

The model predicts the performance in a single horizontal DOF with a contribution due to cross-talk from three other directions. The model is verified by comparison of the results from the existing 6 DOF dynamic error budgeting model used at Mapper. The results from both the models in horizontal direction are almost identical. The created 1 DOF model is considered to give a sufficient approximation of the residual error and can therefore be used for parameter variation.

B.3.1 Stiffness of vibration isolation system

The effect of the stiffness of the vibration isolation system is studied in two ways; (1) only changing the stiffness in the principal direction (constant crosst.) and (2) changing the stiffness in both the principal direction and the crosstalk DOF's with an equal percentage (equal change):

Natural frequency [Hz]	Stiffness [N/m]	Resulting error (constant crosst.)	Diff MOF	Resulting error (equal change)	Diff MOF
0.5	$300 \cdot \pi^2$ (25%)	Floor: 1.0397 nm Force: 2.2978 nm SUSA: 1.4618 nm MOF: 2.522 nm	+86.0%	Floor: 0.92483 nm Force: 2.6341 nm SUSA: 1.4977 nm MOF: 2.7917 nm	+106%
0.75	$675 \cdot \pi^2$ (56.25%)	Floor: 1.0722 nm Force: 1.1228 nm SUSA: 1.1839 nm MOF: 1.5525 nm	+14.5%	Floor: 0.99602 nm Force: 1.2278 nm SUSA: 1.1373 nm MOF: 1.581 nm	+16.6%
1	$1200 \cdot \pi^2$ (100%)	Floor: 1.1234 nm Force: 0.75958 nm SUSA: 1.1737 nm MOF: 1.3561 nm	0%	Floor: 1.1234 nm Force: 0.75958 nm SUSA: 1.1737 nm MOF: 1.3561 nm	0%
1.25	$1875 \cdot \pi^2$ (156.25%)	Floor: 1.1991 nm Force: 0.62241 nm SUSA: 1.231 nm MOF: 1.351 nm	-0.4%	Floor: 1.3235 nm Force: 0.57166 nm SUSA: 1.348 nm MOF: 1.4417 nm	+6.3%
1.5	$4800 \cdot \pi^2$ (400%)	Floor: 2.0148 nm Force: 0.52246 nm SUSA: 2.0283 nm MOF: 2.0814 nm	+53.5%	Floor: 2.6899 nm Force: 0.48198 nm SUSA: 2.6985 nm MOF: 2.7327 nm	+102%

For both an increase or decrease away from the current stiffness the results show a decrease in performance. The current stiffness seems a good trade-off between suppressing the imposed floor and force spectrum. To double the natural frequency the stiffness increases with a factor four. The resulting natural frequency seems relatively insensitive for variation of the stiffness. For a very low natural frequency (< 1 Hz) a very low stiffness is required. Decreasing the stiffness also decreases the robustness for parasitic stiffness; small variations in the realized stiffness.

The stage stability document uses the following formulas for the transmissibility and

compliance of the 1-DOF spring-mass-damper system:

$$T(s) = \frac{s^2 + \left(2q\zeta\omega_n + \frac{\omega_n}{2\zeta}\right)s + q\omega_n^2}{q(s^2 + 2\zeta\omega_n s + \omega_n^2)}$$

$$C(s) = \frac{s^2 + 2\omega_n\sqrt{q}s + q\omega_n^2}{mq\omega_n^2(s^2 + 2\zeta\omega_n s + \omega_n^2)}$$

These transfer functions holds a pair of high-frequency zero such that the roll-off finally turns into a zero slope at a maximum suppression factor q . Setting a maximum suppression factor is more realistic than using the purely theoretic transfer function which rolls-off to infinity since in reality spurious modes limit the roll-off often resulting in a maximum suppression at higher frequencies. The maximum suppression is currently assumed to be 200x, a suppression of -46 dB. Changing this parameter gives the following results;

Max suppression [-]	Decibels [dB]	MOF error [nm]	Diff [%]
10	-20	23.0775	+1602
31,6	-30	7.3526	+442
100	-40	2.4282	+79
178	-45	1.4822	+9.3
200	-46	1.3561	0
224	-47	1.2497	-7.8
316	-50	1.0077	-26
562	-55	0.79406	-41
1000	-60	0.70958	-48

Limiting the roll-off with the stated functions however introduces a gradual transition to the maximum suppression level. This causes that the roll-off is already being limited before reaching the maximum suppression level. This effect is undesirable because no longer a -40 dB/dec slope is obtained before reaching the maximum suppression level. This effect becomes is most prominently present when a lower maximum suppression level is assumed. To investigate the effect of this modelling assumption, the results are compared with a different method for implementing the maximum suppression level. With the alternative method, the transmissibility and compliance are modelled by the standard functions for a single stage passive vibration isolation system;

$$T(s) = \frac{2\zeta\omega_n s + \omega_n^2}{s^2 + 2\zeta\omega_n s + \omega_n^2} \quad (\text{B.1})$$

$$C(s) = \frac{\frac{1}{k}\omega_n^2}{s^2 + 2\zeta\omega_n s + \omega_n^2} \quad (\text{B.2})$$

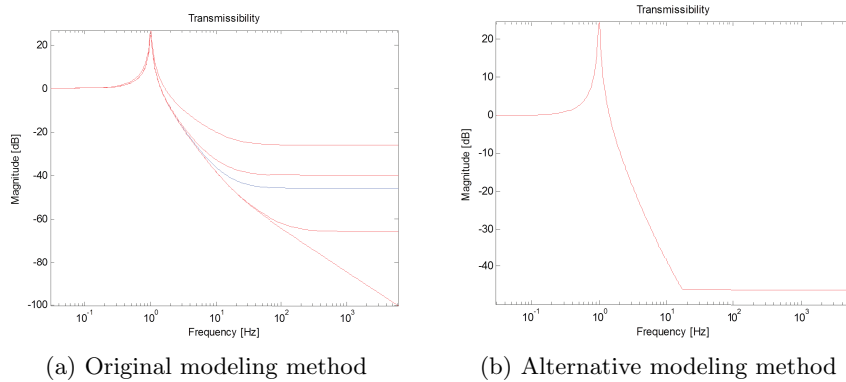


Figure B.1: The two different models for transition to a maximum suppression level. With the implementation of a high frequency zero results in a decreased attenuation before reaching the maximum suppression level, see B.1a.

When these formulas reach the desired maximum suppression level, the transfer functions are set to equal the maximum suppression level resulting in an abrupt transition from a -2 slope to a flat response, see figure B.1b. The following results showed with the standard parameters when using the different method of modelling;

Results with standard parameters:
Resulting error by floor vibrations 1.0193 nm
Resulting error by force disturbance 0.69717 nm
The residual SUSA error is 1.0659 nm
The residual MOF error is 1.2349 nm

This is a difference of 9,3% in resulting error by floor vibrations and 8,2% in resulting error by force disturbances in comparison with the original model.

Changing the maximum suppression level when using the different modelling method offered the following results:

Max suppression [-]	Decibels [dB]	MOF error [nm]	Diff [%]
10	20	21.8824	+1672
31,6	30	6.941	+462
100	40	2.2551	+83
178	45	1.3543	+9.7
200	46	1.2349	0
224	47	1.1349	-8.1
316	50	0.91062	-26
562	55	0.72548	-41
1000	60	0.67362	-45

The percentage change between the different maximum suppression levels is about equal for both methods of modelling the transfer functions.

B.3.2 Damping of the vibration isolation system

Changing the damping affects the attenuation of the natural frequency and the resulting roll-off at increasing frequency. When changing the damping the following results are obtained:

Relative damping (ζ)	Residual error	Diff MOF
0.005	Floor: 1.3095 nm Force: 0.80199 nm SUSA: 1.3578 nm MOF: 1.5356 nm	+24.4%
0.01	Floor: 1.1341 nm Force: 0.74167 nm SUSA: 1.1816 nm MOF: 1.3551 nm	+9.7%
0.02	Floor: 1.0413 nm Force: 0.70866 nm SUSA: 1.0885 nm MOF: 1.2596 nm	+2.0%
0.03 (standard)	Floor: 1.0193 nm Force: 0.69717 nm SUSA: 1.0659 nm MOF: 1.2349 nm	0%
0.05	Floor: 1.0397 nm Force: 0.68757 nm SUSA: 1.0843 nm MOF: 1.2465 nm	+0.9%
0.25	Floor: 2.7488 nm Force: 0.67172 nm SUSA: 2.7651 nm MOF: 2.8297 nm	+129.1%
0.5	Floor: 5.4002 nm Force: 0.66468 nm SUSA: 5.4084 nm MOF: 5.441 nm	+340.6%
1	Floor: 10.4542 nm Force: 0.65527 nm SUSA: 10.4584 nm MOF: 10.4748 nm	+748.2%
2	Floor: 19.6043 nm Force: 0.6443 nm SUSA: 19.6064 nm MOF: 19.6149 nm	+1488.4%

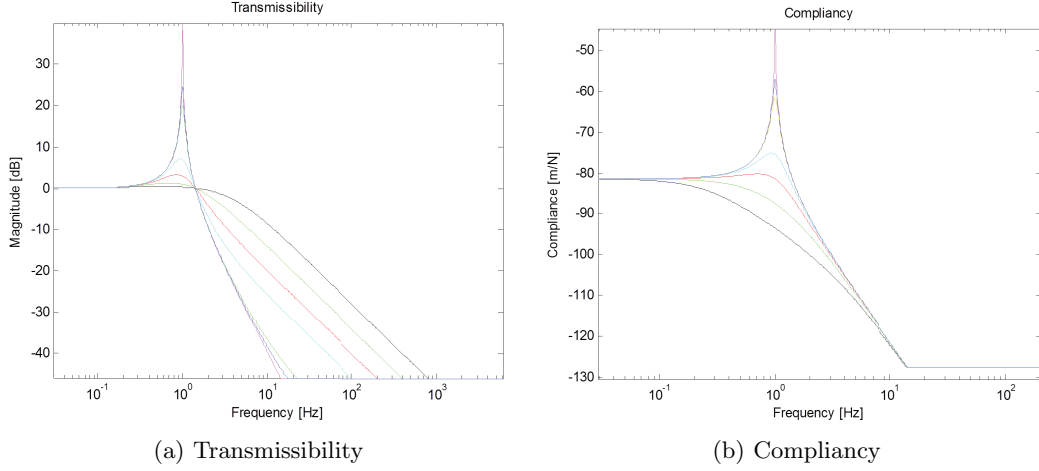


Figure B.2: Transmissibility and compliancy under different levels of viscous damping

As can be noted, changing the damping parameter is performed on the model when using the adjusted implementation of the maximum suppression factor. This is more convenient in order to compare the results when using skyhook damping.

When using a ζ lower than 0.03, the error increases due to the low attenuation of the natural frequency. When increasing the ζ the contribution by the floor vibrations increases due to the reduction in the roll-off due to the use of viscous damping. Since the roll-off is ultimately limited to a -1 slope, the attenuation at higher frequency decreases. When viscous damping is used, the relative damping coefficient is preferably kept around $3 \pm 1\%$. The change in damping has only little effect on the resulting error by the direct disturbance forces. This is due to the fact that use of viscous damping does not limit the attenuation above the natural frequency in the compliancy function. This can easily be seen from the compliancy function (B.2) which holds no zero. Due to the addition of the positioning stage which attenuates low frequency motion well, the effect of improving the low frequency attenuation by the vibration isolation system is only little.

The model is also used to investigate the effect when skyhook damping is implemented. This changes the transmissibility function into:

$$T_{sky}(s) = \frac{\omega_n^2}{s^2 + 2\zeta\omega_n s + 1} \quad (\text{B.3})$$

Results with standard parameters using skyhook damping:
--

Resulting error by floor vibrations 0.99584 nm
Resulting error by force disturbance 0.69717 nm
The residual SUSA error is 1.0435 nm
The residual MOF error is 1.2156 nm

This is a decrease of 2.3% in resulting error by floor vibrations in comparison with using viscous damping.

Changing the ζ while using skyhook damping gave the following results:

Relative damping (ζ)	Residual error	Diff. MOF
0.005	Floor: 1.309 nm Force: 0.80199 nm SUSA: 1.3573 nm MOF: 1.5352 nm	+26,3%
0.03 (standard)	Floor: 0.99584 nm Force: 0.69717 nm SUSA: 1.0435 nm MOF: 1.2156 nm	0%
0.05	Floor: 0.96616 nm Force: 0.68757 nm SUSA: 1.0139 nm MOF: 1.1858 nm	-2.5%
0.25	Floor: 0.92673 nm Force: 0.67172 nm SUSA: 0.97421 nm MOF: 1.1446 nm	-5.8%
0.5	Floor: 0.91798 nm Force: 0.66468 nm SUSA: 0.96491 nm MOF: 1.1334 nm	-6.7%
1	Floor: 0.90787 nm Force: 0.65527 nm SUSA: 0.95399 nm MOF: 1.1196 nm	-7.9%
2	Floor: 0.89691 nm Force: 0.6443 nm SUSA: 0.94206 nm MOF: 1.1043 nm	-9.2%

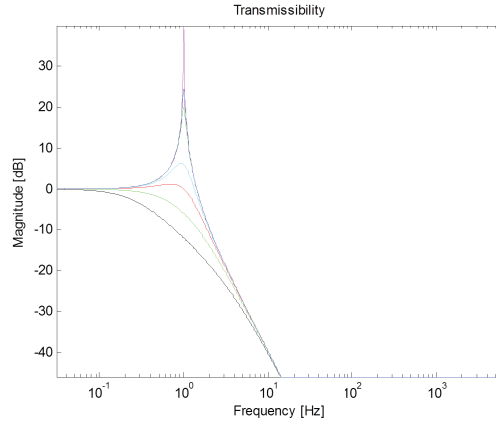


Figure B.3: Transmissibility when using different levels of skyhook damping

With the use of skyhook damping, no zero is present in the resulting transmissibility function (B.3) which makes that the damping does not limit the attenuation at frequencies larger than the natural frequency. Its response to changes in damping becomes equal to that of the compliancy. With increasing ζ , most of the increase in performance results from better attenuation at the natural frequency since the high frequency attenuation is equal for all level of damping.

An important remark is that these values for active skyhook damping are difficult to achieve in reality. Skyhook damping is almost always created by the use of an active system. Correctly measuring vibrations below 1 Hz is hard and the obtaining these idealized curves in reality comes at a price. One should consider if the obtained improvements are worth the costs of introducing an active system for damping (e.g. costs, complexity, electro-magnetic fields etc.).

B.3.3 Weigth of the isolated mass

The natural frequency of the system directly correspond with variations in the weight of isolated load, the MOF. Since there is no exact weight requirement on the components mounted in the MOF, the exact weight of the MOF during the design is unknown. The robustness of the system to an increased weight of the MOF is shown by the following results. Both the weight and inertia are changed by the same factor, changing both the eigenfrequency in the principal direction as well as in the cross-talk directions.

Mass	Error	Diff MOF	Diff Force	Eigfreq
300 (0%)	Floor: 1.1234 nm Force: 0.75958 nm SUSA: 1.1737 nm MOF: 1.3561 nm	0%	0%	1 Hz
250 (-16.7%)	Floor: 1.1906 nm Force: 0.80129 nm SUSA: 1.2434 nm MOF: 1.4351 nm	+5.8%	+5.5%	1.1 Hz
350 (+16.7%)	Floor: 1.0786 nm Force: 0.73375 nm SUSA: 1.1274 nm MOF: 1.3045 nm	-3.8%	-3.4%	0.93 Hz

The natural frequency in rad/s is determined by $\omega_n = \sqrt{k/m}$. When k is small, a variation in m results in only a small variation in the nominal value of k/m , thus also resulting in little variation of the nominal value of ω_n . If m changes by $n\%$ then ω_n will change by a factor $\sqrt{100/(100+n)}$. Since this is a fixed percentage of the desired natural frequency, the nominal change in natural frequency by mass variation will increase with the increase of the desired natural frequency.

With a fixed natural frequency, the attenuation of floor vibrations is independent of the weight of the MOF. Also important in the attenuation of the forces is the resulting inertia of the isolated load:

Mass	Inertia	MOF error / Force error	Diff MOF	Diff Force
250 (-16.7%)	12 – 17	1.402 nm / 0.74039 nm	3.4 %	-2.5%
300	10 – 14,167 (-16.7%)	1.3956 nm / 0.82796 nm	2.9%	9.0%
250 (-16.7%)	10 – 14.167 (-16.7%)	1.4351 nm / 0.80129 nm	5.8%	5.5%
350 (+16.7%)	12 – 17	1.3334 nm / 0.78402 nm	-1.7%	3.2%
300	14 – 19.833 (+16.7%)	1.3318 nm / 0.7152 nm	-1.8%	-5.8%
350 (+16.7%)	14 – 19.833 (+16.7%)	1.3045 nm / 0.73375 nm	-3.8%	-3.4%

Below the natural frequency, the compliancy is determined by the inverse of the stiffness (1/k). The stiffness is related to the mass by the natural frequency. We can thus improve the compliancy by increasing the weight, and via a fixed natural frequency, increase the stiffness. This way the following results are obtained:

Mass / Inertia	Nat. freq.	Error	Diff MOF	Diff Force
250 (-16.7)	1 Hz	Floor: 1.1234 nm Force: 0.91149 nm SUSA: 1.1951 nm MOF: 1.4467 nm	+6.7%	+20%
300 (0%)	1 Hz	Floor: 1.1234 nm Force: 0.75958 nm SUSA: 1.1737 nm MOF: 1.3561 nm	0%	0%
350 (+16.7%)	1 Hz	Floor: 1.1234 nm Force: 0.65107 nm SUSA: 1.1605 nm MOF: 1.2984 nm	-4.3%	-14.3%
410 (+36.7%)	1 Hz	Floor: 1.1234 nm Force: 0.55579 nm SUSA: 1.1506 nm MOF: 1.2534 nm	-7.6%	-26.8%

From the results it shows that proportionally increasing the weight and the stiffness, which results in an equal natural frequency, is very beneficial in the reduction of force vibrations. Increasing the weight and inertia is most beneficial for suppressing low frequency cooling forces. However if the forces mostly occur at higher frequencies, the

suppression of the cooling forces is almost solemnly determined by the set maximum suppression factor and the resulting controller sensitivity.

B.3.4 Cross-talk

The cross-talk to the horizontal direction is normally set to 2% from Z and Rz and 16% from Rx/Ry. The crosstalk is however difficult to control and could well be different in practice. The influence of the crosstalk can be characterized as follows:

Cross-talk percentage [Z Rx/Ry Rz]	Error	Diff MOF	Diff Force
2 16 2	Floor: 1.1234 nm Force: 0.75958 nm SUSA: 1.1737 nm MOF: 1.3561 nm	0%	0%
0 16 2	Floor: 1.1118 nm Force: 0.75956 nm SUSA: 1.1625 nm MOF: 1.3465 nm	-0.7%	-0%
2 0 2	Floor: 1.0159 nm Force: 0.61441 nm SUSA: 1.0524 nm MOF: 1.1873 nm	-12.4%	-19.1%
2 16 0	Floor: 1.1231 nm Force: 0.73775 nm SUSA: 1.1705 nm MOF: 1.3437 nm	-0.9%	-2.9%
0 0 0	Floor: 1.0027 nm Force: 0.58719 nm SUSA: 1.0365 nm MOF: 1.162 nm	-14.3%	-22.7%
2 2 2	Floor: 1.0177 nm Force: 0.61694 nm SUSA: 1.0544 nm MOF: 1.1901 nm	-12.3%	-18.8%

The Rx/Ry crosstalk seems to have the largest influence on the final residual error. Overall it shows that good care has to be taken to minimize crosstalk.

The model furthermore assumes that the input floor and force spectra have different magnitude in different directions. The effect of this assumption is investigated. In the standard settings the floor spectrum in Rx/Ry and Rz is half that of X and Z. Changing the assumption offers the following results:

Floor spectrum multiplication [Z Rx/Ry Rz]	Floor error	Diff. Floor
1 0.5 0.5	1.1234 nm	0%
0.5 0.25 0.25	1.0647 nm	-5.2%
1 1 0.5	1.2215 nm	+8.7%
1 1 1	1.2219 nm	+8.8%
2 1 1	1.2325 nm	+9.7%

The force spectrum is 10 times larger in Z and Rz and 2 times larger in Rx/Ry.

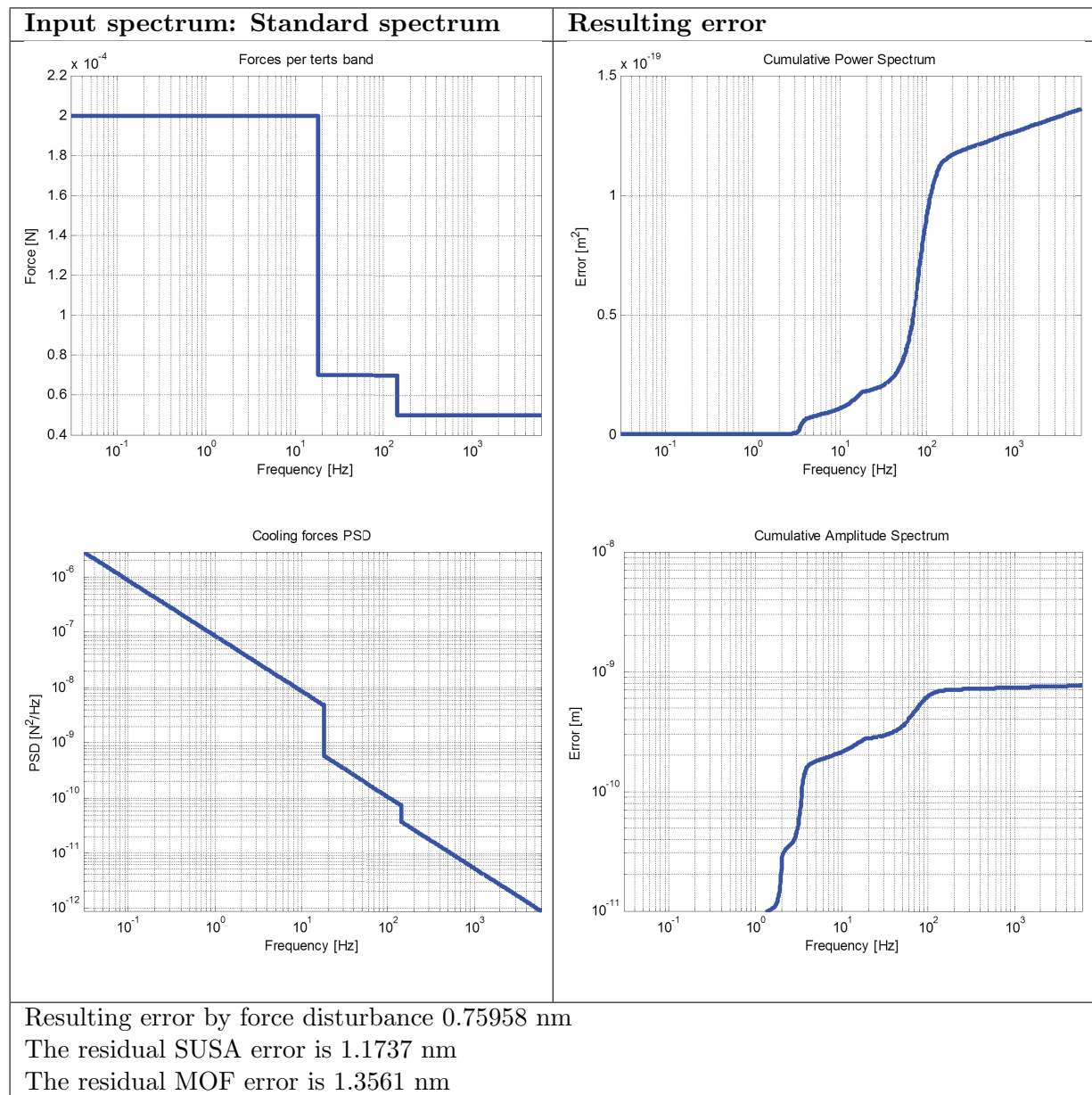
Force spectrum multiplication [Z Rx/Ry Rz]	Force error	Diff. Force
10 2 10	0.75958 nm	0%
10 1 10	0.69082 nm	-9.05%
5 1 5	0.67349 nm	-11.3%
1 1 1	0.65931 nm	-13.2%

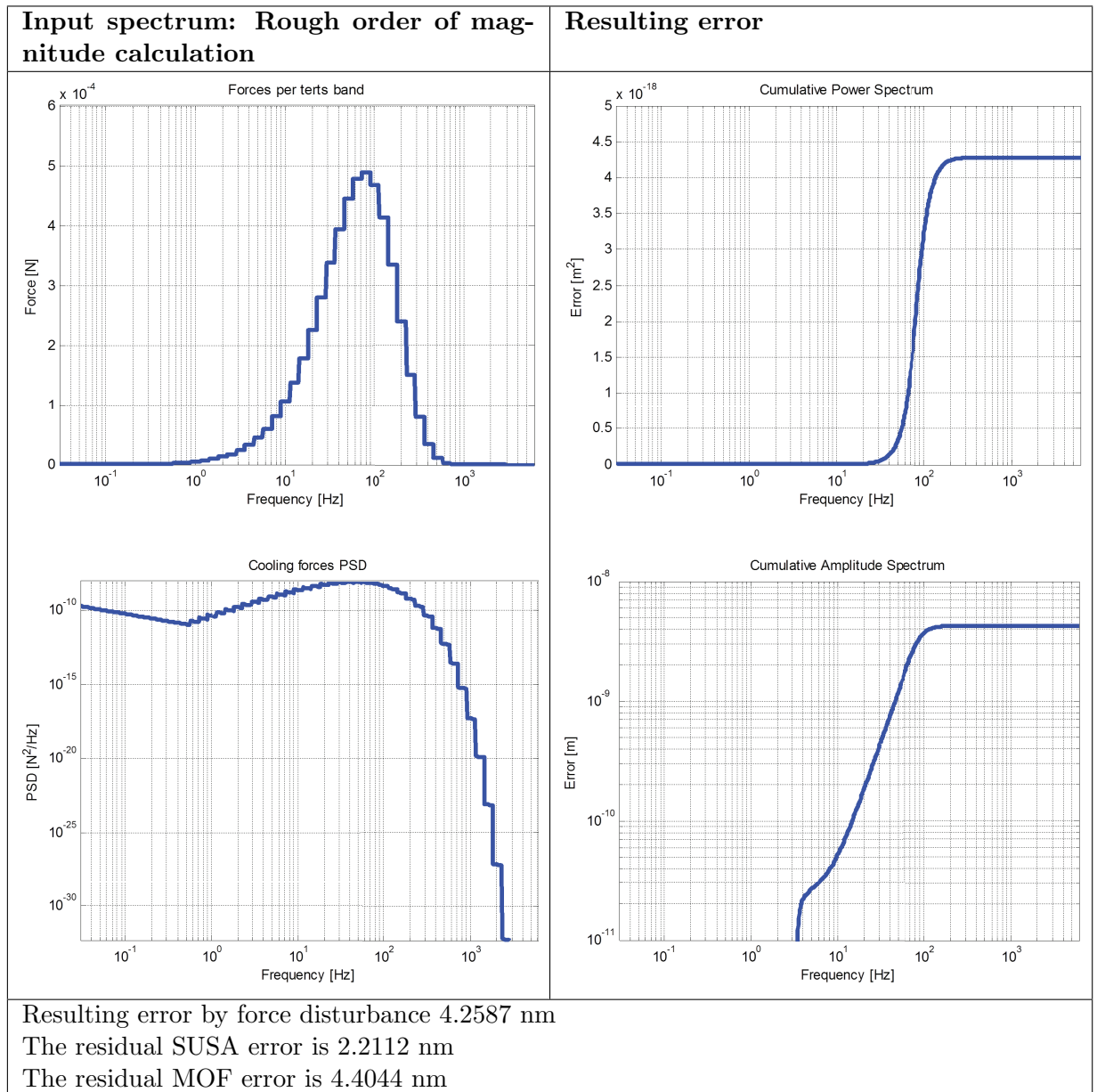
It has not been verified if the spectra differ in magnitude for different DOF. Therefore the use of the multiplication factors for different DOF should be verified in practice.

B.3.5 Direct disturbance forces: magnitude and spectral distribution

Due to the use of a cooling system, direct disturbance forces are present which act on the isolated load. This implicates that for the current passive vibration isolation system a correct balance between transmissibility and compliancy has to be attained. It is therefore important that a good approximation of the forces caused by the cooling system is available. These forces are however difficult to predict because they heavily rely on the geometry of the design. Using standard equations for approximating these forces only results in a rough indication of the order of magnitude.

Currently there are two spectra available as indication of the direct disturbance forces. The first is used as a first input for the Mapper error budgeting model. This spectrum is also used as standard input to our model. The second spectrum is a rough order of magnitude calculation of the forces resulting from cooling of one of the five cooled components; the aperture array (AA). The difference in resulting error by using these two input spectra will be discussed in this section.





The rough order of magnitude calculation shows an increase of 225% in MOF error and 461% in force error. For both spectra most of the error build-up shows in the 20-200 Hz range. Although both the spectra are considered to be conservative estimates, already large errors show for a different spectral distribution of the forces. The large difference in resulting error for the different spectra shows that is obliged to have a good indication of the forces in order to make a correct statement about the performance realized in practice. Without a correct indication of the force spectrum, the error budgeting model can be considered pointless for estimating the performance obtained in practice.

B.3.6 Floor vibration spectrum; magnitude and spectral distribution

The BBN vibration criteria (VC-spectra) are often considered a worst case scenario for floor vibrations. By use of the RMS input per one-third octave band, the criteria often result in an overestimation of the input energy by real floor vibrations [25]. In order to assess the effect of this parameter to the resulting residual error, two variations on the model are studied;

1. Decrease the total PSD of the floor vibrations with a fixed factor
2. Remove the additional input at the specific frequency bands

Using a factor lower PSD for the floor vibrations

The effect of using a factor X times lower PSD for the floor vibrations, results in a factor \sqrt{X} times lower residual error. This is due to using the root of the sum of squares for obtain the resulting error; when the sum of squares reduces by half, the final result reduces with the root of two.

Spectrum	Residual floor error [nm]	Reduction [%]	Allowed nat. freq.
Original Mapper	1.1234	-	1 Hz
1/2 Mapper	0.79438	29,3 ($\sqrt{2}$ x lower)	1.7 Hz
1/5 Mapper	0.50241	55,3 ($\sqrt{5}$ x lower)	2.3 Hz
1/10 Mapper	0.35526	68,4 ($\sqrt{10}$ x lower)	3 Hz

Using a 5 times lower ground vibration spectrum results in a residual error of 0.50241 nm. This is an error reduction of $\sqrt{5}$ times (55,3% lower) in respect to the use of the specified Mapper spectrum. In this case a natural frequency of approximately 2.3 Hz would suffice to attain the original residual error, resulting in a 5.4 times larger VIM stiffness. This would reduce the residual error due to direct disturbance forces to 0.51325 nm (32,4% lower), due to the fundamental trade-off between transmissibility and compliancy. So if the floor vibrations really are overestimated, it offers the possibility of using a higher natural frequency to increase the attenuation of the direct disturbance forces while maintaining a low resulting error by floor vibrations.

Remove the input at the specific frequency bands

The influence of the specific frequency band contributions is relatively small. Overall the narrow band contributions add as little as 0.1 nm to the resulting residual error. As shown in the table below the additions at 16.6, 33 and 100 Hz have the largest contribution. The addition at 100 Hz has the largest influence since the sensitivity of the ShS controller has an overshoot in this frequency band.

Narrow band frequency [Hz]	Added residual error [nm]
16.6	1.1251e-02
33	2.0469e-02
50	2.4188e-03
100	5.2916e-02
660	2.2722e-05
1320	1.1559e-05
Total added residual error:	0.09

The effect of the 100 Hz disturbance becomes even more pronounced when the bandwidth of the ShS controller is increased, moving the peak in the sensitivity closer to the additional disturbance frequency. Although decreasing the total residual error, increasing the ShS bandwidth thus results in a decreased attenuation of this 100 Hz disturbance. This is an important notion as it shows that the general recipe of improving performance of a mechatronic system by increasing controller bandwidth does not always apply. This is illustrated by the following results:

ShS bandwidth [Hz]	100 Hz contribution [nm]	Total added error by narrow bands [nm]	Percentage by 100 Hz contribution [%]	Addition of residual error to total error [%]
75	0.052916	0.08881	58,9	7,8
80	0.073094	0.10178	72,1	9,9
85	0.010087	0.12352	81,7	12,8
95	0.018512	0.19858	93,2	21,6
100	0.23608	0.24628	95,9	26,5
105	0.27480	0.28261	97,2	30
110	0.28011	0.28628	97,8	30,7
115	0.24774	0.25281	98	28,2
120	0.19670	0.20096	97,9	23,6

B.3.7 ShS bandwidth

When changing the set bandwidth of the stage controller the following results are obtained:

Bandwidth	Error	Diff MOF	Diff Force	Diff MOF
60	Floor: 1.6451 nm Force: 0.86834 nm SUSA: 1.6904 nm MOF: 1.8602 nm	+46.4%	+14.3%	+37.2%
70	Floor: 1.2541 nm Force: 0.77491 nm SUSA: 1.3011 nm MOF: 1.4742 nm	+11.6%	+2.02%	+4.06%
75	Floor: 1.1234 nm Force: 0.75958 nm SUSA: 1.1737 nm MOF: 1.3561 nm	0%	0%	0%
80	Floor: 1.0273 nm Force: 0.7574 nm SUSA: 1.0817 nm MOF: 1.2763 nm	-8.55%	-0.29%	-5.88%
90	Floor: 0.92754 nm Force: 0.7829 nm SUSA: 0.99142 nm MOF: 1.2138 nm	-17.4%	+3.07%	-10.5%
100	Floor: 0.92992 nm Force: 0.8457 nm SUSA: 1.0039 nm MOF: 1.257 nm	-17.2%	+11.3%	-7.31%
110	Floor: 0.93301 nm Force: 0.96114 nm SUSA: 1.0273 nm MOF: 1.3395 nm	-16.9%	+26.5%	-1.22%

As shows, increasing the bandwidth does not always improve the attenuation of the disturbances for example with the standard force spectrum. Increasing the bandwidth improves the attenuation of disturbances below unity-gain crossover of the sensitivity function, but this comes at the cost of having a larger multiplication of disturbances the crossover. This so-called waterbed effect, illustrated by figure B.4, is inherent to stable feedback systems and is also discussed by Munnig-Schmidt [8]. Furthermore is should be noted that it is possible that the assumed bandwidth can not be realized in practice.

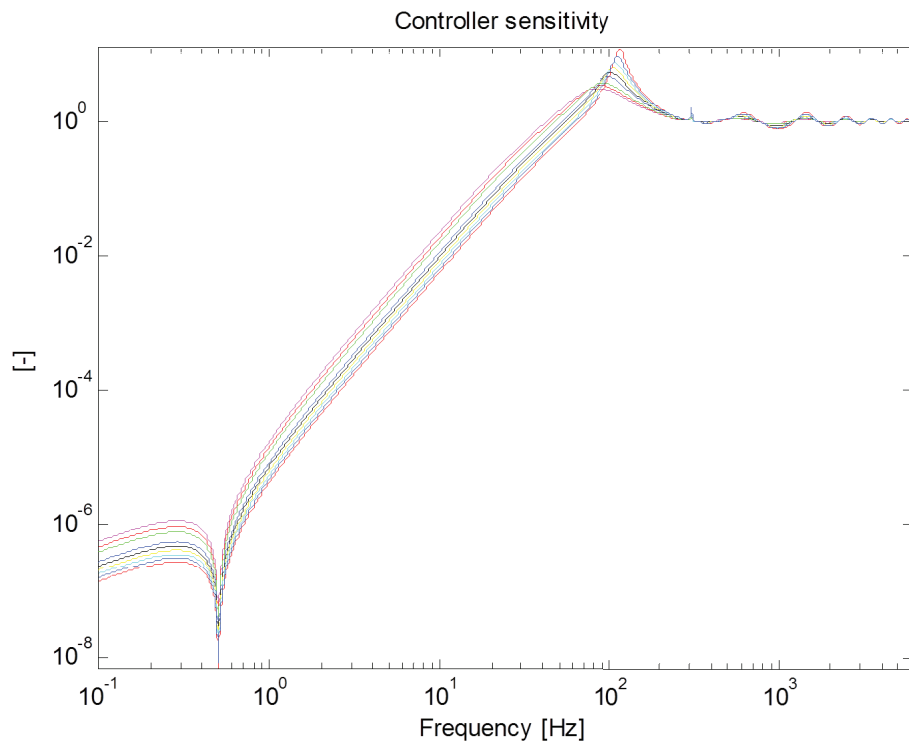


Figure B.4: The waterbed effect when changing the controller bandwidth. This effect is inherent to stable feedback systems.

Appendix C

Vibronix datasheet

This appendix provides additional information to the properties and design of Vibronix.

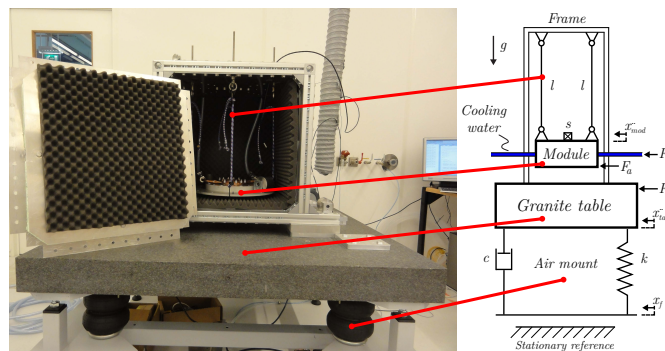


Figure C.1: Vibronix

Component	Properties
Mounting plate	\varnothing 380 x 8 mm aluminum plate, weight of 2,55 kg Designed for first eigenmode > 200 Hz
Pendulums	Elastic string with hooks; stiffness to elongation = ~ 170 N/m, elongated length ~ 400 mm
Frame	Coomach ISB40/8i profile, 40x40 mm Panels are a sandwich of Coomach profile, PUR foam and aluminum plate. Designed for first eigenmode > 200 Hz
Air mounts	Firestone airmount 255-1.5 [81], $k = 59 * 10^3$ N/m
Granite table	Mytri fine black, $E = 1 * 10^5$ N/m
Tubing	Refittex Cristallo soft PVC with braided reinforcement, \varnothing 10 mm
Water pump	Thermo Scientific NESLAB ThermoFlex 2500 [82]
Sensor	Endevco Model 86 seismic accelerometer [30]
DAQ card	NI PCI-4472B [31] - 24 bit



Figure C.2: The components characterized on Vibronix: The straight tube (upper left), Rectangular component (upper right), Aperture Array (middle left), Dummy Aperture Array (middle right) and tubing connected to plate (bottom left). In the bottom right the AA is shown mounted in Vibronix.

C.1 DEB model of Vibronix

The parameters of the model are:

```

1 %% Variables
2 m1 = 7.5; % [kg] mass of interest {module/suspended
    mass from pendulums) (top)
3 k1 = 4*pi^2*1^2*m1; % [N/m] stiffness of pendulums
4 c1 = 2*sqrt(k1*m1)*0.03; % [N*s/m]
5
6 m2 = 70; % [kg] middle mass {frame}
7 k2 = 8*10^7; % [N/m] mounting stiffness of frame
8 c2 = 2*sqrt(k2*(m1+m2))*0.001; % [N*s/m]
9
10 m3 = 390; % [kg] mass closest to floor {granite
    plate} {bottom}
11 k3 = 4*59*10^3; % [N/m] suspension stiffness of air
    springs
12 c3 = 2*sqrt(k3*m3)*0.05; % [N*s/m]
13
14 range = [30 150]; % [-] Frequency range of interest
    in Hz
15 bad_floor = 10; % [-] Multiplication factor of
    standard Mapper spectrum to account for floor flexibility at
    Rotterdamseweg
16 part_force_budget = 1; % [-] Multiplication factor of
    flow-induced forces stating how much the isolated components is to
    account to the submodule budget (0.1 = 10% of budget)

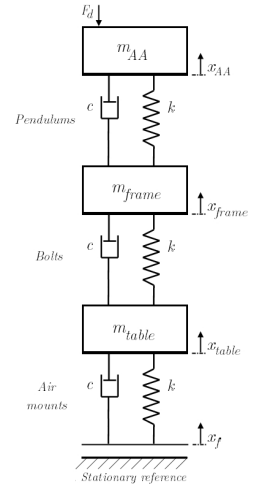
```

The system is modeled as a three-mass-spring-damper system mounted on the ground. The transmissibility is as follows:

```

1 %% Transmissibility three-mass-spring-damper system
2 s = tf('s');
3
4 trans_x2Tox1 = (c1*s+k1)/(m1*s^2+c1*s+k1);
5 trans_x3Tox2 =
6     (c2*s+k2)/(m2*s^2+(c1+c2)*s+k1+k2-(c1*s+k1)*trans_x2Tox1);
7
8 trans_xfTox3 =
9     (c3*s+k3)/(m3*s^2+(c2+c3)*s+k2+k3-(c2*s+k2)*trans_x3Tox2);
10
11 H1 = trans_xfTox3*trans_x3Tox2*trans_x2Tox1;
12 Resp_x1 = freqresp(H1, Sampling_vector_w);
13 X1 = squeeze(abs(Resp_x1))'; % [-]
14
15 H2 = trans_xfTox3*trans_x3Tox2;
16 Resp_x2 = freqresp(H2, Sampling_vector_w);
17 X2 = squeeze(abs(Resp_x2))';
18
19 H3 = trans_xfTox3;
20 Resp_x3 = freqresp(H3, Sampling_vector_w);
21 X3 = squeeze(abs(Resp_x3))';
22 %% Compliancy three-mass-spring-damper system
23 s = tf('s');

```

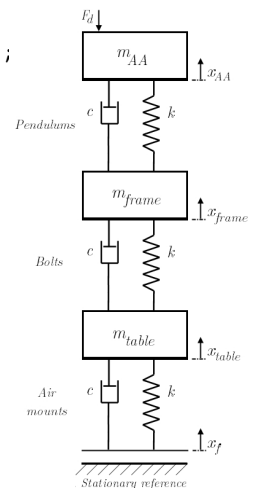


The compliancy is modeled as:

```

1 transF_FloorTox3 = (c2*s+k2)/(m3*s^2+(c2+c3)*s+k2+k3);
2 transF_x3Tox2 =
3     (c1*s+k1)/(m2*s^2+(c1+c2)*s+k1+k2-(c2*s+k2)*transF_FloorTox3);
4
5 transF_x2Tox1 =
6     s^2/(m1*s^2+c1*s+k1-(c1*s+k1)*transF_x3Tox2); % not
7     1/x but s^2/x since compliancy to accelerations is
8     different than compliancy to position
9
10 HF1 = transF_x2Tox1;
11 RespF_x1 = freqresp(HF1, Sampling_vector_w);
12 F_X1 = squeeze(abs(RespF_x1))'; % (m/s^2)/N
13
14 HF2 = transF_x2Tox1*transF_x3Tox2;
15 RespF_x2 = freqresp(HF2, Sampling_vector_w);
16 F_X2 = squeeze(abs(RespF_x2))';
17
18 HF3 = transF_x2Tox1*transF_x3Tox2*transF_FloorTox3;
19 RespF_x3 = freqresp(HF3, Sampling_vector_w);
20 F_X3 = squeeze(abs(RespF_x3))';

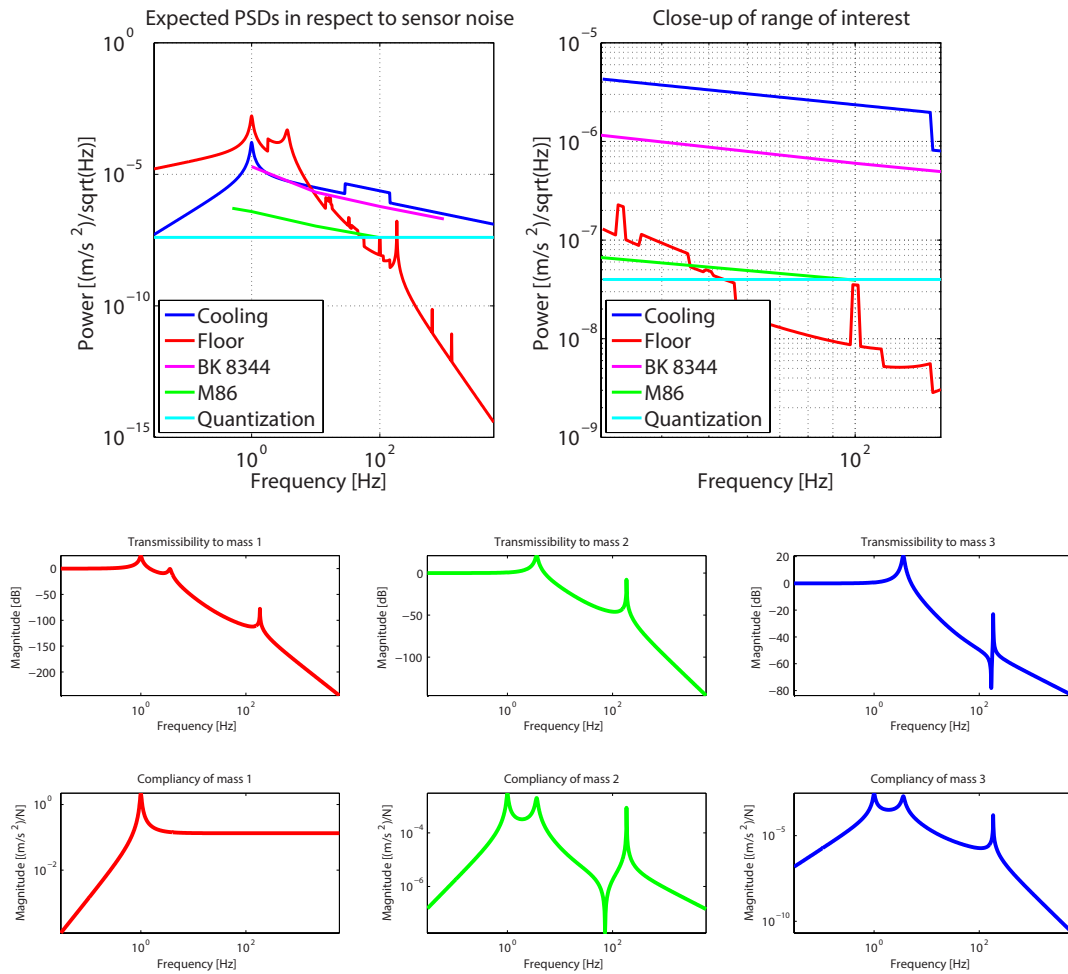
```



The sensor and quantization noise are modelled by their specified values;

```
1 %% Sensors
2
3 % BK8344
4 BK8344vec = [1 10 100 1000];
5 BK8344 = [197e-7 21e-7 6e-7 2e-7]; %[m/s^2/sqrt(Hz)] -
   Specified noise of Bru l & Kjean BK8344 sensor (not used in setup)
6
7 % M86
8 M86vec = [0.5 1 10 100];
9 M86 = [52 39 11 4]*g*10^-9; %[m/s^2/sqrt(Hz)] -
   Specified noise of Endevco M86 sensor (used in setup)
10
11 % Maximum quantization noise
12 quant = 1.589e-15*ones(size(Sampling-vector)); %[(m^2/s^4)/Hz] -
   Expected level of quantization noise
```

The following results are obtained with the model;



Resulting 3-sigma acceleration by floor vibrations over frequency range of interest 208.4292 ng
 Resulting 3-sigma acceleration by direct disturbances forces over frequency range of interest 12816.6573 ng

Similar models were created to evaluate the possible use of force sensors or a laser vibrometer.

By the use of finite element analysis, the setup frame and table is designed to have all its internal natural frequencies above 200 Hz. The detailed design of CAD and production drawings is performed by the author, as well as a large part of the production and assembly of the designed parts.

Bibliography

- [1] M. M. Group. (2012, June 30) Internet world stats. [Online]. Available: <http://www.internetworldstats.com/stats.htm>
- [2] Facebook. (2012, December) Facebook key-facts. [Online]. Available: <http://newsroom.fb.com/Key-Facts>
- [3] Transistor count and moore's law. [Online]. Available: http://en.wikipedia.org/wiki/File:Transistor_Count_and_Moore%27s_Law_-_2011.svg
- [4] Comparison semiconductor process nodes. [Online]. Available: http://en.wikipedia.org/wiki/File:Comparison_semiconductor_process_nodes.svg
- [5] G. E. Moore, "Cramming more components onto integrated circuits," *Electronics*, vol. 38, 1965. [Online]. Available: http://download.intel.com/museum/Moores_Law/Articles-Press_Releases/Gordon_Moore_1965_Article.pdf
- [6] M. Kanello, "Moore's law to roll on for another decade," *CNET News*, 2003. [Online]. Available: <http://news.cnet.com/2100-1001-984051.html>
- [7] ITRS. (2012) International technology roadmap for semiconductors. [Online]. Available: <http://www.itrs.net/>
- [8] R. H. M. Schmidt, *The Design of High-Performance Mechatronics*, D. U. Press, Ed. IOS Press, 2011, ISBN 978-1-60750-825-0.
- [9] Mapper lithography b.v. [Online]. Available: www.mapperlithography.com
- [10] G. t. B. R. J. T. d. P. J. P. E. S. S. S. T. T. A. v. V. B. K. M.J. Wieland, G. de Boer, "Mapper: High throughput maskless lithography," *Proc. of SPIE*, vol. 7271 72710O-1, 2009. [Online]. Available: <http://144.206.159.178/FT/CONF/16429058/16429076.pdf>
- [11] M. Vervoordeldonk, "Development of a novel active isolation concept," 2004.
- [12] K. K.-L. Miu, "A low cost, dc-coupled active vibration isolation system," Master's thesis, Massachusetts Institute of Technology, 2008.

- [13] J. v. S. B. Bakker, “The revolutionary hummingbird technology,” *Mikroniek*, vol. 2, pp. 14–20, 2010. [Online]. Available: http://www.dspe.nl/files/Mikroniek_2010-2-2.pdf
- [14] J. Winterflood, “High performance vibration isolation for gravitational wave detection,” Ph.D. dissertation, University of Western Australia, 2001.
- [15] E. Chin, “High performance vibration isolation techniques for the aigo gravitational wave detector,” Ph.D. dissertation, University of Western Australia, 2007.
- [16] M. Plissi, “Geo 600 triple pendulum suspension system: Seismic isolation and control,” *Review of Scientific Instruments*, vol. 71, no. 6, pp. 2539–2545, 2000.
- [17] N. Robertson, “Seismic isolation and suspension systems for advanced ligo,” *Proceedings of SPIE*, vol. 5500, pp. 81–91, 2004.
- [18] T. Accadia, “The seismic superattenuators of the virgo gravitational waves interferometer,” *Journal of Low Frequency Noise, Vibration and Active Control*, vol. 30, no. 1, pp. 63–79, 2011.
- [19] D. T. P.K. Subrahmanyam, “Synthesis of passive vibration isolation mounts for machine tools; a control system paradigm,” *Proceedings of the 2000 American Control Conference*, vol. 4, pp. 2886 – 2891, 2000.
- [20] C. Gordon, “Generic criteria for vibration-sensitive equipment,” *Proceedings of SPIE*, vol. 1619, pp. 71–85, 1991.
- [21] ———, “Generic vibration criteria for vibration-sensitive equipment,” *Proceedings of SPIE*, vol. 3786, pp. 22–33, 1999.
- [22] T. B. C. G. M. Gendreau, H. Amick, “Evolving criteria for research facilities: Vibration,” *Proceedings of SPIE*, vol. 5933, pp. 1–13, 2005.
- [23] J. Peterson, “Observations and modeling of seismic background noise,” U.S. Department of Interior Geological Survey, Tech. Rep. Open-File Report 93-322, 1993. [Online]. Available: <http://aslwww.cr.usgs.gov/Publications/>
- [24] L. Jabben, “Chp. 3 - dynamic error budgeting,” in *Mechatronic Design of a Magnetically Suspended Rotating Platform*, December 2007, pp. 31 – 66.
- [25] J. E. W. A. T. M. S. v. d. B. J. van Eijk, D. Laro, “The ‘ultimate performance’ in floor vibration isolation,” *Mikroniek*, vol. 51, no. 2, pp. 13 – 19, 2011.
- [26] M. Boogaard, “Machines with high accuracy on factory floors,” Master’s thesis, TU Delft, 2012. [Online]. Available: <http://repository.tudelft.nl/view/ir/uuid%3A41b743d8-f3a9-4737-b443-4ebb2be9914a/>

- [27] W. Monkhorst, “Dynamic error budgeting - a design approach,” Master’s thesis, Mechanical Engineering, Delft University of Technology, Cambridge, MA, USA, May 2004.
- [28] —, “Feasibility study of the dynamic error budgeting design approach,” Mechanical Engineering, Delft University of Technology, Tech. Rep., January 2003.
- [29] J. van Nieuwstadt, “Estimate of vibrations due to cooling water flow in beam generator module v01-02,” Mapper Lithography, Internal document, 2012.
- [30] Endevco, *Model 86 Seismic accelerometer datasheet*, Megitt’s Endevco Corporation Std., 2012. [Online]. Available: <https://www.endevco.com/>
- [31] N. Instruments, *NI 4472 series Dynamic Signal Acquisition Card datasheet*, National Instruments Std., 2012. [Online]. Available: <http://www.ni.com/pdf/products/us/3sv414-416.pdf>
- [32] L. Zuo, “Element and system design for active and passive vibration isolation,” Ph.D. dissertation, Massachusetts Institute of Technology, 2004.
- [33] R. Ibrahim, “Recent advances in nonlinear passive vibration isolators,” *Journal of Sound and Vibration*, vol. 314, pp. 371–452, 2008.
- [34] G. van der Poel, “An exploration of active hard mount vibration isolation for precision equipment,” Ph.D. dissertation, University of Twente, 2010.
- [35] D. Platus, “Negative-stiffness-mechanism vibration isolation systems,” *SPIE*, vol. 3786, pp. 98–105, July 1999.
- [36] —, “Negative-stiffness vibration isolation in laser and optical systems,” *SPIE*, 2008.
- [37] Technical manufacturing corporation. [Online]. Available: <http://www.techmfg.com/>
- [38] A. Carrella, “Passive vibration isolators with high-static-low-dynamic-stiffness,” Ph.D. dissertation, University of Southampton, April 2008.
- [39] Minus k vibration technology inc. [Online]. Available: <http://www.minusk.com/>
- [40] Newport - optical tables. [Online]. Available: <http://www.newport.com/Vibration-Control/988043/1033/content.aspx>
- [41] Thorlabs inc. - optical tables. [Online]. Available: http://www.thorlabs.de/navigation.cfm?guide_id=41
- [42] Aei 10m prototype. Leibniz Universitt Hannover. [Online]. Available: <http://10m-prototype.aei.uni-hannover.de/>

- [43] A. Takamori, “Inverted pendulum as low frequency pre-isolation for advanced gravitational wave detectors,” *Nuclear Instruments & Methods in Physics Research, Section A: Accelerators, Spectrometers, Detectors, and Associated Equipment*, vol. 582, pp. 683–692, 2007.
- [44] I. Taurasi, “Inverted pendulum studies for seismic attenuation,” Master’s thesis, California Institute of Technology, 2005.
- [45] C. Johnson, “Design of passive damping systems,” *Transactions of the ASME*, vol. 117, pp. 171–176, June 1995.
- [46] S. Chikkamaranahalli, “Damping mechanisms for precision applications in uhv environment,” *ASPE*, 2006. [Online]. Available: http://www.aspe.net/publications/spring_2006/spr06abs/1876.pdf
- [47] R. Stanway, “Applications of electro-rheological fluids in vibration control: a survey,” *Smart Materials and Structures*, vol. 5, no. 4, pp. 464–482, 1996.
- [48] Y. Choi, “Semi-active isolators using electrorheological/magnetorheological fluids,” *Noise & Vibration Worldwide*, pp. 16–19, 2002.
- [49] A. Tonoli, “Dynamic characteristics of eddy current dampers and couplers,” *Journal of Sound and Vibration*, vol. 301, pp. 576–591, 2007.
- [50] D. I. W. B. H.A. Sodano, J.S. Bae, “Improved concept and model of eddy current damper,” *Journal of Vibration and Acoustics*, vol. 128, pp. 294–302, June 2006.
- [51] A. Bejeddou, “Use of shunted shear-mode piezoceramics for structural vibration passive damping,” *Computers and Structures*, vol. 84, pp. 1415–1425, 2006.
- [52] J. Holterman, “Vibration control of high-precision machines with active structural elements,” Ph.D. dissertation, University of Twente, 2002. [Online]. Available: <http://doc.utwente.nl/38639/1/t000001f.pdf>
- [53] —, “Active dampin using piezoelectric smart discs,” *Mikroniek*, vol. 3, pp. 46–55, 2008. [Online]. Available: <http://www.dspe.nl/files/2008-3%20actieve%20demping.pdf>
- [54] D. Karnopp, “Vibration control using semi-active force generators,” *Journal of Engineering for Industry*, vol. 96, pp. 619–626, May 1974.
- [55] C. Collette, “Active vibration isolation of high precision machines,” *Diamond Light Source Proceedings*, vol. 1, pp. 1–5, January 2010. [Online]. Available: <http://cdsweb.cern.ch/record/1323818>
- [56] S. N. L. Zuo, “Active vibration isolation using a postbuckled spring,” *ASPE Proceedings, Control of Precision Systems*, 2004. [Online]. Available: http://www.aspe.net/publications/Spring_2004/04SP%20Extended%20Abstracts/1412-zuo-nayfeh%20New.PDF

- [57] Geospace technologies. [Online]. Available: <http://www.geospace.com/>
- [58] Ion geo geophones. [Online]. Available: <http://www.geophone.com/contact.asp>
- [59] J. Dams, "Low frequency geophone with passive magnetic spring," *Mikroniek*, vol. 3, pp. 24–28, 2009.
- [60] Ussi seismic systems inc. - optical geophone. [Online]. Available: <http://www.ussensorsystems.com/USSI-Geophone-brochure.pdf>
- [61] Meggitt endevco corporation. [Online]. Available: <https://www.endevco.com/>
- [62] Colibrys ltd. [Online]. Available: <http://www.colibrys.ch/>
- [63] Brel & kjaer sound and vibration measurement a/s. [Online]. Available: <http://www.bksv.com/>
- [64] Hewlett packard and shell central nerval system of the earth (cense) project. [Online]. Available: <http://www.hpl.hp.com/news/2009/oct-dec/cense.html>
- [65] H. Packard, "Hp mems seismic sensor for oil and gas exploration," 2011. [Online]. Available: http://www.hp.com/hpinfo/newsroom/press_kits/2011/sensingsolutions/HP_Seismic_Sensor_wp.pdf
- [66] Sercel/tronics/leti mems geophone - slide 16-20. [Online]. Available: http://www.aaafasso.fr/dossiersaaaf/ACTES_COLLOQ.LIBRES/ActColloq.06/NanoTechno.06.NonCompress/004.Le%20potentiel%20des%20MEMS.pdf
- [67] Sercel. [Online]. Available: <http://www.sercel.com/>
- [68] L. Scarborough, "Fluidic composite tunable vibration isolators," *Journal of Vibration and Acoustics*, vol. 134, pp. 011 010–1 – 011 010–7, 2012.
- [69] M. Unsal, "Semi-active vibration control of a parallel platform mechanism using magnetorheological damping," Ph.D. dissertation, University of Florida, 2006.
- [70] J. Ginder, "Magnetorheological elastomers in tunable vibration absorbers," *Proceedings of SPIE*, vol. 4331, pp. 103–110, 2001.
- [71] R. Sarban, "A tubular dielectric elastomer actuator: Fabrication, characterization and active vibration isolation," *Mechanical Systems and Signal Processing*, vol. 25, pp. 2879–2891, 2011.
- [72] N. v. L. A. Katalenic, "Reluctance force in high precision engineering," *Precisiebeurs*, 2011. [Online]. Available: <http://www.precisiebeurs.nl/assets/Uploads/TU-Eindhoven-dhr.-Katalenic.pdf>
- [73] C. Nijse, "Linear motion systems; a modular approach for improved straightness performance," Ph.D. dissertation, TU Delft, 2001, chapter 5:Zero stiffness actuators in straight motion systems.

- [74] T. Mizuno, "Development of an active vibration isolation system using linearized zero-power control with weight support springs," *Journal of Vibration and Acoustics*, vol. 132, pp. 041 006–1 – 041 006–9, 2010.
- [75] A. F. A.M. Beard, D.W. Schubert, "A practical product implementation of an active/passive vibration isolation system," *Proc. of SPIE, Vibration Monitoring and Control*, vol. 2264, pp. 38–49, October 1994.
- [76] S. et al., "Stiff actuator active vibration isolation system," U.S. Patent US5 660 255, 1997.
- [77] *Piezo Film Sensors Technical Manual*, Measurement Specialities, Inc., 950 Forge Avenue, Norristown, PA, April 1999. [Online]. Available: <http://resenv.media.mit.edu/classes/MAS836/Readings/MSI-techman.pdf>
- [78] C. Hansen and S. Snyder, *Active Control of Noise and Vibration*, 1st ed. E & FN SPON, 1997.
- [79] M. Kwak, "Development of the passive-active vibration absorber using piezoelectric actuators," *Smart Structures and Materials 2002: Damping and Isolation*, vol. 4697, pp. 292–300, 2002.
- [80] Z. Lu, "Simulation study of robust h-inf control system for the optical ultra-precision vibration isolation system," *IMACS Multiconference on Computational Engineering in Systems Applications*, pp. 1787–1791, 2006.
- [81] Firestone, *Firestone airmount 255-1.5*, Firestone Std. [Online]. Available: <http://www.firestoneip.com/site-resources/fsip/literature/pdf/EMDG.pdf>
- [82] T. Scientific, *Neslab Thermoflex 2500*, Thermo Scientific Std., 2012. [Online]. Available: <https://static.thermoscientific.com/images/D11083~.pdf>

